EFFECTS OF GEOMETRY AND ANISOTROPY ON PERMEABILITY MEASUREMENTS FROM DRILL CUTTINGS

BY

SHEHARYAR MANSUR

A Thesis Presented to the
DEANSHIP OF GRADUATE STUDIES

KING FAHD UNIVERSITY OF PETROLEUM & MINERALS

DHAHRAN, SAUDI ARABIA

In Partial Fulfillment of the
Requirements for the Degree of

MASTER OF SCIENCE

In

PETROLEUM ENGINEERING

JUNE, 2009

KING FAHD UNIVERSITY OF PETROLEUM & MINERALS
DHAHRAN 31261, SUADI ARABIA

DEANSHIP OF GRADUATE STUDIES

This thesis, written by **SHEHARYAR MANSUR** under the direction of his thesis advisor and approved by his thesis committee, has been presented to and accepted by the Dean of Graduate Studies, in partial fulfillment of the requirements for the degree of **MASTER OF SCIENCE IN PETROLEUM ENGINEERING**.

Thesis Committee

H.Y. al-Yousef
Dr. Hassan Y. Al-Yousef (Thesis Advisor)

Dr. Ezeddin Shirif (Member)

Alberto Marsala
Dr. Alberto F. Marsala (Member)

Dr. Sidqi A. Abu-Khamsin
(Department Chairman)

Dr. Salam A. Zummo
(Dean of Graduate Studies)

7/9/09
Date

Dedicated

to

The loving memory of my late Mother

For instilling in me the morals, values and principles

that define me for the person I am today.

Acknowledgment

All praises and adorations are due to Allah, the lord of incomparable majesty. May Allah bestow peace on his Prophet Mohammed (Peace and Blessings of Allah be upon him), and his family.

Acknowledgement is due to the King Fahd University of Petroleum & Minerals for supporting this research.

I acknowledge, with deep gratitude and appreciation, the inspiration, encouragement, supervision and support rendered to me by my thesis advisor, Dr. Hasan Y. Al-Yousef. I also wish to thank the other members of my thesis committee Dr. Ezeddin Shirif and Dr. Alberto F. Marsala for their constructive guidance, technical support and patronage.

Numerous gratitude and thanks goes to the Petroleum Engineering Department and the KFUPM Research Institute for making the necessary facilities and resources available to accomplish this research.

I would also like to express my immense gratitude to Dr. Hasan S. Al-Hashim and Dr. Mahmoud El Awdy Doklah for their tutelage throughout my Masters Degree to which I owe my success and rapid prowess in acquiring the necessary concepts in the field of Petroleum Engineering.

Further, I would like to thank Mr. Abdulrahim A. Muhammadain and my dear friends Hisham Saeed, Jubran Akram and Babar Hassan for their constructive advice, support and companionship in the long hours that lead to fulfillment of my research work.

Table of Contents

List of Figures

List of Tables

Thesis Abstract

Full Name : Sheharyar Mansur
Thesis Title : Effects of Geometry and Anisotropy on Permeability Measurements from Drill Cuttings
Major Field : Petroleum Engineering
Date of Degree : June, 2009

Recent advances in technology have lead to the development of techniques aimed at the estimation of a reservoir's petro-physical parameters from drill cuttings.

The present study investigates the effects of cutting geometry and anisotropy on the responses from the pressure diffusion technique of direct permeability measurements from drill cuttings. The drill cuttings are modeled as rectangular cuboids in the Cartesian coordinate system and the resultant diffusivity equation is solved using an implicit finite difference technique. In addition, experimental testing was conducted using the Darcy Log equipment to assess the impact of shape and anisotropy and validate the simulator.

The results obtained from the study highlight the deviations in the interpreted value of permeability arising from the shape variations. Furthermore, it was noticed that the interpreted permeability becomes roughly equivalent to that obtained from a cutting having permeability equivalent to some area weighted average of the individual axial permeabilities. The permeability normal to the largest surface area had the greatest influence upon the interpreted permeability for rectangular cuboids. Also, the cutting shape was found to have the most significant influence on the resultant responses.

خلاصة الرسالة

الإســـــم : شهريـار منصور
عنوان الرسالة : تـأثير الـشكل الهندسي والـتبايـن على قيـاس الـنفـاذيـة مـن قطع الحفر
التخصص : هندسة بترول
تاريخ التخرج : جمادى الآخر 1430

الـتطورات الأخيرة في مجال الـتكنولـوجيـا أدت إلى تطويـر تـقنيـات تهدف إلى تـقديـر الخصائص الـنفطية الـفيـزيـائية من قطع الحفر.

الـدراسة الحـاليـة تـبحث في الـتحقق من تـأثير الـشكل الهندسي لـلقطع وتـبايـن خواصها على الـردود الحاصلة من تـقنية انـتشار الضغط على الـقيـاسات المباشرة لـلنفـاذية بـاستخدام قطع الحفر. لـعمل الـبحث تم استخدام حل رقمي لـتمثيل الـقطع كمكعبات مستطيلة على نظام ديـكارت وحل معـادلـة الانـتشار الـنـاتجة بـاستخدام نظام الـفرق المحدود الـضمني. إضافة إلى ذلـك فـإن الاختبـار المعـملي يـتم بـاستخدام جهاز قيـاس خصائص دارسي لـتقيـيم تـأثير الـشكل وتـبايـن الخواص ولـلتثبت من المحاكي الـرقـمي.

الـنـتائج الـتي تم الحصول عليـها من هذه الـدراسـة تـسـلط الـضـوء عـلـى الاختلافـات في قيـمة الـنفـاذية الـنـاجمـة عـن تـغـيرات الـشـكل الهندسـي. وعلاوة على ذلـك ، لـوحظ أن الـنفـاذية المقدرة تصبح معـادلـة تـقريـبـا لـتلك الـتي تم الحصول عليـها من الـقطعة صاحبة نـفـاذية تـسـاوي مـعـدل المسـاحة المتوسـطة لـلمحـاور الـرئيسـية لـلنفـاذيـات. الـنفـاذيـة الـعمودية على أكبر مساحة تـؤثـر تـأثيرا كبيرا على الـنفـاذية المقـدرة لـلعينات المكعبة المستطيلة. كما وجد أن شكل الـقطعة يـؤثـر تـأثيرا هامـا على الـردود الـنـاتجة.

CHAPTER 1

INTRODUCTION

Permeability, defined as the rock fluid conductivity, is one of the most important petro-physical parameters for reservoir characterization. It is influenced by various factors such as degree of cementation, net overburden, pore geometry and presence of clays amongst others.

When a new well is drilled, the key concerns for the liable companies are to accurately establish the expected reserves (porosity and saturation are key parameters) and the well productivity (permeability being of significance).

Knowledge of reservoir permeability and pressure is important to field development. Such knowledge prior to well completion and, in circumstances, before stimulation treatment is especially critical to optimal well performance. Determination of in-situ permeability not only aids the well completion and stimulation but can be used to calibrate the log and core derived estimates of formation permeability improving performance prediction and field development.

With the recent advances in the knowledge of sciences governing the petro-physical properties of reservoir rocks, a reasonably accurate estimate of the porosity and permeability can be established. In many reservoirs, permeability values are often available from one to as many as four sources. These permeability sources include core

analysis, nuclear magnetic resonance logs, wire-line formation testers (MDT) and well testing. An inherent constraint, however, of all these processes is their inability to provide real time data which renders them useless in making strategic decisions.

Drill cuttings provide a cost effective means to characterize formations when and where cores are not available. Analysis on cuttings allows for availability of coincident data, helping in the achievement of real time decision making. A continuous permeability log can be obtained which aids in improving the real time well-bore stability models. It is these benefits and the recent advancements in technology that can be attributed for invoking interest in the use of drill cuttings to evaluate petro-physical properties of the reservoir rock. Various research projects have been undertaken in recent years, with those aimed at the estimation of permeability from drill cuttings, being sub-divided into two categories: the direct and indirect evaluations.

An inherent inadequacy of the direct methods proposed for permeability measurement so far is their inability to address the influence of geometry and directionality of permeability of the available cuttings upon such a permeability measurement. Cuttings coming out from the well-bore are not regularly shaped and more often than not, a significant directional anisotropy exists which needs to be addressed in order to obtain a more accurate permeability estimate. In this work, the effects of cuttings geometry and anisotropy will be studied to help quantify their impact upon the measureable permeability through the use of the pressure diffusion technique.

CHAPTER 2

LITERATURE REVIEW

Drill cuttings, in recent times, have invoked the industry's interest as a possible inexpensive means to characterize formations when and where cores are not available. Analysis on cuttings carries the added advantage of making available real time data, which can consequently aid in real time decision making. A continuous permeability log can be obtained which aids in improving the real time well-bore stability models. It is these benefits and the recent advancements in technology that can be attributed for much of the recent interest in the use of drill cuttings to evaluate petro-physical properties of the reservoir rock. This section reviews the latest work done in the area of making use of drill cuttings for permeability measurements. The measurement techniques may be classified into Indirect and Direct methods.

Swanson (1981) [14] developed a new correlation between brine and air permeabilities with mercury capillary pressure data. The relationship was expressed as a monograph which offers a ready application for improved estimation of permeability from capillary pressure measurements on small portions of side-wall core samples and drill cuttings.

Nigh & Taylor (1985) [12] developed a technique to estimate cutting permeability from NMR measurements. A special tool was designed to make NMR measurements on cuttings under the rigorous conditions at the rig site. The porosity can then be derived from the measured volume of water while the permeability is evaluated form the whole T_2 relaxation signal using the **Timur** (1968) [15] Law.

Kamath (1992) [5] examined published theoretical and correlative models and extensions to evaluate the accuracy of predicting air permeability from mercury injection data. He also reported a possible use of mercury porosimeter curves obtained from cuttings for the estimation of permeability.

Luffel *et al* (1993) [8] developed three laboratory methods to measure matrix gas permeability of Devonian Shale cores and drill cuttings at native water saturations. Permeability of core chips or drill cuttings was determined through pulsed pressure testing with helium and was found to be in good agreement with that obtained form the pulse tests on core plugs for samples displaying permeability in the range of 0.25 mD to 45 X 10^{-8} mD. An important finding was that the analysis from drill cuttings, though could not be carried out at the net over-burden stress, yielded results that were uninfluenced by coring induced micro fractures which are not actually present in the reservoir.

Marsala *et al* (1996) [10] characterized in real time the formations encountered during drilling by means of measurements on drill chips. A procedure for the measurement of permeability from cuttings of low and very low permeability values (ranging from 0.1 millidarcies to a few nanodarcies) by employing the pulse decay technique under unsteady state conditions was detailed. The project also demonstrated the feasibility of obtaining representative values of P- and S- wave velocities, rock strength and deformability, permeability, porosity, density, residual fluid content and saturation from drill cuttings. A steady state method [11] was also developed to make measurements on cuttings having permeability up to 500 mD.

Egermann *et al* (2002) [2] presented a new methodology to measure the permeability directly from cuttings. The method was based on the principal of pressure diffusion similar to that proposed by **Luffel** [8], only the compression of trapped gas existing as disconnected ganglia was affected by establishing an effective flow of viscous oil into the cuttings. Owing to the simplicity and consistency, it was proposed that the method could be used in the field for a fast evaluation of reservoir permeability in quasi real time during drilling.

CHAPTER 3

PROBLEM STATEMENT AND OBJECTIVE OF STUDY

3.1 Problem Statement

It is clear from the review of the latest works aimed at the estimation of permeability from drill cuttings that the methods proposed and developed pose some serious limitations when addressing the issue of permeability anisotropy and cutting shape. Though not all the methods exhibit inadequacy in the face of geometric inconsistency, the method being in-sensitive to the cutting shape, but inherently, all the techniques have been designed considering a uniform isotropic value of permeability. In view of the sedimentary origin of most reservoir rocks, this is an oversimplification.

A definite science capable of completely describing and defining the physical processes concerning the petroleum reservoir can be very complex. The available data can be extremely scanty in the event of difficult conditions or in other cases just far too expensive to acquire. For the sake of deducing conclusions, the industry relies heavily on theoretical correlations to construe a meaningful representation for properties which are otherwise not directly obtainable. These correlations, however, cannot be universally relevant and have been known to produce significant errors, when applied to other formations, as a consequence.

Given the inherent simplicity in concept and application, most of the latest works on techniques aimed at direct measurement of permeability from drill cuttings have evolved upon the principal of pressure diffusion. A pressure pulse is applied to a chamber containing cuttings. As the fluid moves into the cuttings initially saturated with the fluid at atmospheric conditions, the pressure in the chamber declines which is recorded over time. Permeability of drill cuttings can then be estimated by history matching the experimental data against a numerical model.

Unlike the case where the flow is forced across the cuttings along a particular direction (**Marsala** [10] method), with all the faces exposed to flow and contributing to the influx and the resultant pressure drop, these techniques appear quite susceptible to divergence from the ideal response characteristic for a homogeneous and isotropic cutting of a spherical shape in the event of anisotropy or geometrical inconsistencies.

3.2 Objectives of Study

The general objective of this work is to study the effect of cutting geometry and anisotropy on the obtainable pressure diffusion response from drill cuttings. The specific objectives can be stated as:

1) Study the impact of cutting shape on permeability measurements obtained from drill cuttings.
2) Study the influence of permeability anisotropy on permeability measurements obtained from drill cuttings.

CHAPTER 4

MODEL DEVELOPMENT AND VALIDATION

As a result of our survey, the **Egermann** [2] model presented the most logical option for the attainment of the aforementioned objectives. Though similar in terms of principle to the one proposed by **Luffel** [8], the method is more versatile in terms of the range of measureable permeability values.

4.1 Principle and Model Development

The principle of pressure diffusion (pulse decay) is structured upon the concept of the inherent compressibility of gases. When vessels containing compressible fluids at dissimilar pressures are brought into dynamic contact with each other, fluid flow takes place. The fluid effusion from the vessel at higher pressure will be accompanied by a pressure decline while its influx into the vessel at lower pressure will be translated as an increase in the pressure inside the respective vessels. The process continues until pressure equilibrium is attained, the time required for which will ultimately be dependent upon the mobility of the flowing fluids and the pressure contrast.

Recent advancements in the technology of pressure sensors and the knowledge regarding rock fluid interaction has kindled interest in the concept of making use of pressure diffusion for the estimation of permeability from drill cuttings. To allow for

measurement of higher permeability values, an effective flow of viscous oil, effectively to keep the mobility (k/μ) small enough to have an impact on the pressure regime, is established into the cuttings by compression of a residual gas initially trapped into the cuttings. The pressure history can then be history matched against a numerical model to obtain the value of permeability.

4.1.1 Model Assumptions

The model used to generate the pressure responses for the cutting is based on the following assumptions:

1) The cuttings are rectangular cuboids with each of the three major lengths parallel with the three axes.
2) The gas follows the perfect gas law.
3) The residual gas after imbibitions is disconnected as ganglia homogeneously distributed into the rock volume.
4) The gas remains immobile because it is already trapped and disconnected.
5) The Darcy Law applies inside the cuttings. It has already been established that even a size of 1mm is large enough to represent an elementary volume (**Larson and Morrow** [6]).
6) The capillary pressure is not taken into account.

4.1.2 Cartesian System

For a rectangular cuboid cutting, application of a material balance leads to the equation,

$$\nabla . \vec{v_o} + \phi \times \frac{\partial S_o}{\partial t} = 0 \qquad 4.01$$

In our system, we are assuming that the cuttings have been imbibed with a viscous liquid, which has trapped a small amount of gas, present as disconnected, immobile medium. Thus,

$$S_o + S_g = 1 \qquad 4.02$$

Or,

$$S_o = 1 - S_g \qquad 4.03$$

Considering the trapped gas obeys perfect gas law, we have,

$$P_{ini} \times V_{ini} = P \times V \qquad 4.04$$

Since,

$$V_{fluid} = S_{fluid} \times V_p \qquad 4.05$$

Equation 4.04 may be written as,

$$P_{ini} \times S_{g_{ini}} \times V_p = P \times S_g \times V_p \qquad 4.06$$

Re-arranging,

$$S_g = S_{g_{ini}} \times \frac{P_{ini}}{P} \qquad 4.07$$

So,

$$S_o = 1 - S_{g_{ini}} \times \frac{P_{ini}}{P} \tag{4.08}$$

Since the fluid entering the pore space enters to compress the trapped gas, thereby increasing its pressure, therefore the fluid saturations can be assumed to be a function of pressure, so applying the chain rule, we can write,

$$\frac{\partial S_o}{\partial t} = \frac{\partial S_o}{\partial P} \times \frac{\partial P}{\partial t} \tag{4.09}$$

And,

$$\frac{\partial S_o}{\partial P} = \frac{\partial}{\partial P}\left(1 - S_{g_{ini}} \times \frac{P_{ini}}{P}\right) \tag{4.10}$$

Solving, we get,

$$\frac{\partial S_o}{\partial P} = S_{g_{ini}} \times \frac{P_{ini}}{P^2} \tag{4.11}$$

So,

$$\frac{\partial S_o}{\partial t} = S_{g_{ini}} \times \frac{P_{ini}}{P^2} \times \frac{\partial P}{\partial t} \tag{4.12}$$

Also, in the absence of capillary forces, Darcy's law gives,

$$\vec{v}_x = -\frac{k_x}{\mu} \times \frac{\partial P}{\partial x} \tag{4.13}$$

So,

$$\vec{v}_o = -\frac{1}{\mu_o} \times \left(k_x \times \frac{\partial P}{\partial x}\hat{i} + k_y \times \frac{\partial P}{\partial y}\hat{j} + k_z \times \frac{\partial P}{\partial z}\hat{k}\right) \tag{4.14}$$

Substituting back into Equation 4.01, we get,

$$-\frac{1}{\mu_o}\times\left[\nabla.\left(k_x\times\frac{\partial P}{\partial x}\hat{i}+k_y\times\frac{\partial P}{\partial y}\hat{j}+k_z\times\frac{\partial P}{\partial z}\hat{k}\right)\right]+\phi\times S_{g_{ini}}\times\frac{P_{ini}}{P^2}\times\frac{\partial P}{\partial t}=0 \quad 4.15$$

Re-arranging,

$$\nabla.\left(k_x\times\frac{\partial P}{\partial x}\hat{i}+k_y\times\frac{\partial P}{\partial y}\hat{j}+k_z\times\frac{\partial P}{\partial z}\hat{k}\right)=\phi\times\mu_o\times S_{g_{ini}}\times\frac{P_{ini}}{P^2}\times\frac{\partial P}{\partial t} \quad 4.16$$

Assuming the permeability in each direction is homogeneous throughout the cutting, we get,

$$k_x\times\frac{\partial^2 P}{\partial x^2}+k_y\times\frac{\partial^2 P}{\partial y^2}+k_z\times\frac{\partial^2 P}{\partial z^2}=\phi\times\mu_o\times S_{g_{ini}}\times\frac{P_{ini}}{P^2}\times\frac{\partial P}{\partial t} \quad 4.17$$

4.1.3 Spherical System

For a spherical cutting, **Egermann et al** [2] made use of the application of a material balance to derive the diffusivity equation given by,

$$\frac{\partial}{\partial r}\left(r^2\times\frac{\partial P}{\partial r}\right)=\alpha\times\frac{r^2}{P^2}\times\frac{\partial P}{\partial t} \quad 4.18$$

Where,

$$\alpha=\frac{\mu_o\times\phi\times S_{g_{ini}}\times P_{ini}}{k} \quad 4.19$$

This equation will be used for curve fitting the responses generated from the Cartesian model.

4.2 Finite Difference Solution

The model was solved implicitly to mitigate any possible problems of instability. A detailed derivation of the finite difference solution used is presented for the Cartesian system in Appendix A, while that for the spherical model is presented in Appendix B.

4.3 Model Testing and Validation

The diffusivity equation describing the cutting, immersed in glycerin, in Cartesian co-ordinates was solved using an implicit finite difference scheme. The system was then programmed using Matlab, the resulting system of equations solved simultaneously using a binary conjugate gradient method.

After the programming was completed, the code needed to be tested both for anisotropic and geometric consistency using various techniques, as well as accuracy before conducting the simulation runs to validate the claims and verify the objectives set forth for the intended research.

The properties which have been kept constant throughout all the various testing and validation runs have been described in Table 4.1.

Table 4.1: Constant Properties in Model Testing

φ	0.2
S_{gi}	0.2
μ_o	1000 cp
P_i	1 atm.
P_{cell}	10 atm.

4.3.1 Grid Sensitivity

With all finite difference schemes, the accuracy of the result depends upon the time and space differential elements. The number of grid elements used, however can affect the net required simulation time, which beyond a certain number of nodes increases tenfold without having a significant impact on the resultant accuracy.

A sensitivity study was carried out to ascertain a minimum number of grid nodes which would produce a certain degree of accuracy repeatedly for cutting sizes as might be encountered in the field.

Rock and fluid properties and initial and final pressure conditions are as have been described in Table 4.1. The base system is defined by a uniform isotropic permeability of 10 mD for the cutting. Simulation runs were made for cubic cuttings of 2 mm, 5 mm and 10 mm lengths. Though a cutting size of 10 mm is an impractical assumption, the purpose here was just to ascertain the gridding scheme for the subsequent simulation runs. Each cutting size was tested for 3, 6, 9, 12 and 15 nodes in each direction. The results were plotted together as well as a separate analysis or curve fitting based on the spherical model was carried out for each case to realize the impact the gridding will have on the obtainable results.

A first run was made for a 2 mm cubic cutting. The ensuing plots can be seen in Figure 4.1.

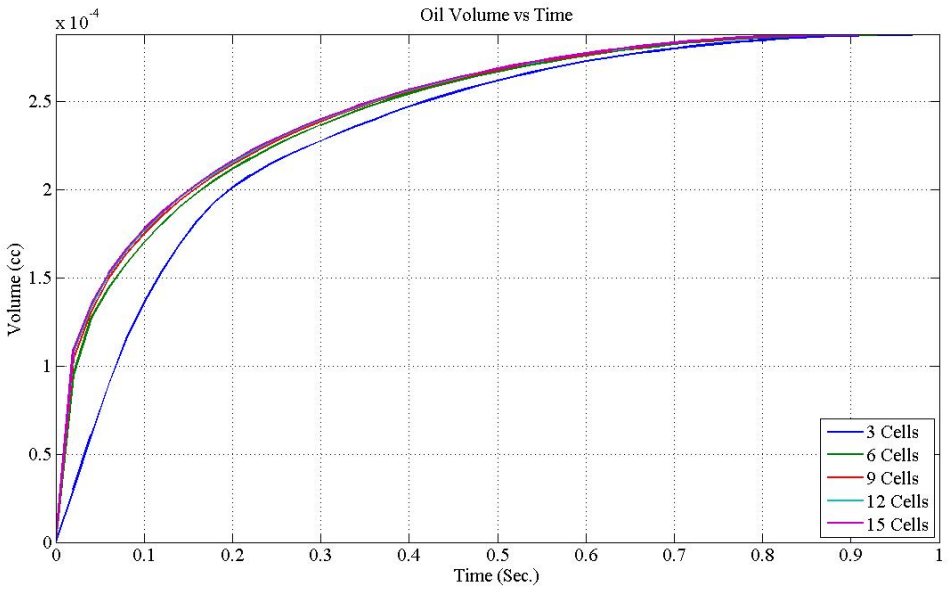

Figure 4.1: Grid Sensitivity 2 mm

As can be seen from the plot, apart from the model using three nodes in each direction, the remaining curves appear to be in very close agreement. The individual curves were then interpreted using a spherical model to assess the permeability interpreted for each curve. Figures ranging from Figure 4.2 to Figure 4.6 show the curve fitted plots.

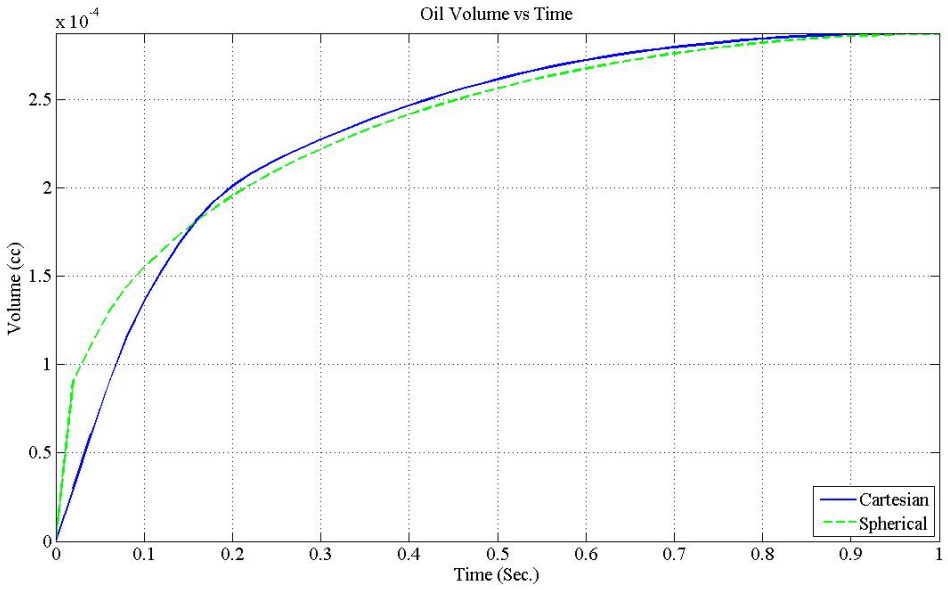

Figure 4.2: 2 mm, 3 nodes (Interpreted k=10.29 mD)

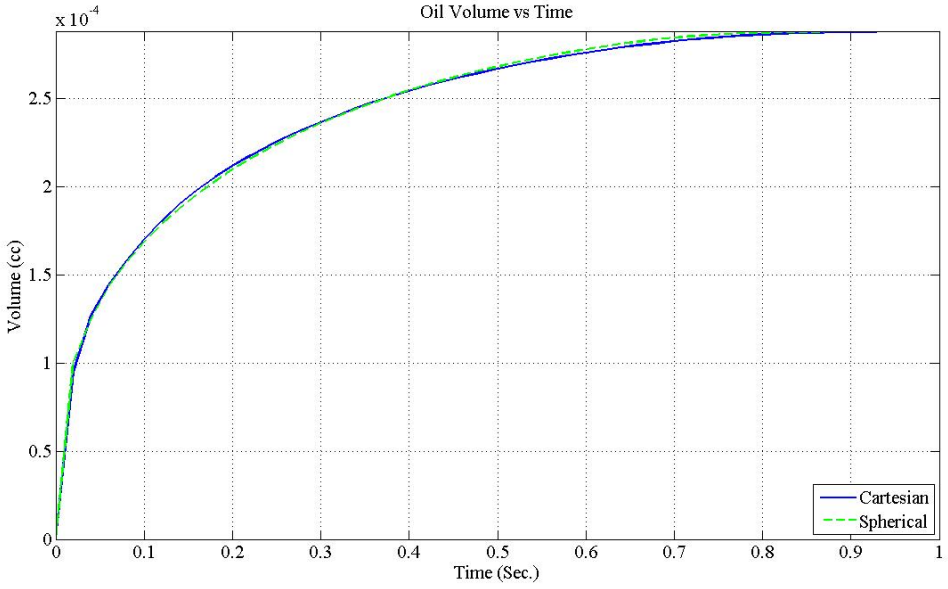

Figure 4.3: 2 mm, 6 nodes (Interpreted k=11.94 mD)

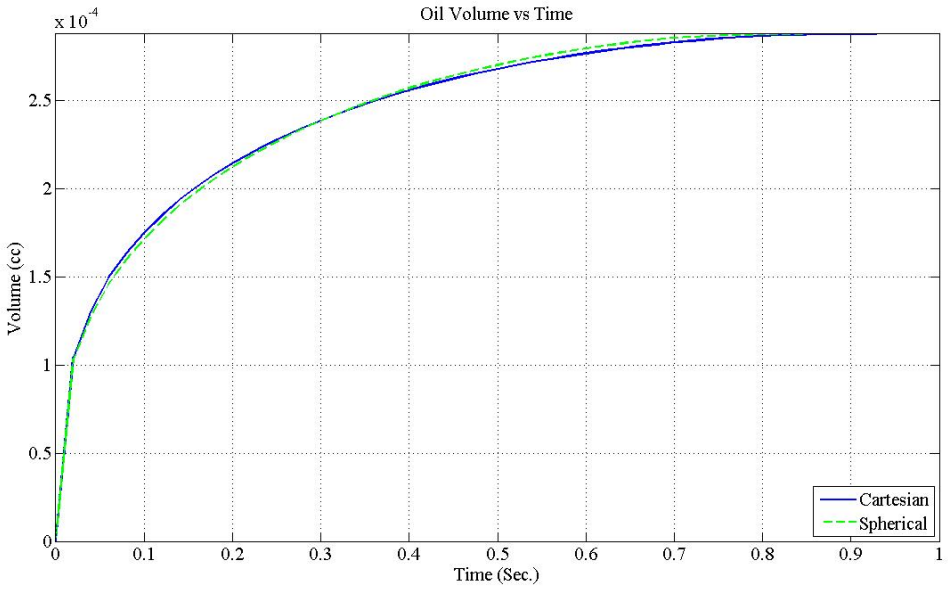

Figure 4.4: 2 mm, 9 nodes (Interpreted k=12.27 mD)

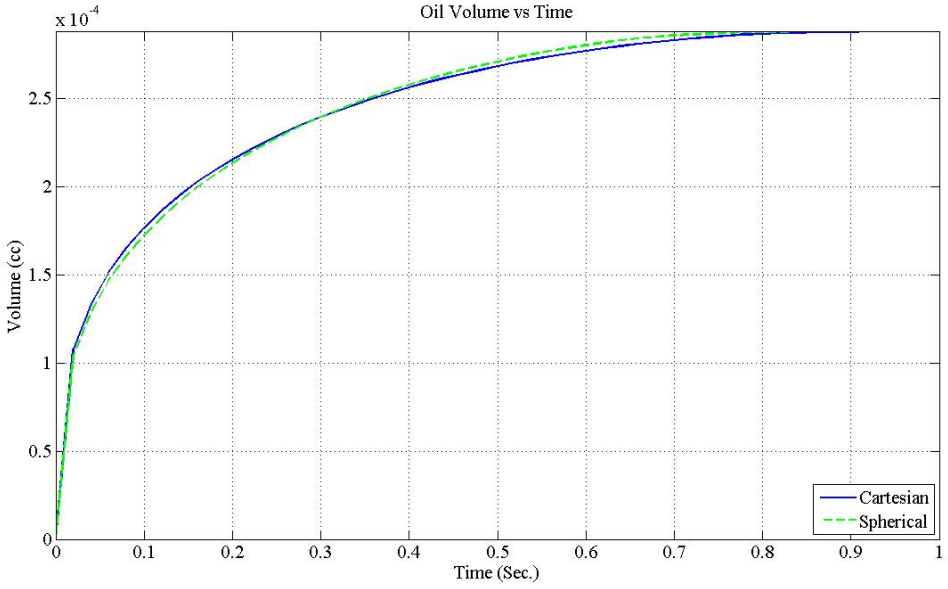

Figure 4.5: 2 mm, 12 nodes (Interpreted k=12.42 mD)

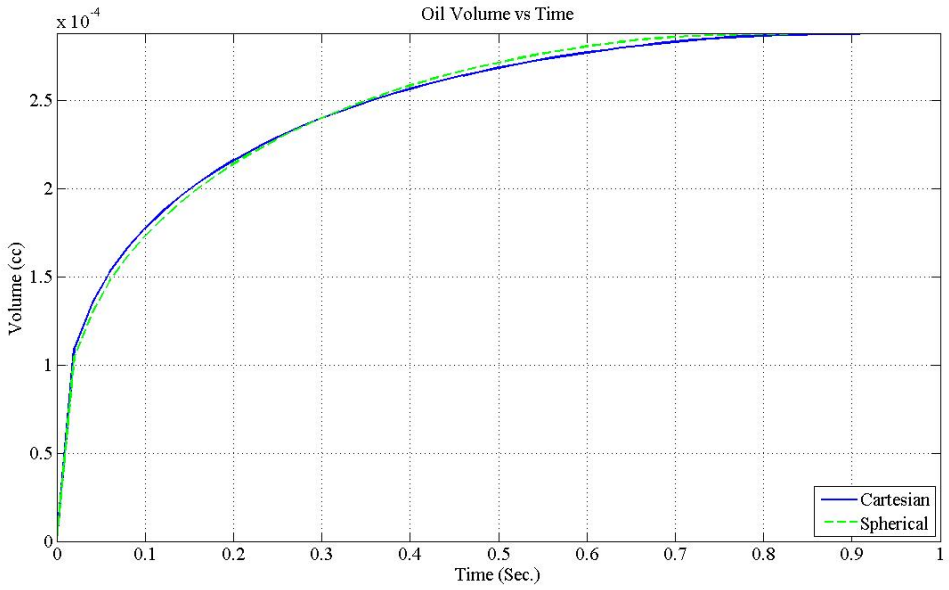

Figure 4.6: 2 mm, 15 nodes (Interpreted k=12.51 mD)

The permeability for the sample, estimated using the spherical model, reveals the 3 node system to give a more accurate reading when compared to the input value. That aspect, however, will be discussed in the ensuing chapter. For now, the task at hand is to establish the optimal number of grid nodes which would render a significant degree of accuracy without cramming the system resources. The computational time can range from a couple of minutes for the three node system to several hours for the grid system comprising of 15 nodes in each direction. As is evident from the results, the permeability values estimated using the spherical model do not show a significant variation over a range of nodes extending from 9 up to 15, a range in which the permeability displayed by the system changes by only a maximum of 1.96%.

In an attempt to generalize our findings over a significant cutting size range, the proceeding figures from Figure 4.7 to Figure 4.18 display plots obtained from simulation

runs for the 5 mm and 10 mm cuttings. Note that for comparative purposes, all other system properties apart from cutting size are identical to those used for the 2 mm cutting.

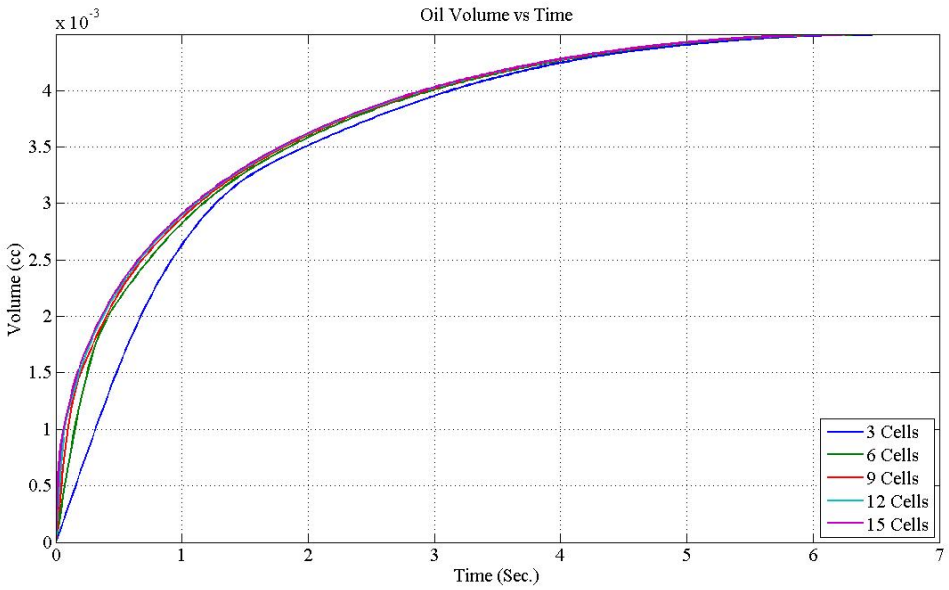

Figure 4.7: Grid Sensitivity 5 mm

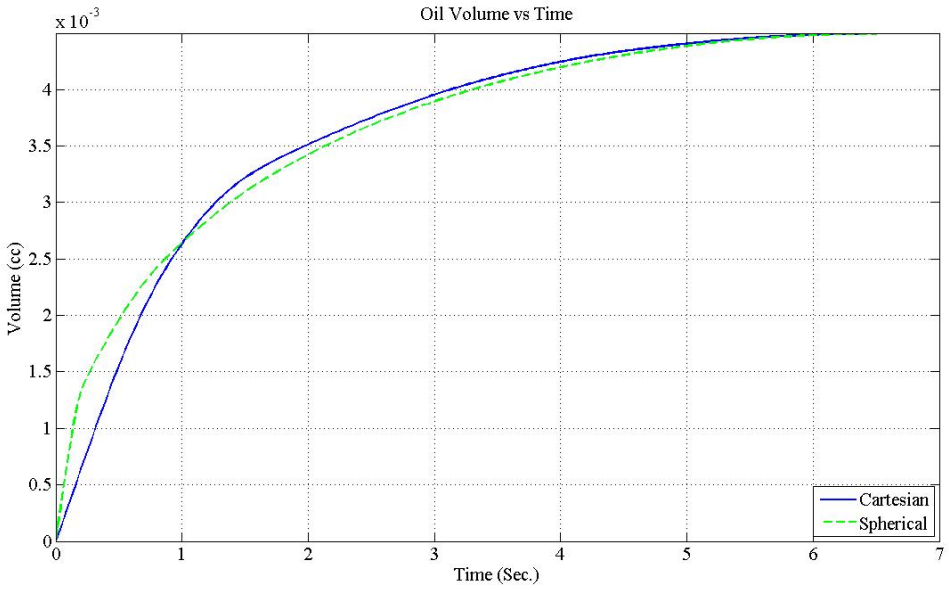

Figure 4.8: 5 mm, 3 nodes (Interpreted k=11.07 mD)

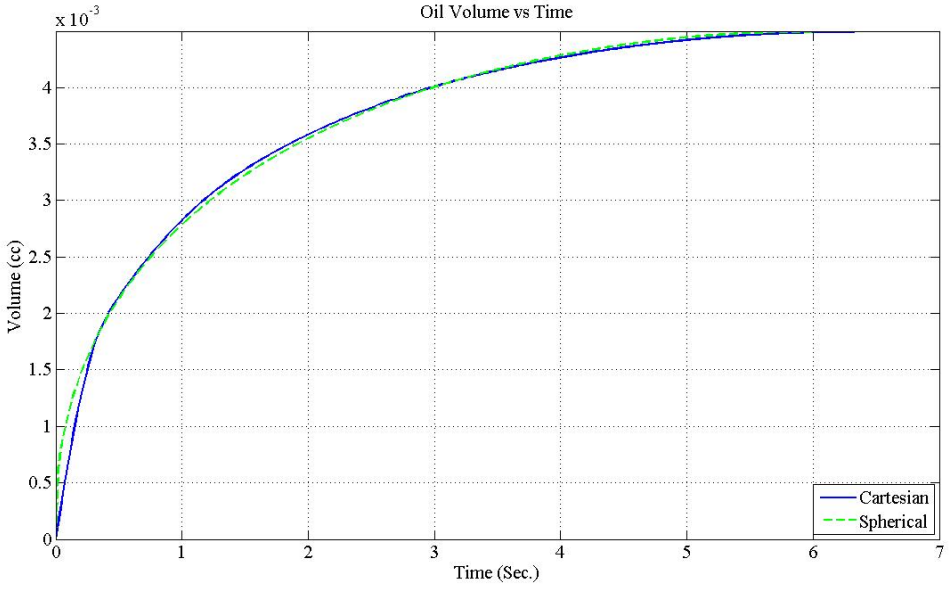

Figure 4.9: 5 mm, 6 nodes (Interpreted k=12.02 mD)

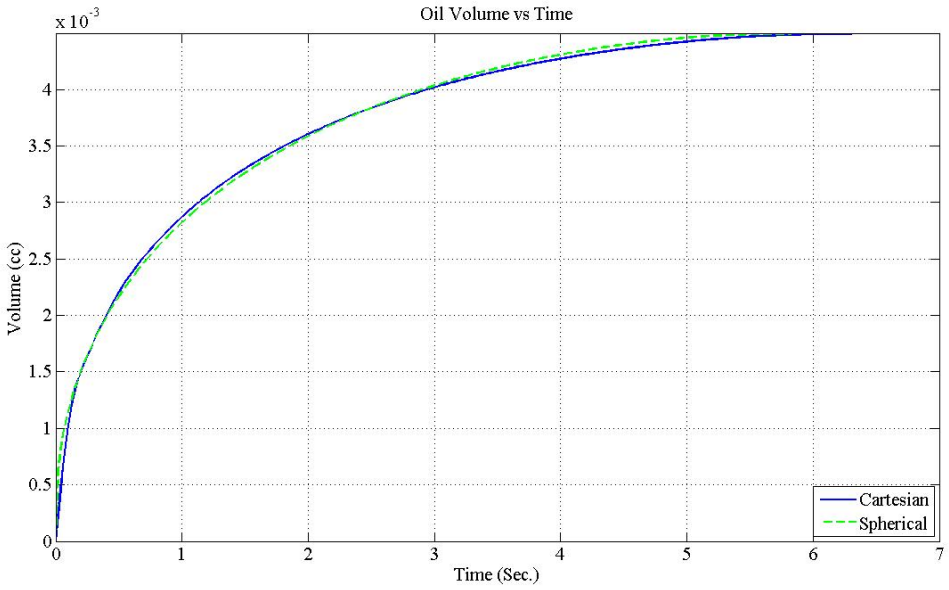

Figure 4.10: 5 mm, 9 nodes (Interpreted k=12.34 mD)

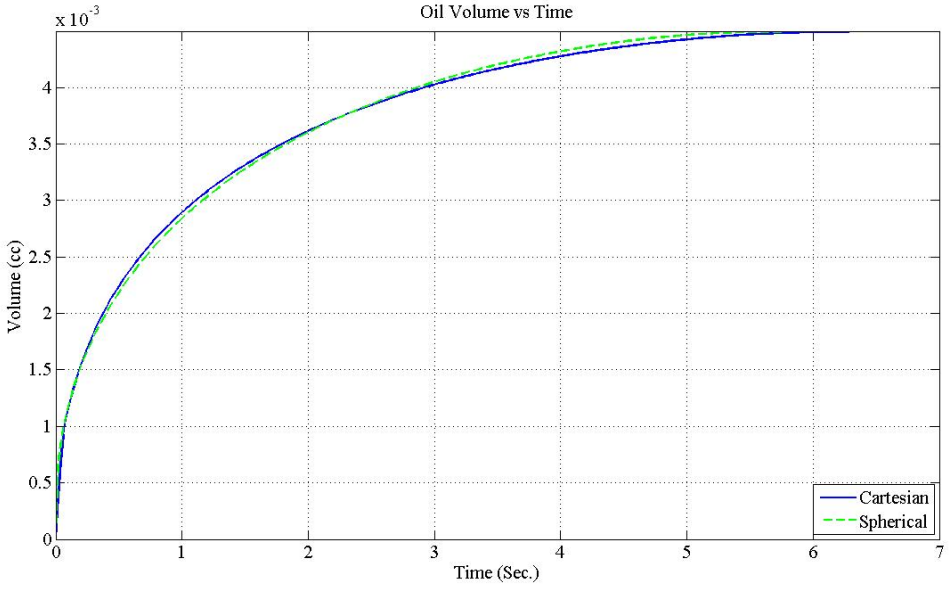

Figure 4.11: 5 mm, 12 nodes (Interpreted k=12.49 mD)

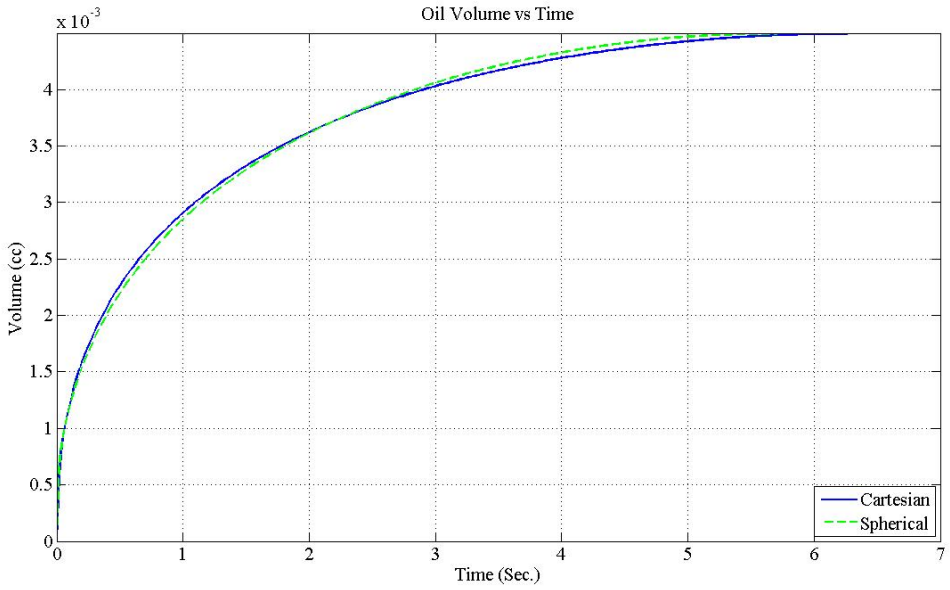

Figure 4.12: 5 mm, 15 nodes (Interpreted k=12.6 mD)

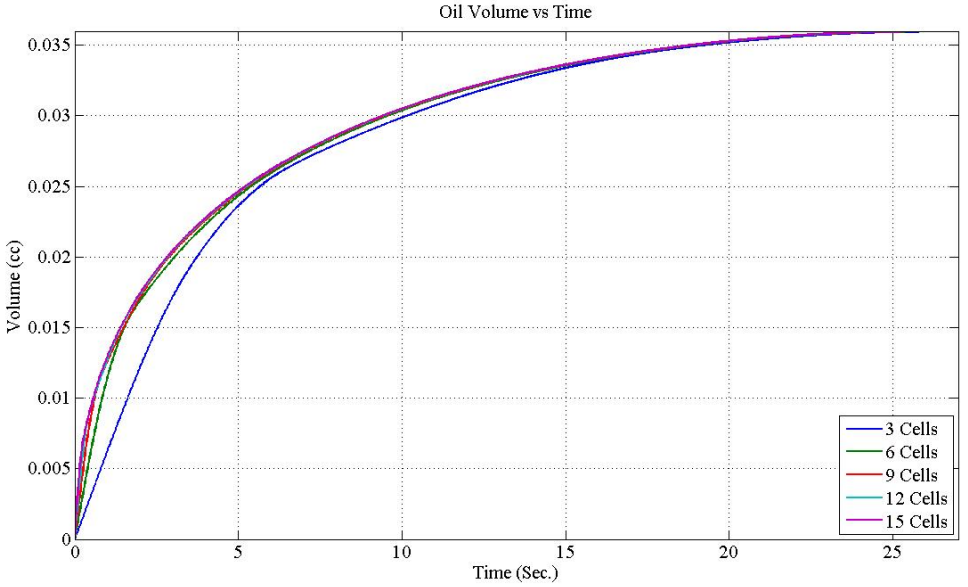

Figure 4.13: Grid Sensitivity 10 mm

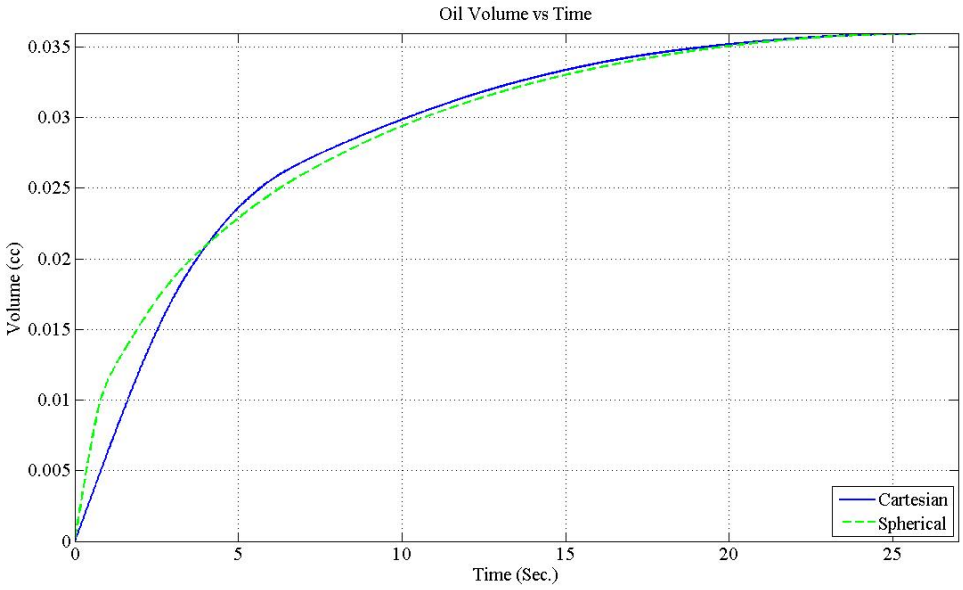

Figure 4.14: 10 mm, 3 nodes (Interpreted k=11.22 mD)

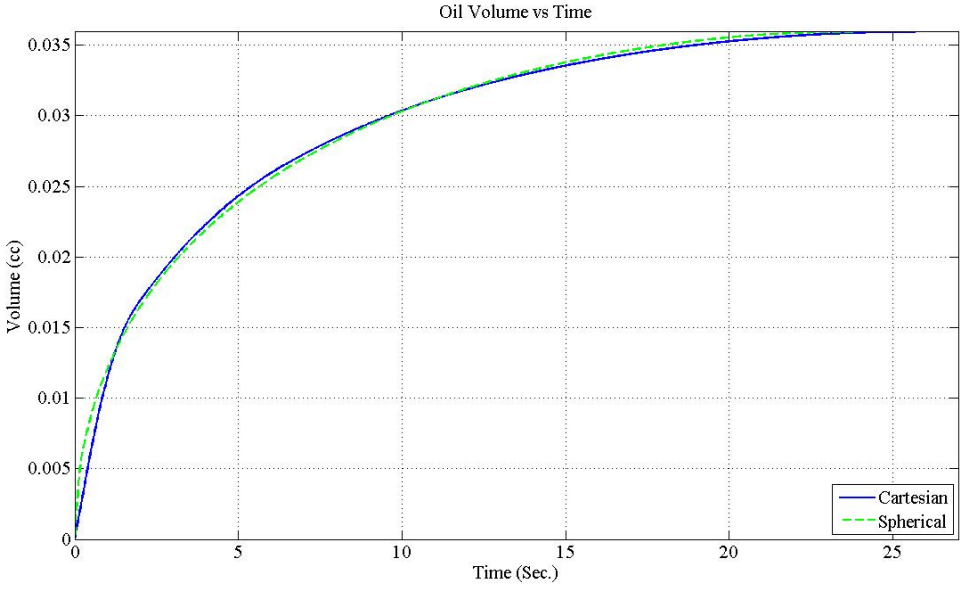

Figure 4.15: 10 mm, 6 nodes (Interpreted k=12.26 mD)

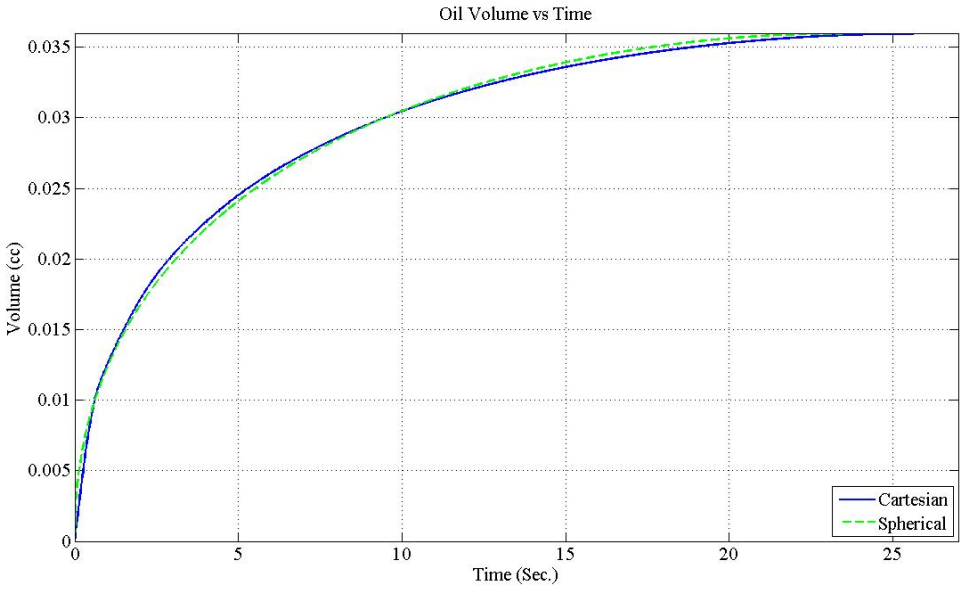

Figure 4.16: 10 mm, 9 nodes (Interpreted k=12.48 mD)

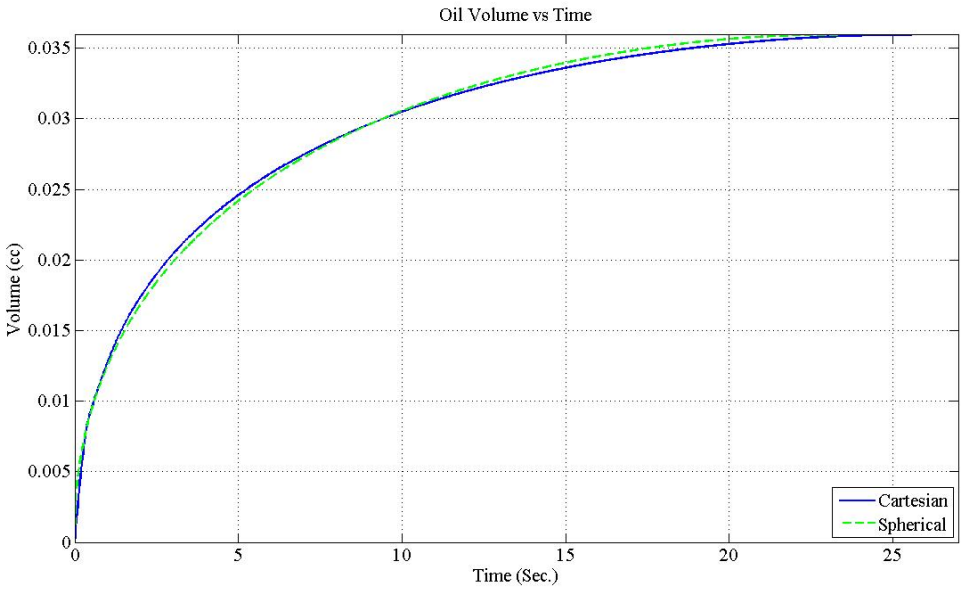

Figure 4.17: 10 mm, 12 nodes (Interpreted k=12.54 mD)

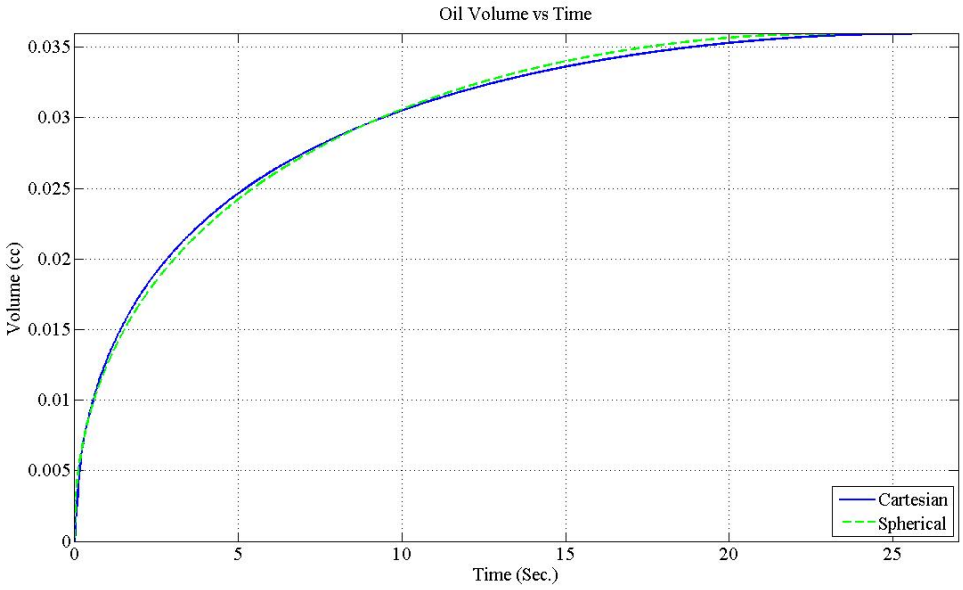

Figure 4.18: 10 mm, 15 nodes (Interpreted k=12.6 mD)

A close observation and analysis of the results reveals that the results for the same number of nodes for the three cutting sizes are in quite close agreement. The three node system displays the highest degree of variation but the comparative difference diminishes as the number of nodes is increased. The results indicated that the 9 percent error resulting from the three node system falls to less than 3 percent for any number of nodes amounting to 6 or greater. It is thus safe to assume that using any number of nodes between 9 and 12 can produce the degree of accuracy to conduct the study effectively.

4.3.2 Debugging and Directional Consistency

With the code finalized, it was imperative to check if the program was generating repeatable results. If the equations have been solved and programmed correctly, flow

caused along any one direction while considering the other two directions impermeable would generate similar responses for similar boundary and system characteristics.

A uniform cutting of cubic proportions having lengths of each side of 2 mm was modeled in the program, dividing it into 9 nodes in each direction. The permeability of the arbitrary length permeable to flow was kept constant at 10 mD while that for each of the other two directions was set to zero. Other matrix and fluid properties and the initial and final pressure conditions were kept consistent with those presented in Table 4.1.

Three simulation runs were required to get the pressure responses while allowing flow along any one direction at each instant. The accuracy was checked to the 6^{th} place of decimal. A plot of the results given by Figure 4.19 displays the absolute agreement in the results.

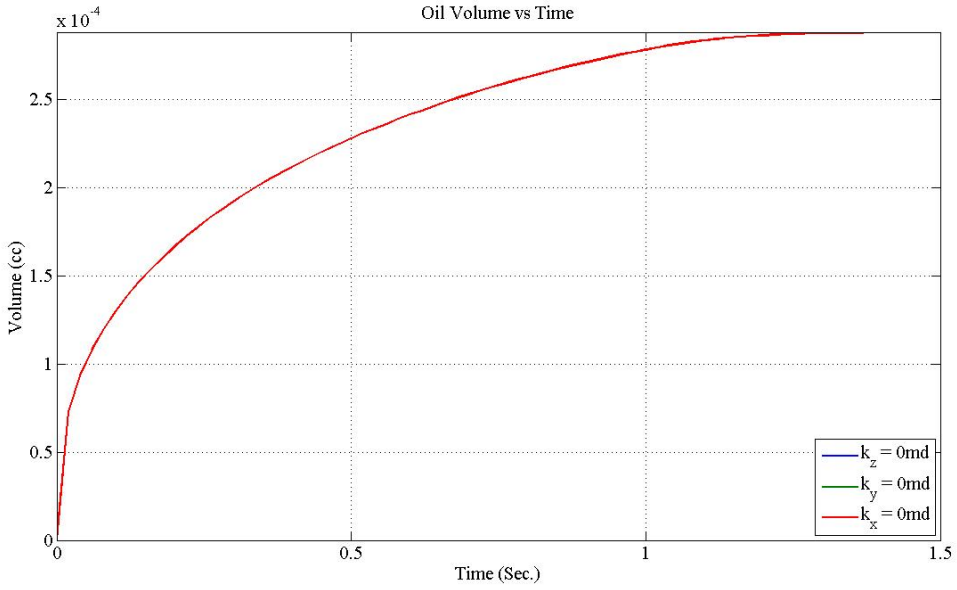

Figure 4.19: Directional Permeability Check

To further ascertain the repeatability of the simulation model, a similar test was conducted for an asymmetric cutting keeping the directional permeability constant. For the same conditions as described in Table 4.1, this time, the permeability along each of the axes was kept constant at 10 mD, the lengths along any two directions were set to 2 mm while that of the third was increased to 4 mm for each of the three directions one at a time. The simulation results displayed an excellent agreement as can be seen in Figure 4.20.

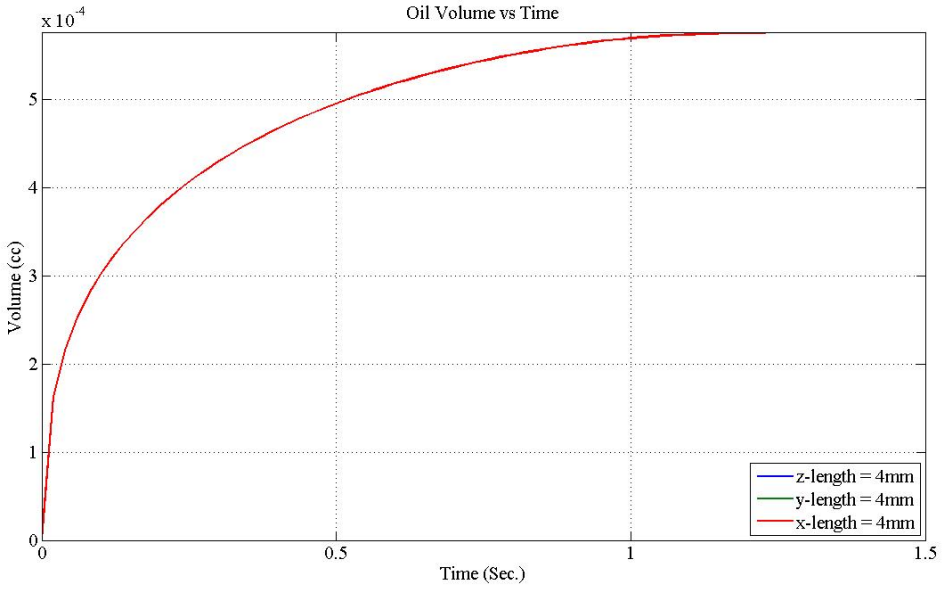

Figure 4.20: Asymmetry Check

4.3.3 Code Validation

Before progressing with the task at hand, it was essential to validate the model against actual test conditions. Two possibilities remained at hand.

A first test carried out to validate the finite difference code was to compare the results produced from the Cartesian model against an existing and tested spherical model. The research revolves around the basic idea that a cubic or rectangular cuboid cutting cannot be accurately modeled using a spherical model. Based on the basic laws of physics, however, the results can be used to ascertain the expected trend. A sphere always displays the minimum surface area to volume ratio. For two cuttings having the same total volume, but with one being spherical and the other cubic, with all the other factors being the same for the two cases, it can be expected that the higher surface area presented by any a-spherical cutting would help facilitate a higher fluid flow rates. Though the net volume entered into the two cuttings would eventually become equal since both the cuttings have the same total volume and same porosity and trapped gas saturation, the non-spherical cutting will achieve this state quicker than the spherical cutting. Figure 4.21 displays the results plotted for a uniform cutting of cubic proportions having lengths of each side of 2 mm, divided into 9 nodes in each direction. The cutting is modeled to be homogeneous and isotropic with a constant permeability of 10 mD. Other properties and conditions are kept the same as those defined in Table 4.1. A second curve plotted alongside the pressure response for the cubic cutting represents the pressure response when the same volume of cutting is assumed to be spherical.

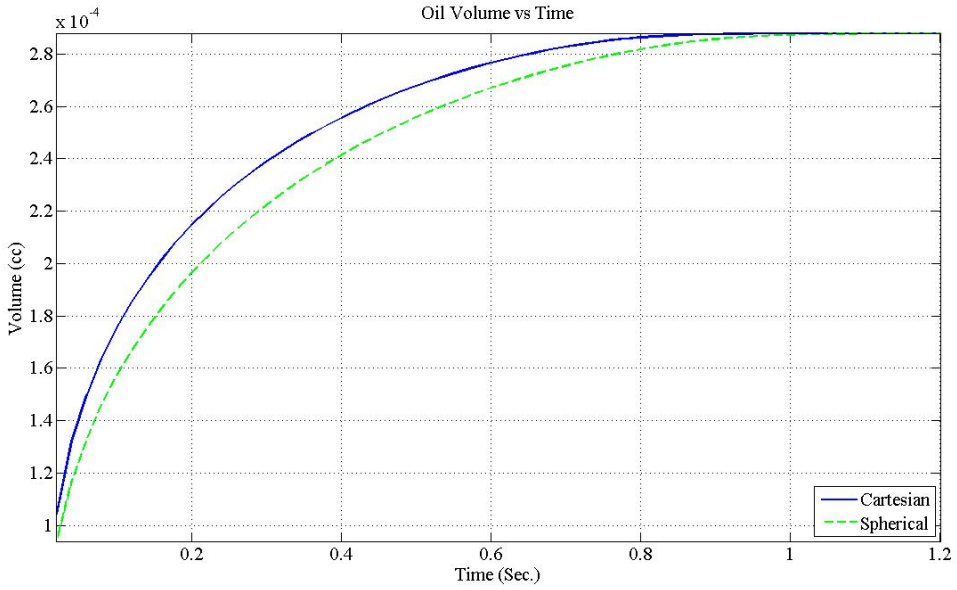

Figure 4.21: Cartesian vs. Spherical (Validation Run)

As is evident from the plot, the model is behaving in the manner as expected, thus establishing a reasonable degree of reliability for the code.

A second way to validate the ability of the code to replicate the actual experimental conditions was to actually test the simulation results against the actual experimental data. Although these results will be discussed in subsequent chapters, it is note worthy to mention here that the simulation results were in good agreement with the experimental data.

4.3.4 Summary of Model Testing and Validation

From the above testing into the applicability of the model to simulate actual testing conditions, the following observations are noted:

1) Nodes numbering nine and greater along each of the three axes will generate reasonably accurate and consistent results.
2) The simulation code is accurate in capturing flow along each of the three axes.
3) The validation results are consistent with the physics of the process and produces results in close agreement with those obtained from experimental procedures.

CHAPTER 5

RESULTS AND DISCUSSIONS

Simulation runs were made using the numerical simulator for the specific objective of ascertaining the influence cutting geometry and anisotropy might have on the obtainable pressure diffusion (pulse decay) responses. As an added benefit, experimental results obtained from the Darcy Log equipment further helped authenticate the conclusions drawn from the results of the sensitivity study carried out using the numerical simulator. In this chapter, we shall be presenting the experimental and numerical results emphasizing:

1) The influence of cutting geometry on permeability measurements
2) The influence of cutting anisotropy on permeability measurements
3) An assessment of the accuracy of numerical model in contrast to the experimental results

5.1 Geometry Effects

Cuttings of cubic geometry in three volume sizes representing equivalent spherical diameters of 2.5 mm, 3.5 mm and 5 mm, a range more representative of the cuttings encountered in the field, were selected to study the impact of cutting geometry on the resultant pressure responses. Interpreting the results thus obtained from the non-

spherical cuttings using a spherical model goes to highlight the degree of deviation and error one can expect from adopting the pulse decay or pressure diffusion technique for measuring permeability from drill-cuttings.

With y length and z length kept equal to each other in all cases, keeping the volume constant, the simulation runs were made for three different aspect ratios (A.R.) with the x length as defined in Table 5.1.

Table 5.1: Defined Aspect Ratios

Definition	Ratio	Defined A.R.
x length : (y length = z length)	1 : 1	1
x length : (y length = z length)	2 : 1	2
x length : (y length = z length)	3 : 1	3

The following properties have been assumed and kept constant for all of the subsequent simulation runs.

Table 5.2: Defined Properties

φ	0.2
S_{gi}	0.2
P_i	1 atm.
P_{cell}	10 atm.

The value of porosity and gas saturation are a rough average of the values obtained from the multiple experimental runs conducted in the laboratory using the Darcy-Log apparatus. The value of viscosity was adjusted for each case to control the pressure stabilizing times, for the medium to high permeability cases subject to our study, to a

realistic range which is easily interpretable and closely emulating the physical Darcy-Log system.

The cuttings were modeled with 10 grid cells along each of the three axes, a number sufficient to help accurately capture the influx without exceeding the system resources available.

Each cutting size is further tested in three ranges of permeability starting with a minimum value of 1 mD, 20 mD and goes on to a maximum of 50 mD. Note that this range was proven to be sufficient to highlight the influence of cutting shape in conjunction with the prescribed permeability values.

The responses obtained for the various shapes for a single permeability, volume and identical initial and boundary conditions have been plotted together to enumerate the significant change in the response for a specific volume of cutting simply because of a variation in shape. Plots of the individual curves, curve fitted with the spherical model, can be seen to highlight the extent of error resulting from introducing the shape factor.

All the cutting sizes shall hence forth be defined in terms of equivalent diameter (E.D.) which represents the cutting of a specific volume in terms of a diameter equivalent to that of a spherical cutting having the same volume.

5.1.1 Geometry case 1 (k = 1 mD)

A first set of simulation runs were made for a permeability of 1 mD. Results for the various cutting size variations are presented hereunder.

5.1.1.1 Equivalent diameter = 2.5 mm

Figure 5.1 shows the plots for a cutting with a volume equivalent to a spherical cutting of 2.5 mm diameter, having a uniform isotropic permeability of 1 mD. To keep the response time short, the viscosity of the oil was kept at 200 cp. The three individual curves in Figure 5.1 show the responses for the three variations of shape for the same volume.

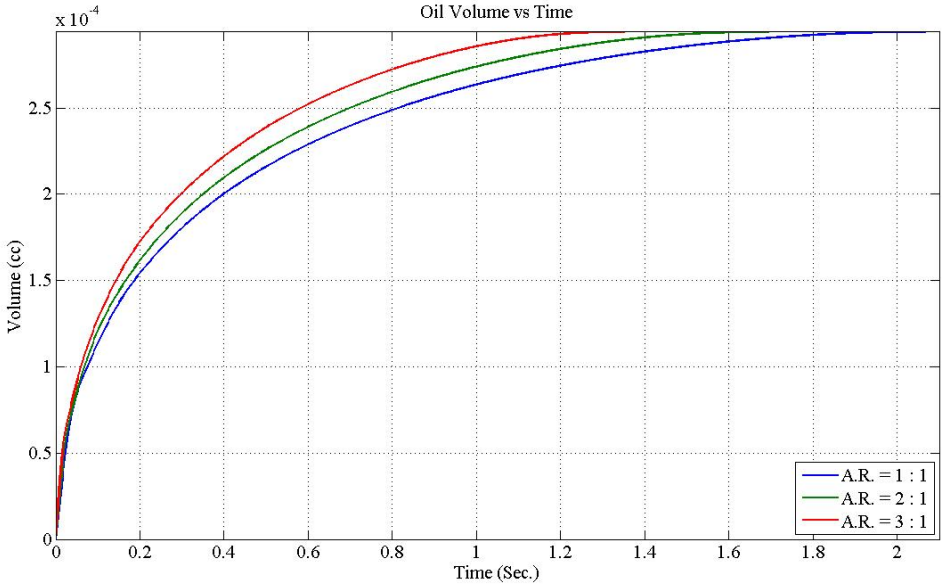

Figure 5.1: k=1 mD, E.D.=2.5 mm

As is evident from the plot, any variation of shape from the cubic has an effect of increasing the rate of influx of the viscous oil (glycerin in our case) into the cutting. The consequent response curves thus display a shorter equilibrium or settling time. Figures ranging from Figure 5.2 to Figure 5.4 show the individual curves fitted with the spherical model to emphasize the significance of the cutting shape on the attainable results.

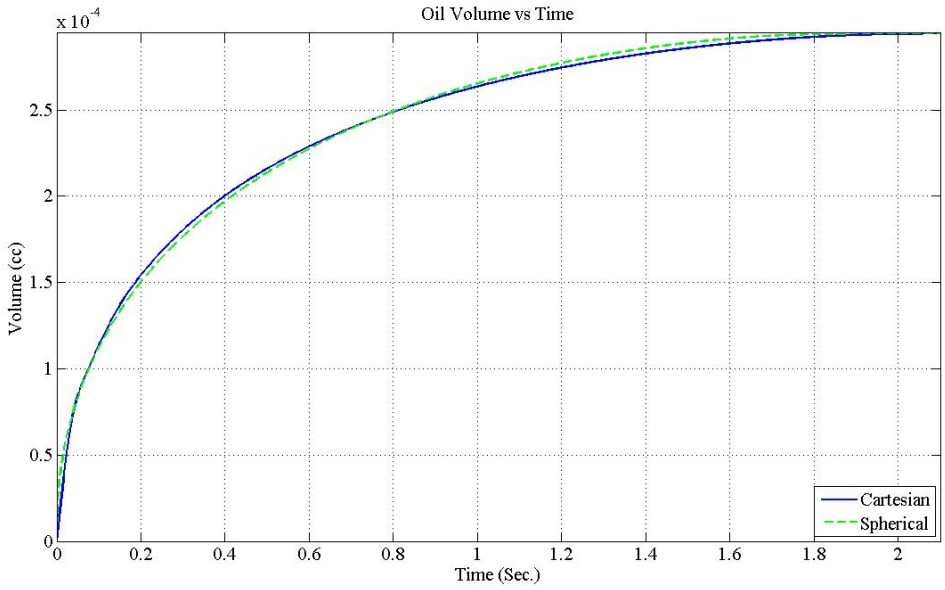

Figure 5.2: k=1 mD, E.D.=2.5 mm, A.R.=1 (Interpreted k=1.26 mD)

Curve fitting with the spherical model reveals that such an interpretation of this cutting would give the measured value of permeability to be around 1.26 mD, displaying an error of about 26% from the actual, when in physical terms we would have considered the results to be fairly accurate, being off by a mere 0.26 mD.

Figure 5.3 displays the curve fitted response for the first non-cubic formulation of the cutting. Interpretation of the impulse response curve using the spherical model reveals an interpreted value of permeability of approximately 1.45 mD, an exaggeration on the original value by almost 45%, an increase upon its predecessor by approximately 15.4%.

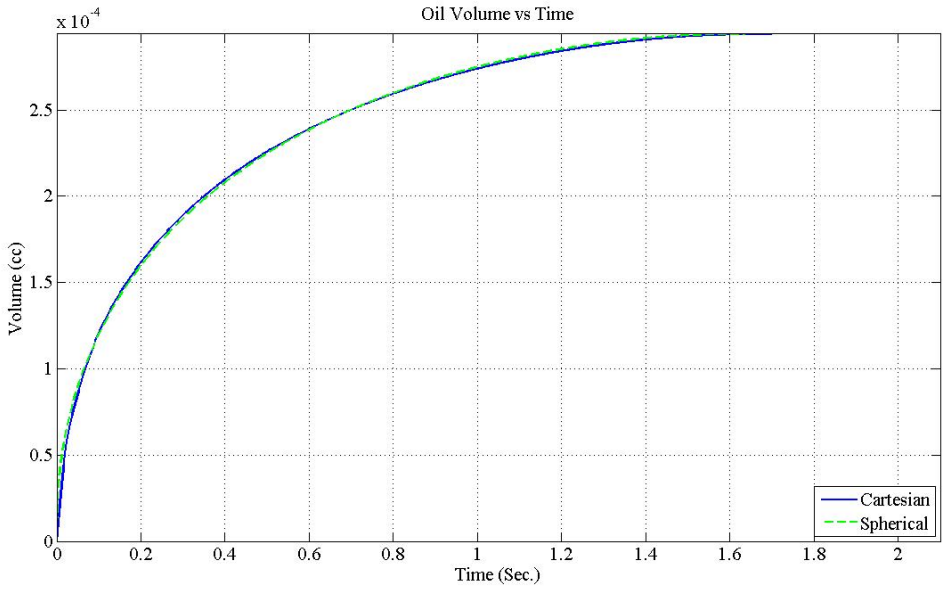

Figure 5.3: k=1 mD, E.D.=2.5 mm, A.R.=2 (Interpreted k=1.45 mD)

Altering the lengths further, the repercussions become more severe as the response time is further condensed. As the aspect ratio is changed to 3:1, the resultant curve fit can be seen in the Figure 5.4.

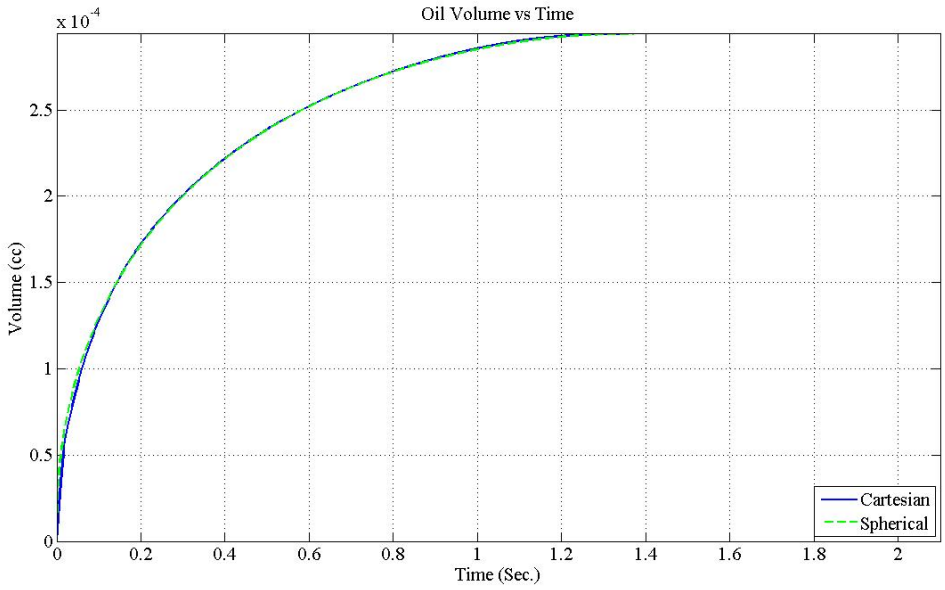

Figure 5.4: k=1 mD, E.D.=2.5 mm, A.R.=3 (Interpreted k=1.73 mD)

An interpreted value of permeability of 1.73 mD for this case comes to be off the actual value by 73%.

5.1.1.2 Equivalent diameter = 3.5 mm

For the same initial and boundary conditions defined in Table 5.1, results obtained from the simulator for the three defined aspect ratios, this time using an oil of viscosity 100 cp, are plotted in Figure 5.5.

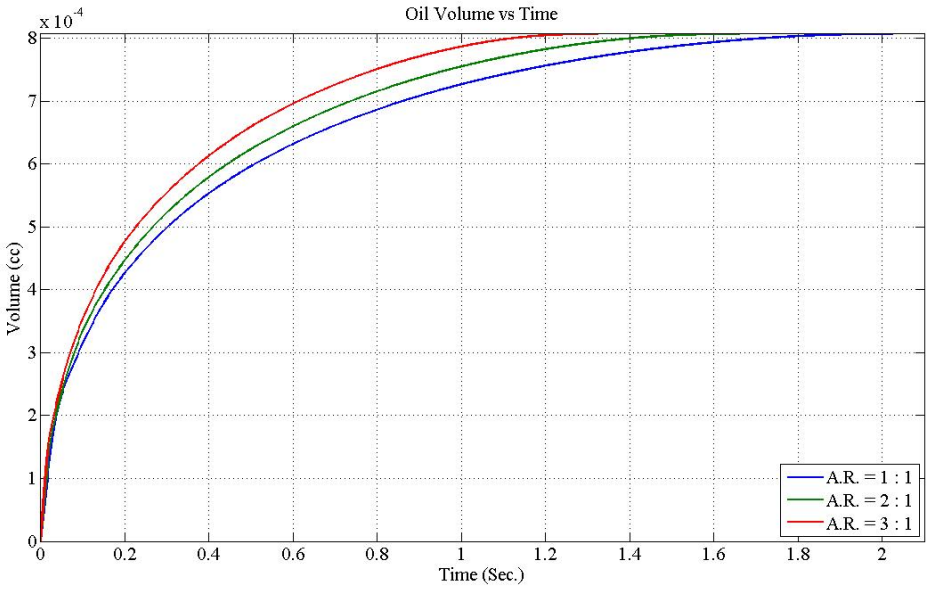

Figure 5.5: k=1 mD, E.D.=3.5 mm

Each of the three responses was then curve fitted with the spherical model. Plots for the curve fitting can be seen in figures ranging from Figure 5.6 to Figure 5.8

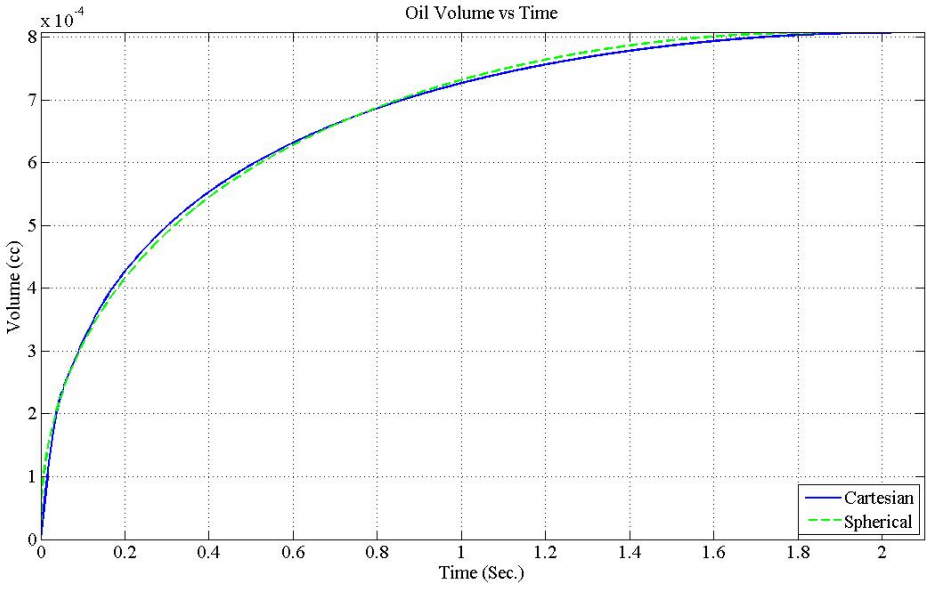

Figure 5.6: k=1 mD, E.D.=3.5 mm, A.R.=1 (Interpreted k=1.26 mD)

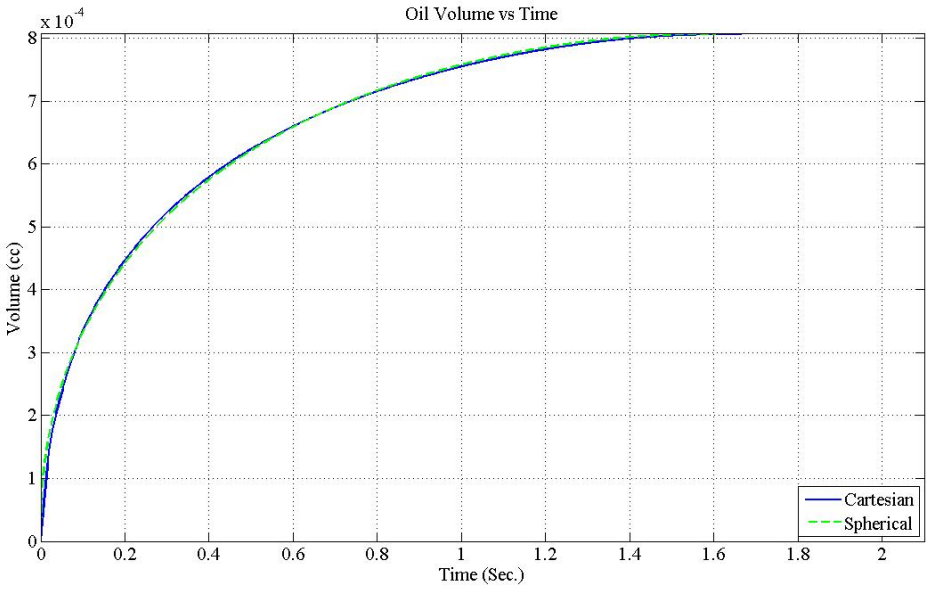

Figure 5.7: k=1 mD, E.D.=3.5 mm, A.R.=2 (Interpreted k=1.45 mD)

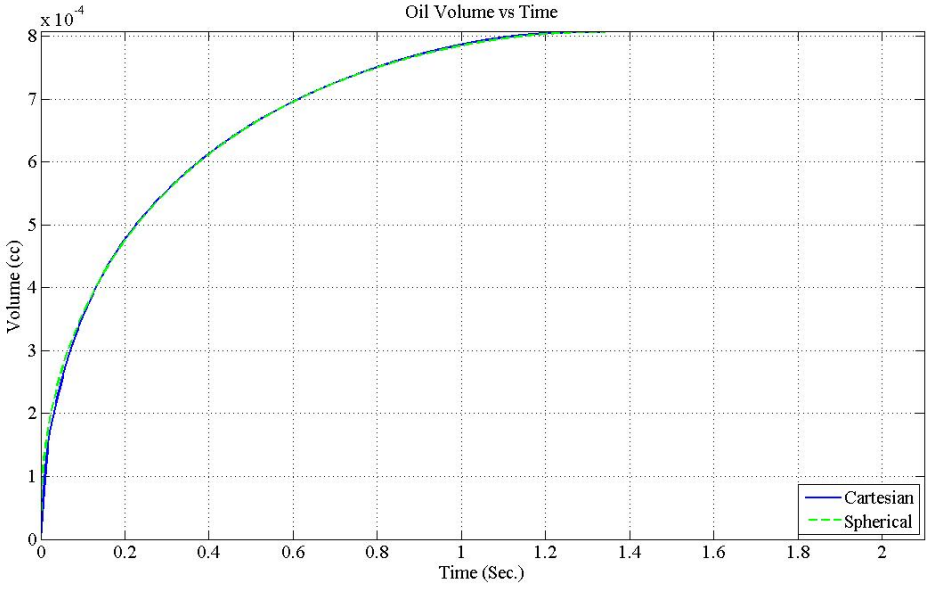

Figure 5.8: k=1 mD, E.D.=2.5 mm, A.R.=3 (Interpreted k=1.73 mD)

Curve fitting reveals a permeability of 1.26 mD, 1.45 mD and 1.73 mD respectively for the three responses. Note that even though the volume of the cutting has increased, the results obtained from the spherical model interpretation are in absolute agreement with the 2.5 mm equivalent diameter cutting.

5.1.1.3 Equivalent diameter = 5 mm

The results for a cutting with equivalent spherical diameter of 5mm are displayed in Figure 5.9. The simulated results represent the two non-cubic aspect ratios along with the standard cubic representation. The viscosity of the oil used is again kept constant at a value of 100 cp.

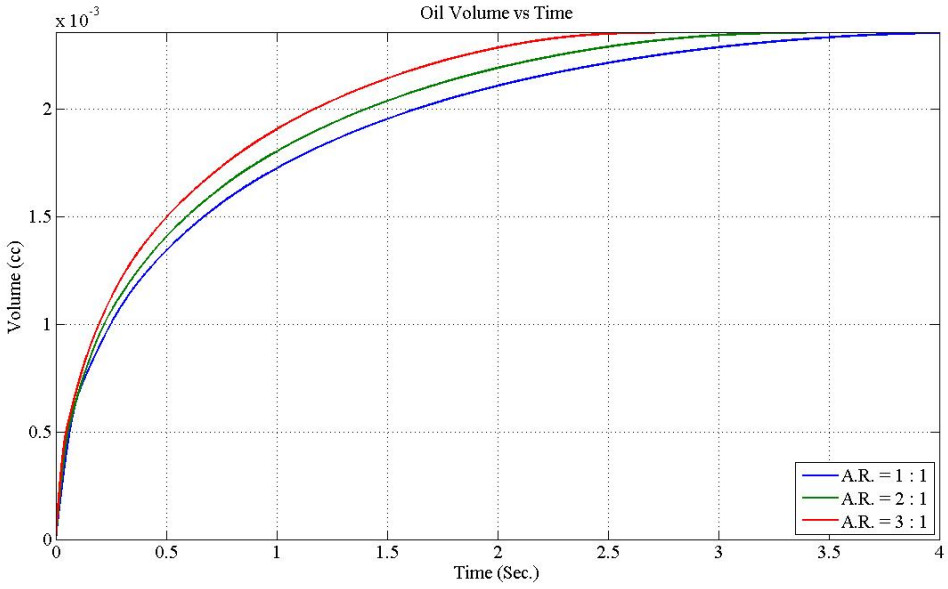

Figure 5.9: k=1 mD, E.D.=5 mm

Each of the three responses was then curve fitted with the spherical model. Plots for the curve fitting can be seen in figures numbering from Figure 5.10 to Figure 5.12.

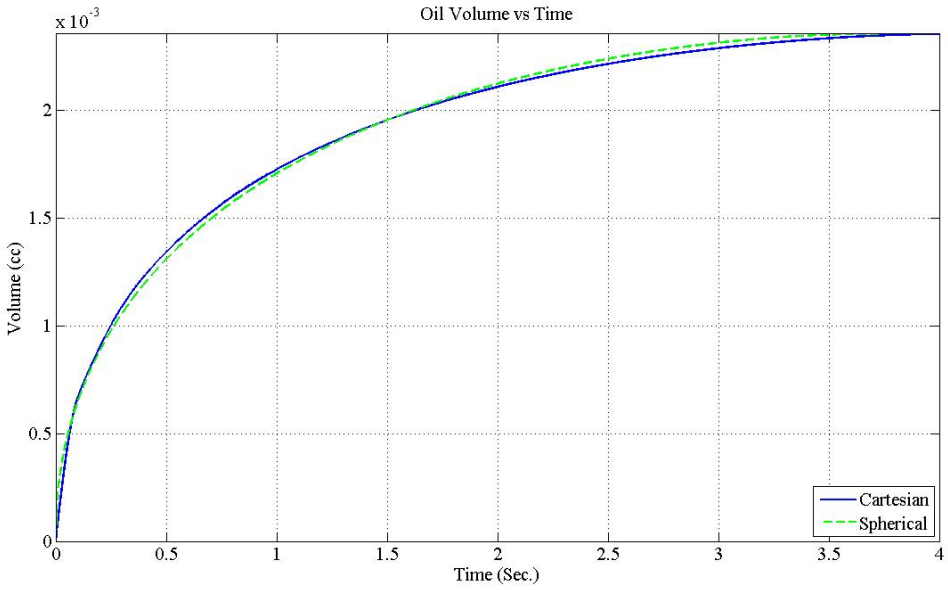

Figure 5.10: k=1 mD, E.D.=5 mm, A.R.=1 (Interpreted k=1.26 mD)

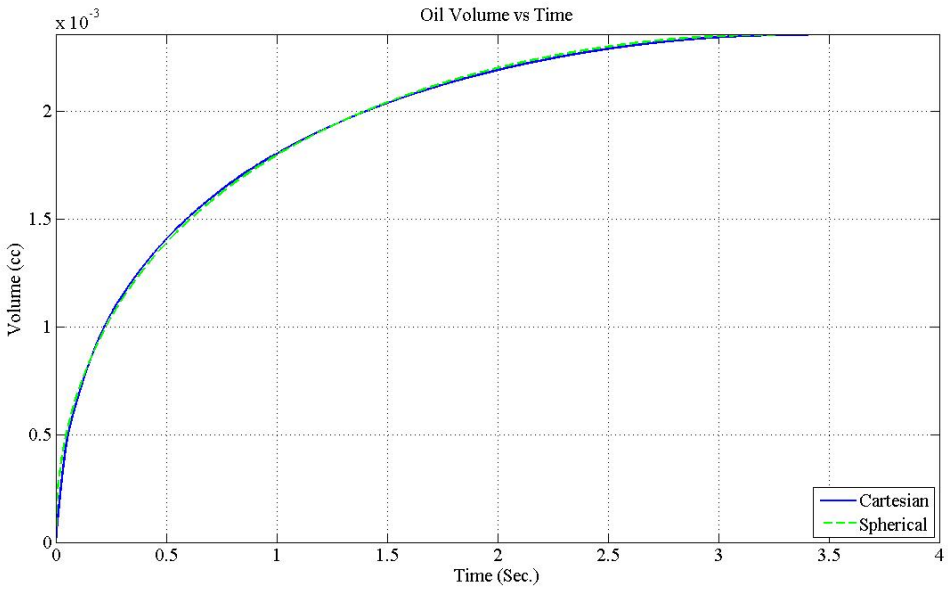

Figure 5.11: k=1 mD, E.D.=5 mm, A.R.=2 (Interpreted k=1.46 mD)

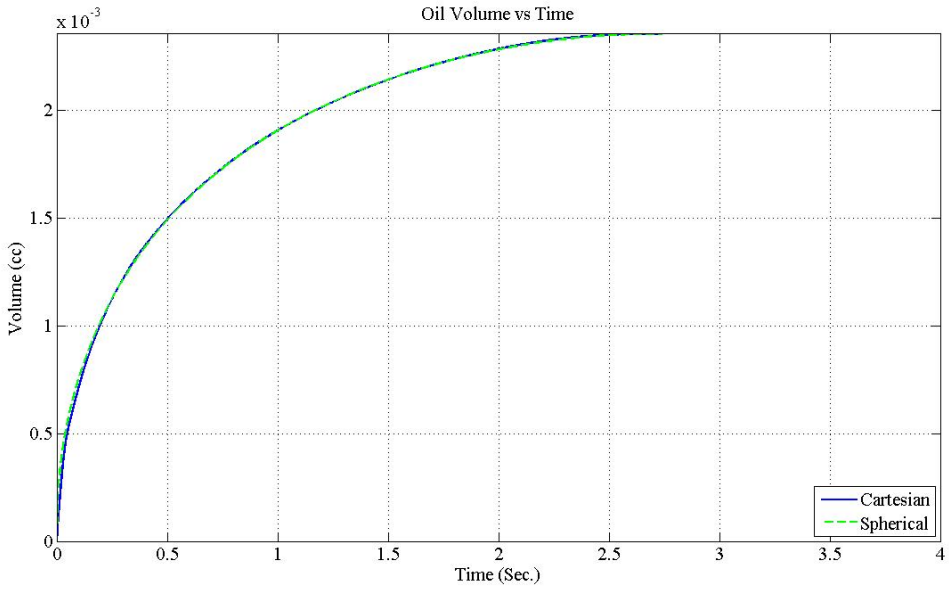

Figure 5.12: k=1 mD, E.D.=5 mm, A.R.=3 (Interpreted k=1.74 mD)

Curve fitting reveals a permeability of 1.26 mD, 1.46 mD and 1.74 mD respectively for the three responses.

5.1.2 Geometry case 2 (k = 20 mD)

Next we address the same cases of volume for the defined aspect ratios but this time for a uniform isotropic permeability of 20 mD.

5.1.2.1 Equivalent diameter = 2.5 mm

Figure 5.13 shows the plots for a cutting of 2.5 mm equivalent diameter. A minimum viscosity of 4000 cp was required to keep the responses in the prescribed range. The three individual curves in Figure 5.13 show the responses for the three defined aspect ratios for the same volume.

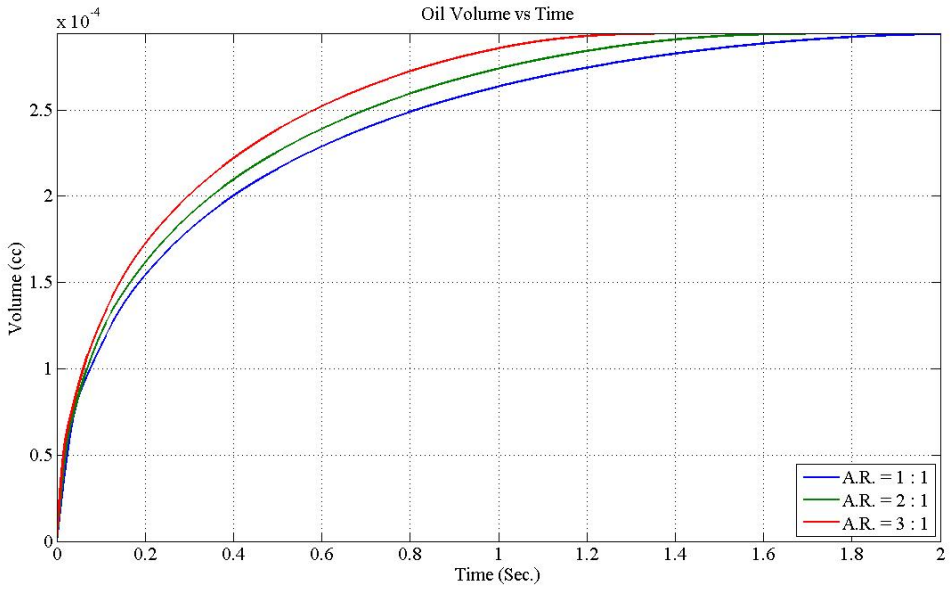

Figure 5.13: k=20 mD, E.D.=2.5 mm

It is again evident from the plot that any variation of shape from the cubic has an effect of increasing the rate of influx of the viscous oil into the cutting. The consequent response curves thus display a shorter equilibrium or testing time. The subsequent figures (Figure 5.14 to Figure 5.16) show the individual curves fitted with the spherical model emphasizing the significance of the cutting shape on the obtainable results.

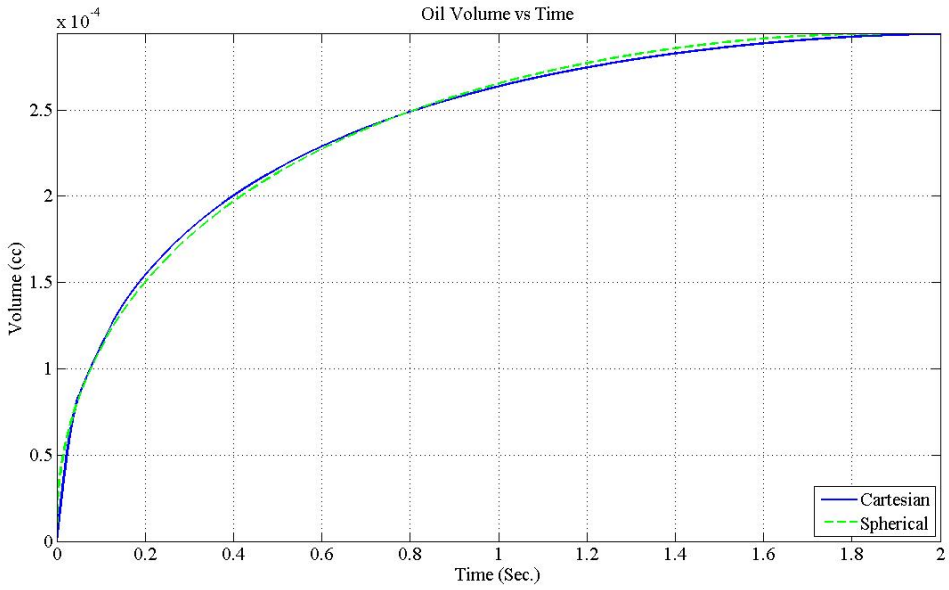

Figure 5.14: k=20 mD, E.D.=2.5 mm, A.R.=1 (Interpreted k=25.07 mD)

Curve fitting with the spherical model reveals that such an interpretation of this cutting would give the measured value of permeability to be around 25.07 mD, thus displaying an error of about 25.36% from the actual.

Figure 5.15 displays the curve fitted response for the first non-cubic formulation of the cutting.

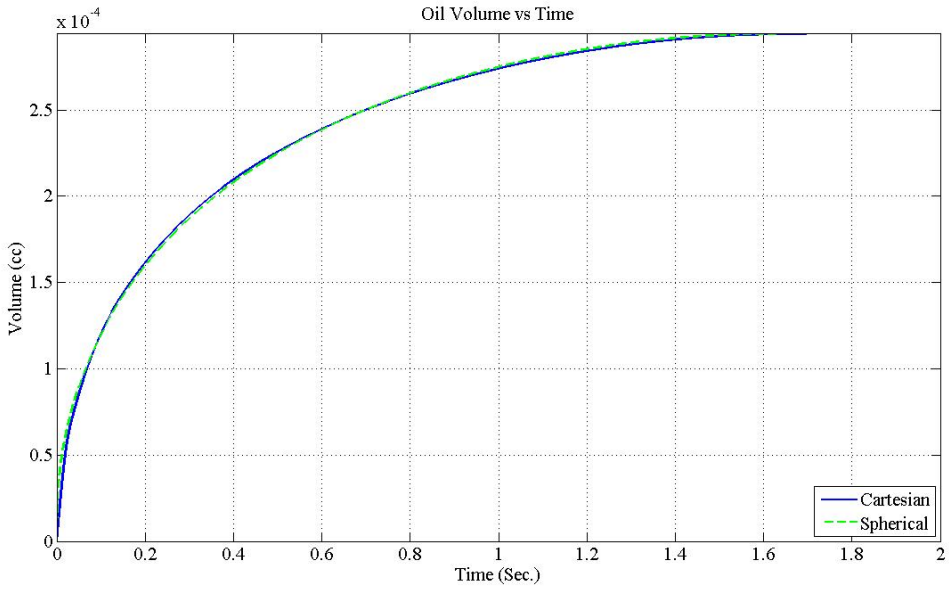

Figure 5.15: k=20 mD, E.D.=2.5 mm, A.R.=2 (Interpreted k=29 mD)

Interpretation of the impulse response curve using the spherical model reveals an interpretable value of permeability of approximately 29 mD, an exaggeration on the original value by almost 45%.

As the length contrast between the three sides is increased to make the aspect ratio 3, the resultant curve fit can be seen in the Figure 5.16.

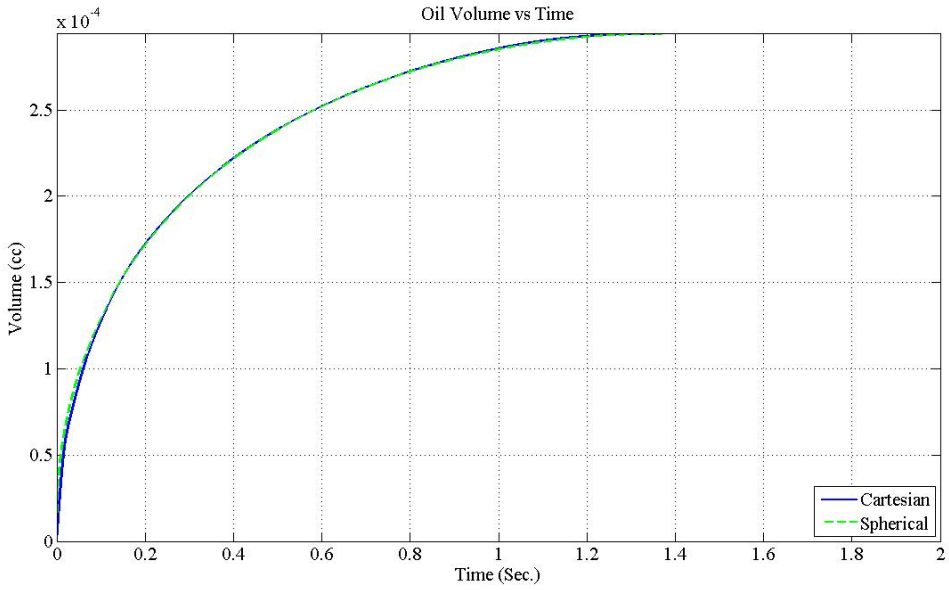

Figure 5.16: k=20 mD, E.D.=2.5 mm, A.R.=3 (Interpreted k=34.6 mD)

An interpreted value of permeability of 34.6 mD for this case comes to be off the actual value by 73%.

5.1.2.2 Equivalent diameter = 3.5 mm

The results from the simulator for a volume of cutting representing an equivalent spherical diameter of 3.5 mm are given in Figure 5.17. The simulator was assigned a viscosity value of 2000 cp to keep the responses within the desired time range.

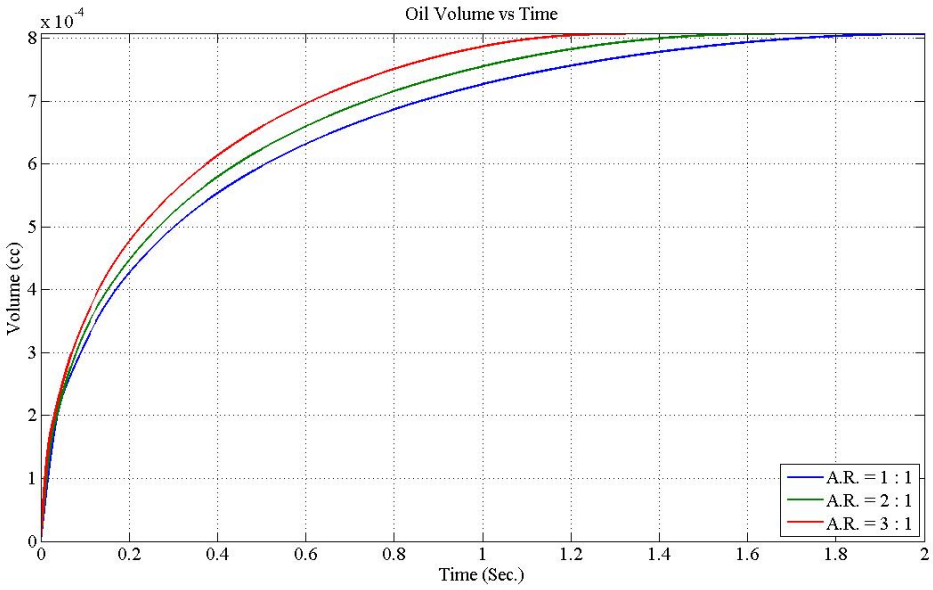

Figure 5.17: k=20 mD, E.D.=3.5 mm

Plots for the curve fitting can be seen in figures ranging from Figure 5.18 to Figure 5.20.

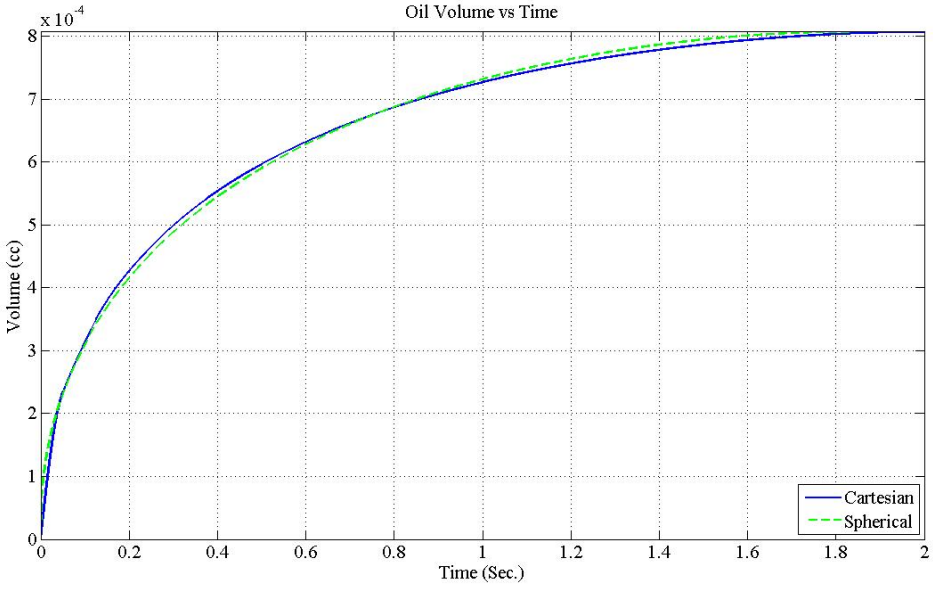

Figure 5.18: k=20 mD, E.D.=3.5 mm, A.R=1 (Interpreted k=25.07 mD)

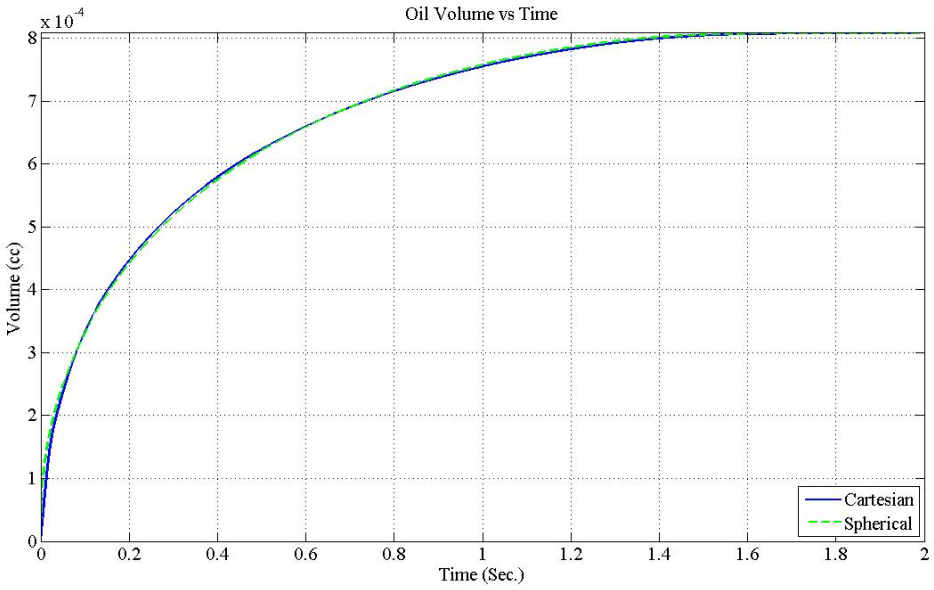

Figure 5.19: k=20 mD, E.D.=3.5 mm, A.R.=2 (Interpreted k=29 mD)

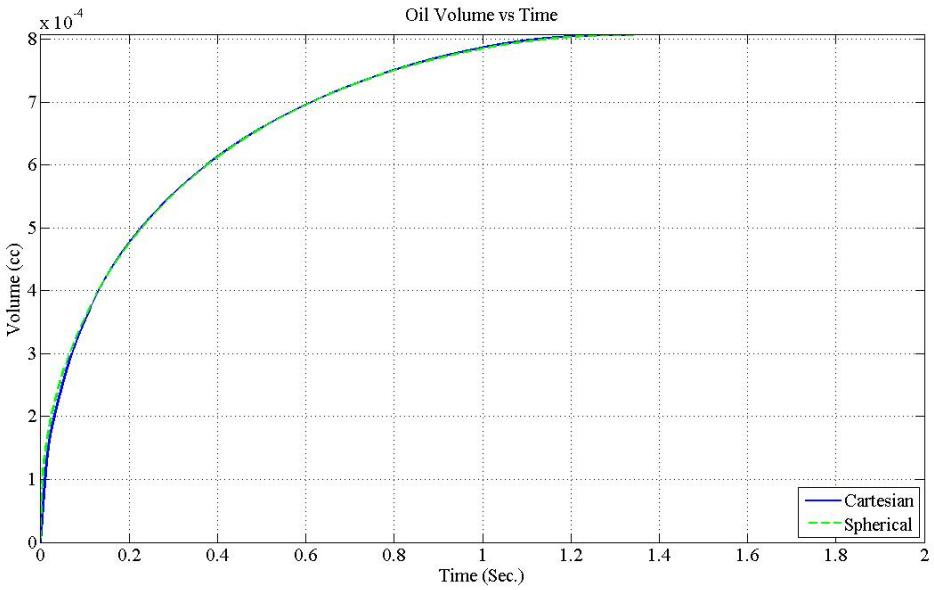

Figure 5.20: k=20 mD, E.D.=3.5 mm, A.R.=3 (Interpreted k=34.58 mD)

Curve fitting reveals a permeability of 25.07 mD, 29 mD and 34.58 mD respectively for the three responses.

5.1.2.3 Equivalent diameter = 5 mm

Plots given in the figures below (Figure 5.21 to Figure 5.24) represent the responses for a cutting having a volume equivalent to that of a 5 mm diameter sphere and a uniform isotropic permeability of 20 mD. A viscosity value of 1000 cp was deemed suitable for the simulation runs.

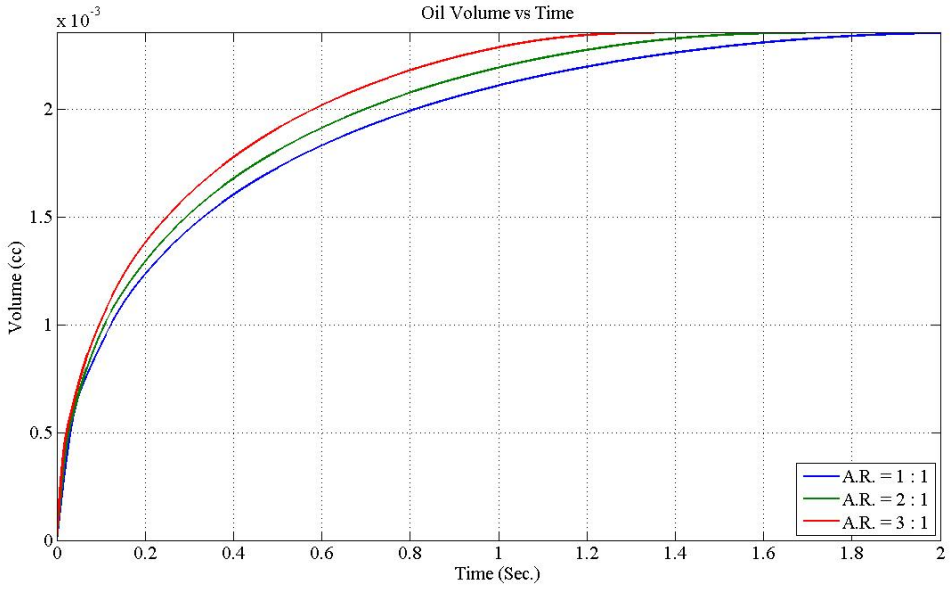

Figure 5.21: k=20 mD, E.D.=5 mm

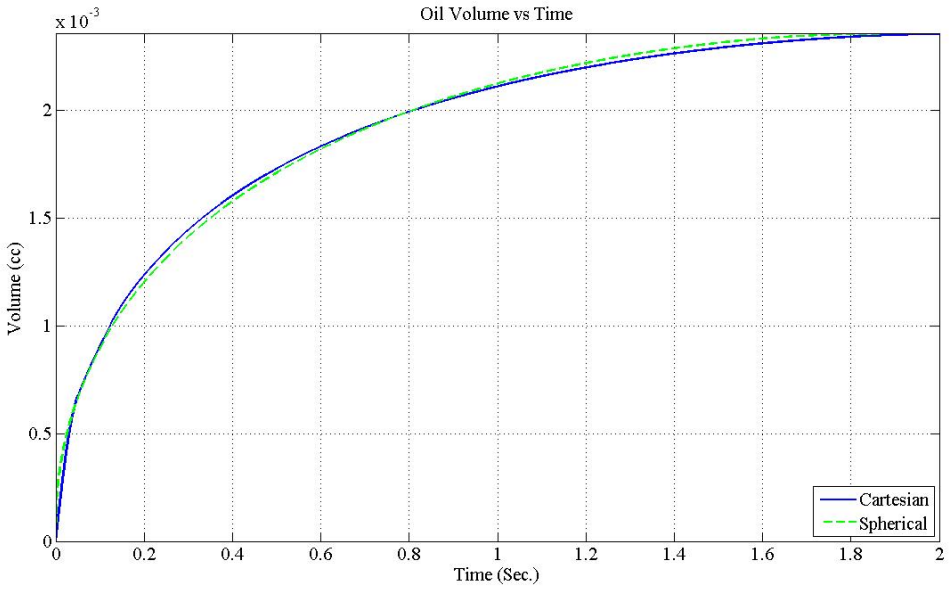

Figure 5.22: k=20 mD, E.D.=5 mm, A.R.=1 (Interpreted k=25.07 mD)

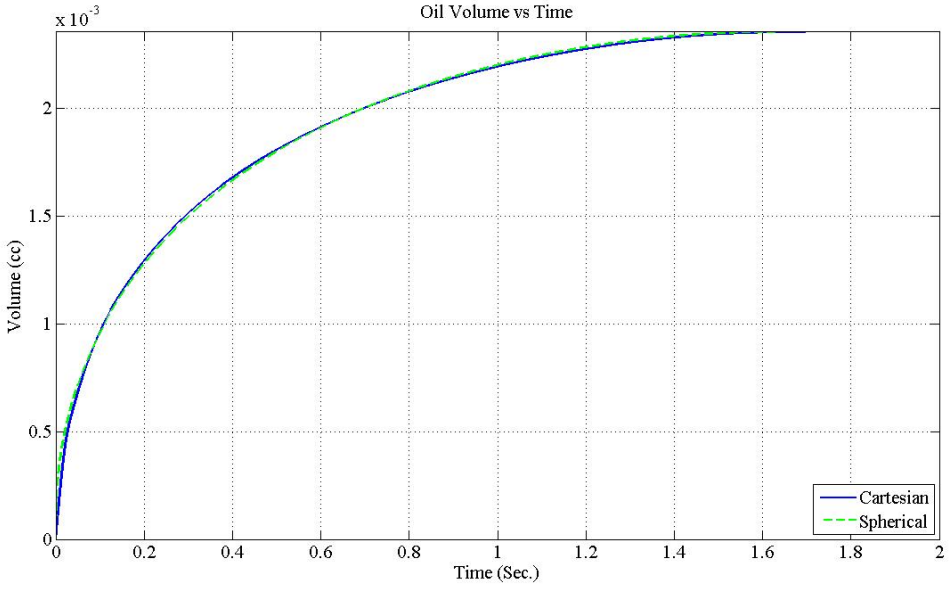

Figure 5.23: k=20 mD, E.D.=5 mm, A.R.=2 (Interpreted k=29 mD)

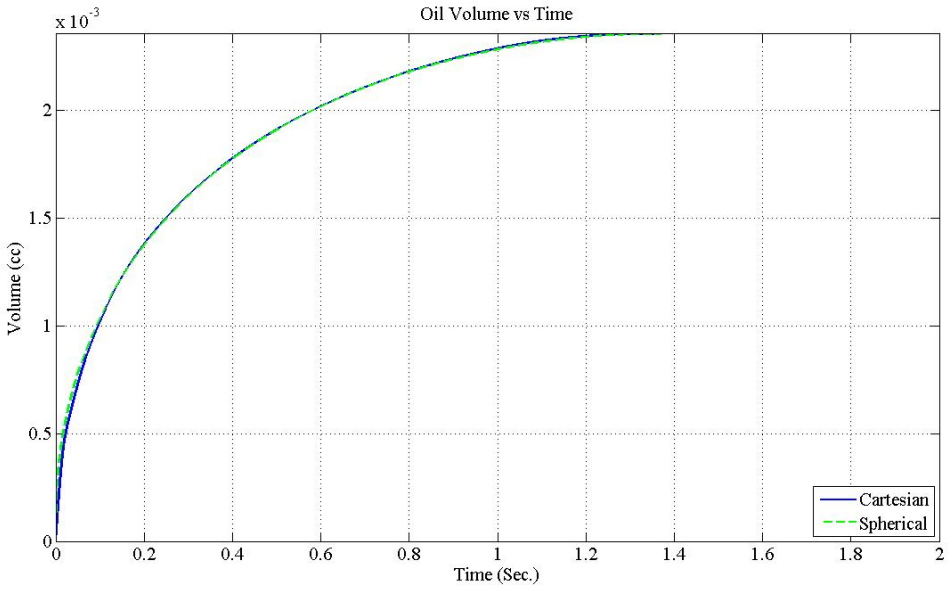

Figure 5.24: k=20 mD, E.D.=5 mm, A.R.=3 (Interpreted k=34.6 mD)

5.1.3 Geometry case 3 (k = 50 mD)

The third and last value of permeability used in the study was 50 mD.

5.1.3.1 Equivalent diameter = 2.5 mm

Figure 5.25 shows the plots for a 2.5 mm diameter equivalent volume cutting having a uniform isotropic permeability of 50 mD. The three individual curves show the responses for the three variations of aspect ratios for the same volume.

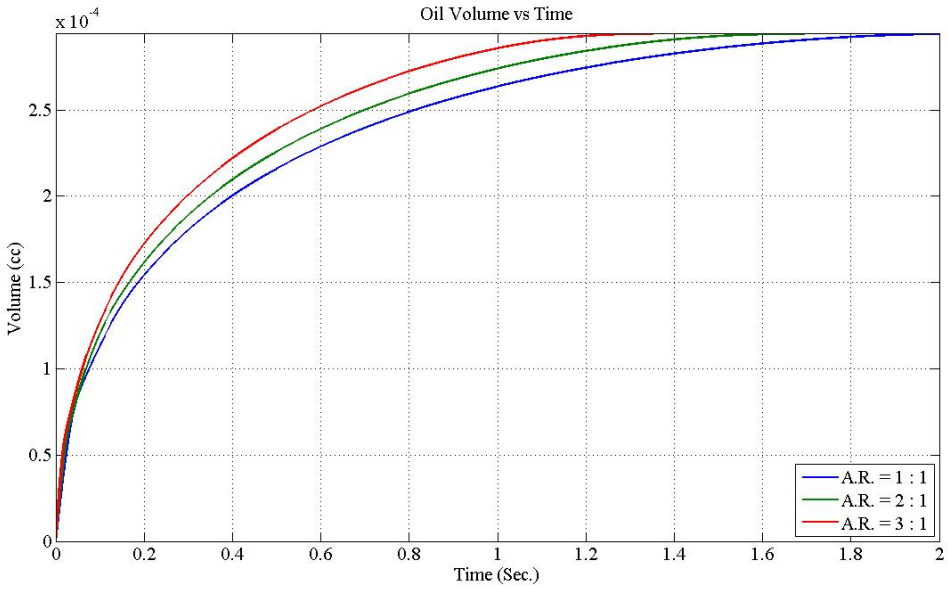

Figure 5.25: k=50 mD, E.D.=2.5 mm

The results of the curve fitting are displayed in the concerned figures (Figure 5.26 to Figure 5.28).

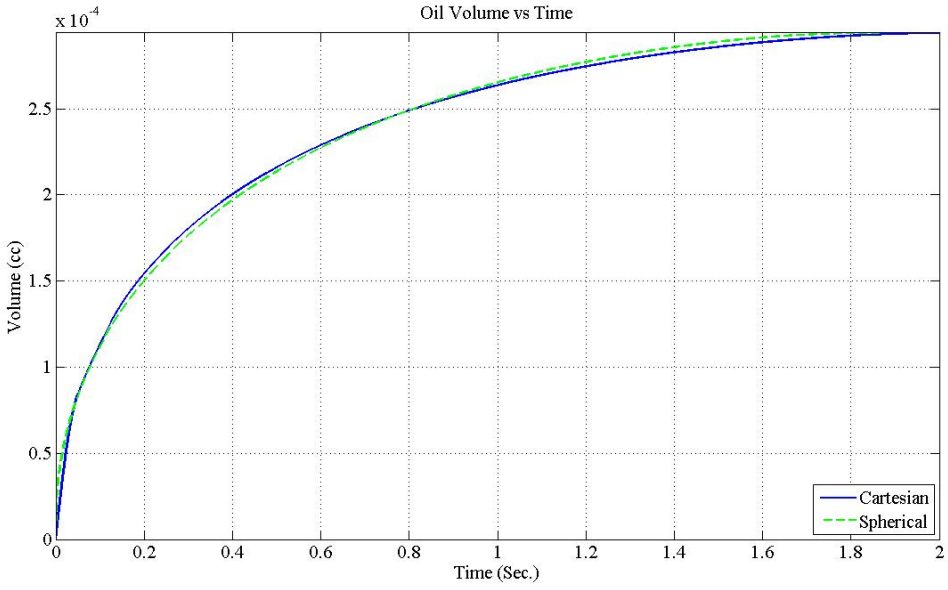

Figure 5.26: k=50 mD, E.D.=2.5 mm, A.R.=1 (Interpreted k=62.68 mD)

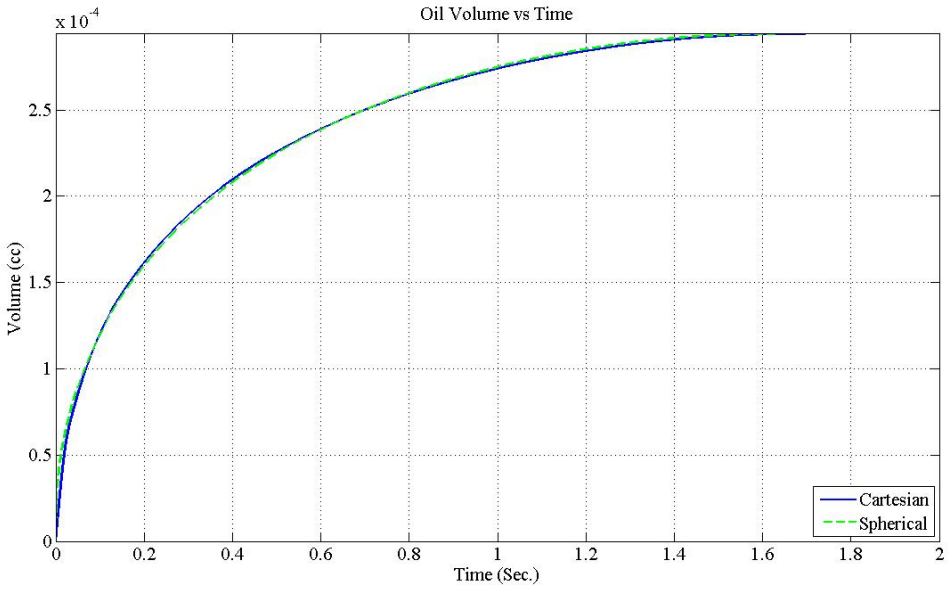

Figure 5.27: k=50 mD, E.D.=2.5 mm, A.R.=2 (Interpreted k=72.52 mD)

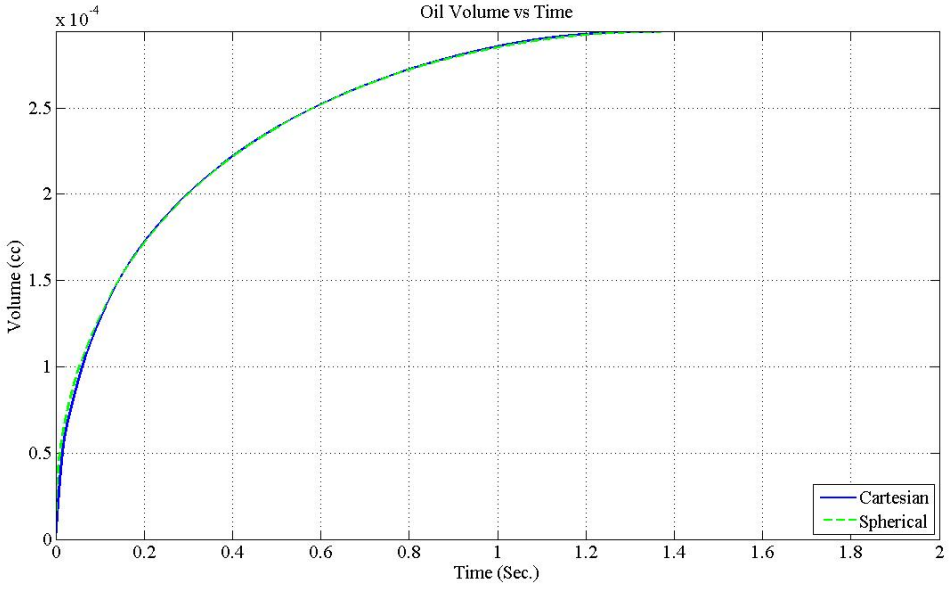

Figure 5.28: k=50 mD, E.D.=2.5 mm, A.R.=3 (Interpreted k=86.48 mD)

5.1.3.2 Equivalent diameter = 3.5 mm

Results have been plotted in Figure 5.29 for a cutting of volume equivalent to that of a sphere of diameter 3.5 mm.

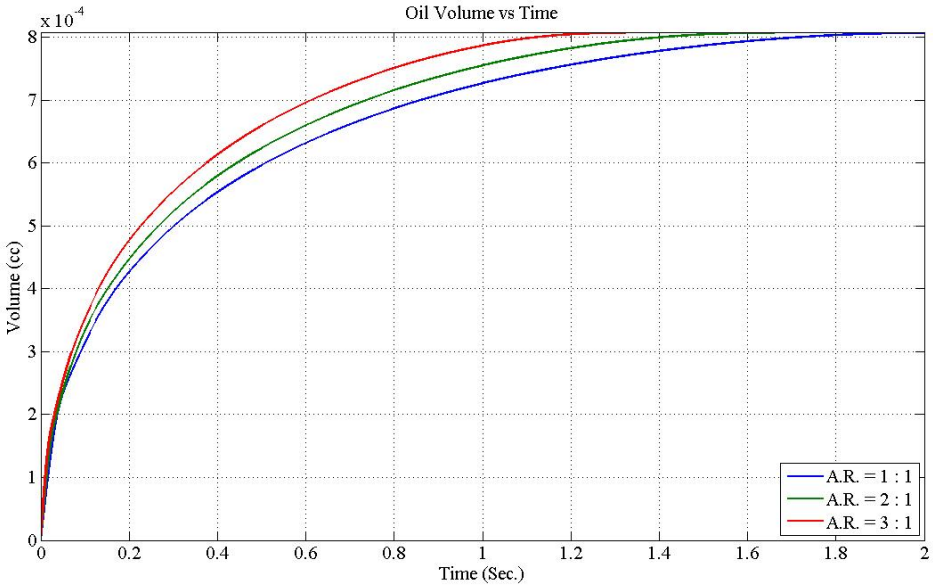

Figure 5.29: k=50 mD, E.D.=3.5 mm

Plots for the curve fitting can be seen in figures ranging from Figure 5.30 to Figure 5.32.

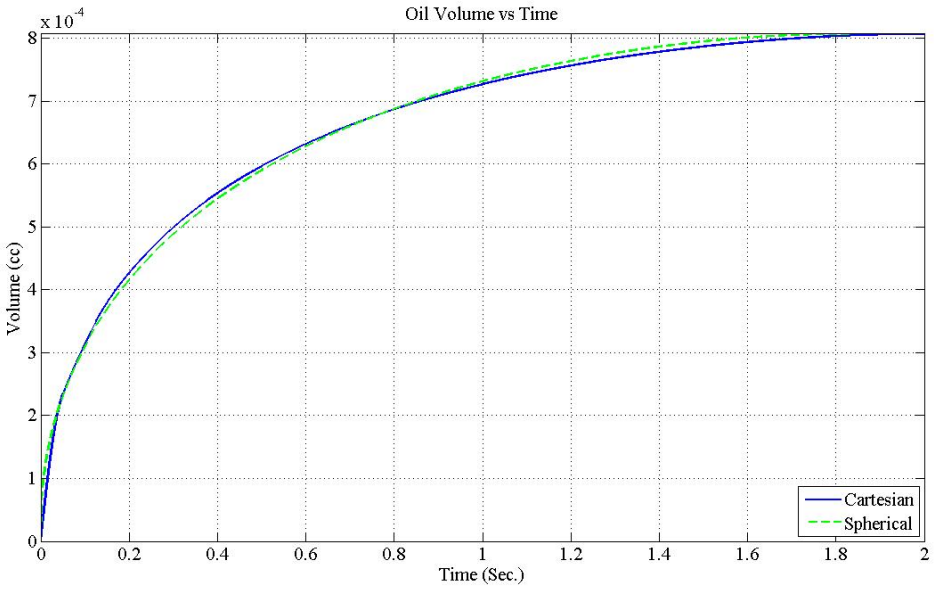

Figure 5.30: k=50 mD, E.D.=3.5 mm, A.R.=1 (Interpreted k=62.67 mD)

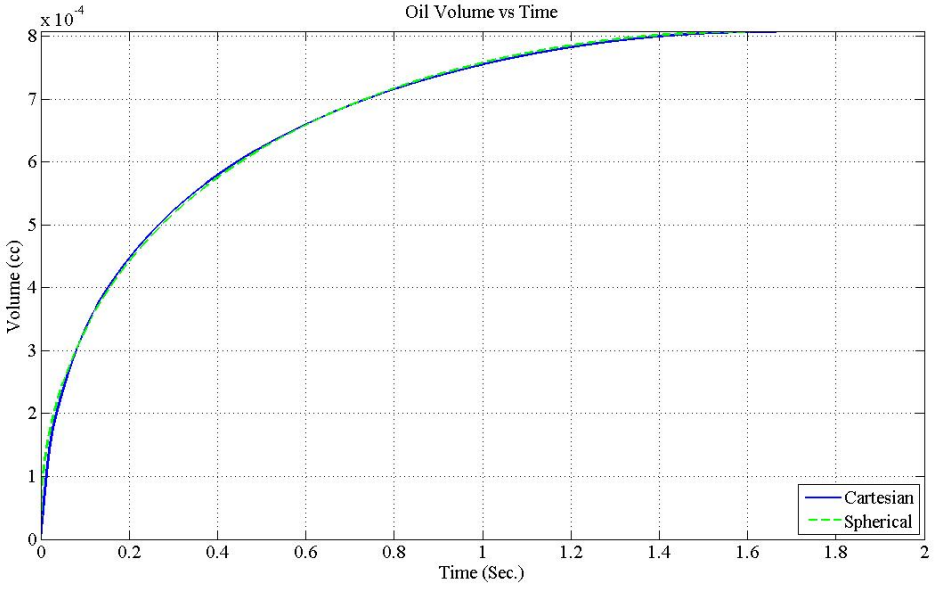

Figure 5.31: k=50 mD, E.D.=3.5 mm, A.R.=2 (Interpreted k=72.51 mD)

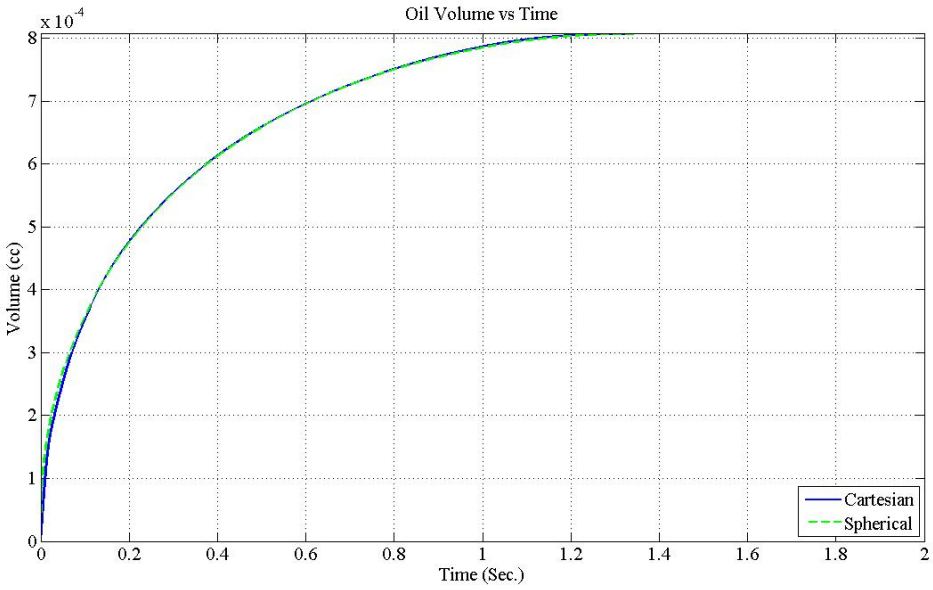

Figure 5.32: k=50 mD, E.D.=3.5 mm, A.R.=3 (Interpreted k=86.46 mD)

5.1.3.3 Equivalent diameter = 5 mm

Given below are the results for non-spherical representations of a cutting with volume equal to a 5 mm diameter sphere.

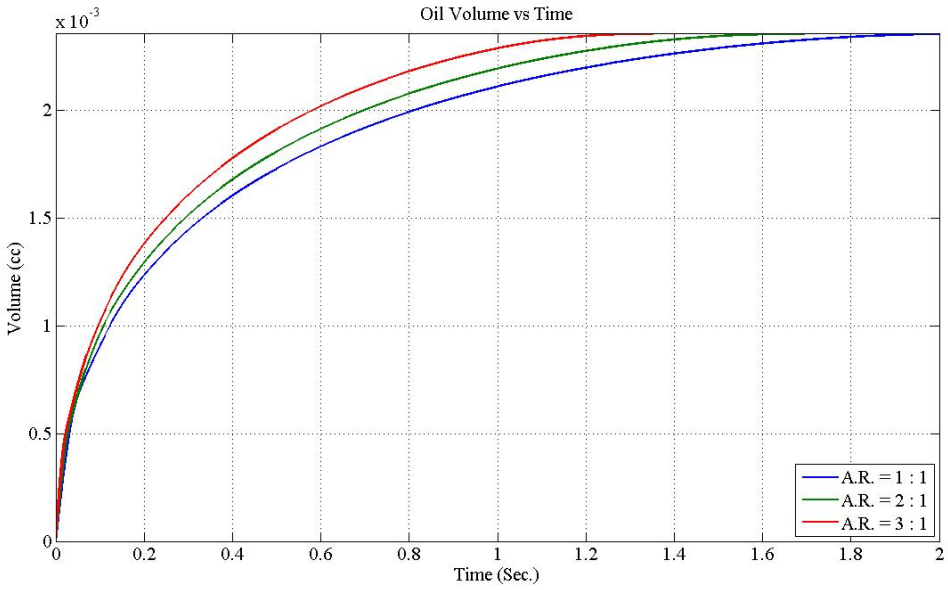

Figure 5.33: k=50 mD, E.D.=5 mm

Given in figures numbering from Figure 5.34 through Figure 5.36 are the plots for the curve fitting for these cases.

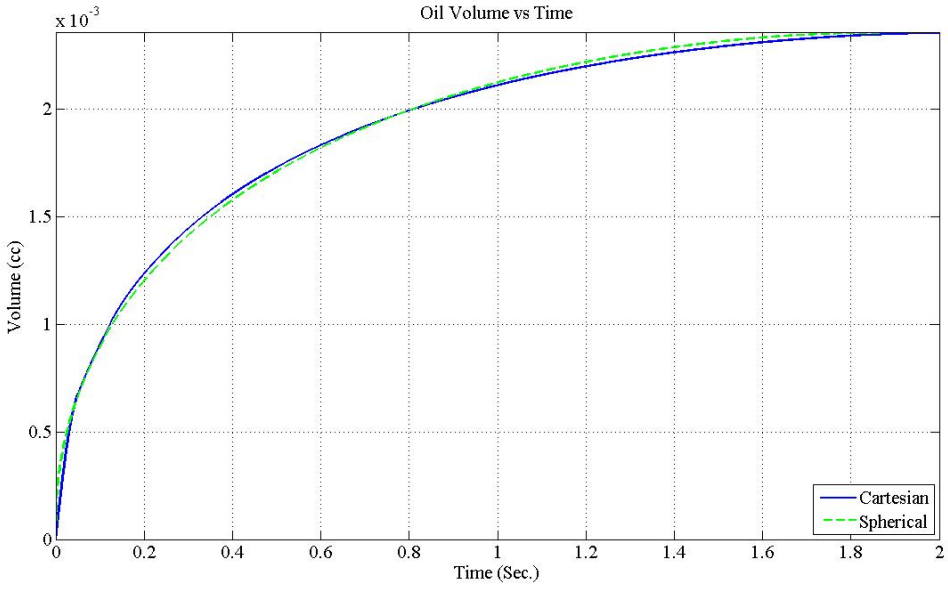

Figure 5.34: k=50 mD, E.D.=5 mm, A.R.=1 (Interpreted k=62.67 mD)

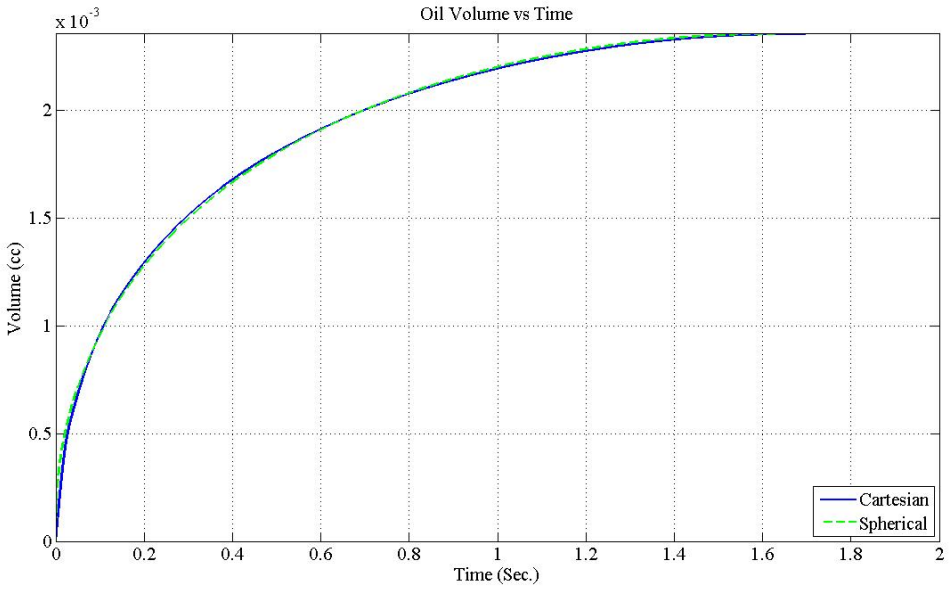

Figure 5.35: k=50 mD, E.D.=5 mm, A.R.=2 (Interpreted k=72.52 mD)

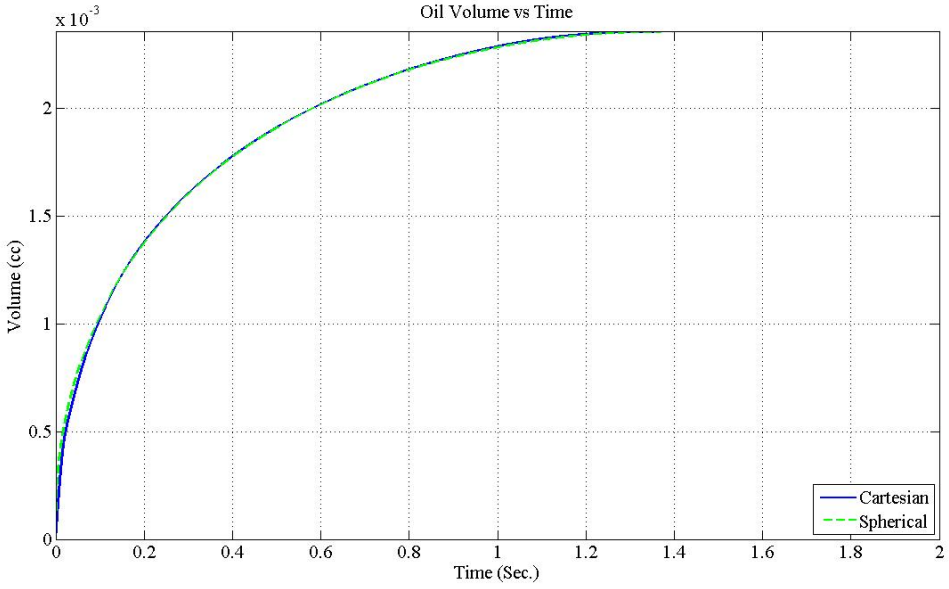

Figure 5.36: k=50 mD, E.D.=5 mm, A.R.=3 (Interpreted k=86.48 mD)

A summary of all the key results is presented in the Table 5.3. Note that we have brought the results for similar aspect ratios for the different sizes and permeabilities together to explain the significance of the results obtained.

Table 5.3: Geometry Effects

Permeability	E.D.	Aspect Ratio	Estimated Permeability	Error
mD	mm	x/(y=z)	mD	%
1	2.5	1	1.26	25.6
1	3.5	1	1.26	25.6
1	5.0	1	1.26	26.2
20	2.5	1	25.07	25.4
20	3.5	1	25.07	25.3
20	5.0	1	25.07	25.4
50	2.5	1	62.68	25.4
50	3.5	1	62.67	25.3
50	5.0	1	62.68	25.4
1	2.5	2	1.45	45.0
1	3.5	2	1.45	45.0
1	5.0	2	1.46	46.0
20	2.5	2	29.01	45.0
20	3.5	2	29.01	45.0
20	5.0	2	29.01	45.0
50	2.5	2	72.52	45.0
50	3.5	2	72.51	45.0
50	5.0	2	72.52	45.0
1	2.5	3	1.73	73.0
1	3.5	3	1.73	73.0
1	5.0	3	1.74	74.2
20	2.5	3	34.60	73.0
20	3.5	3	34.58	72.9
20	5.0	3	34.60	73.0
50	2.5	3	86.48	73.0
50	3.5	3	86.46	72.9
50	5.0	3	86.48	73.0

The slight variations in the percentage error probably exist owing to the difference in the rates of influx for the various cutting sizes and permeability. The influx is captured more accurately when the rates are low, as opposed to the larger cutting dimensions where the rates are high but the response time is comparable with the other results owing to the larger volume of influx required to achieve equilibrium. Analysis of the results obtained for the three permeability cases studied for the various cutting sizes reveals that the percentage change in the error appears to be independent of the cutting size or the permeability values being studied. A closer inspection tends to highlight the fact that the percentage error is primarily dependent on the aspect ratio which goes to affect the net surface area exposed to flow in any case. The spherical shape has the smallest surface area to volume ratio. A ratio which tends to grow as the shape deviates further from spherical. The larger surface area facilitates a higher flow rate, thus, when the response curve is fitted assuming the cutting to be spherical, the higher surface area is interpreted instead as a higher permeability. Furthermore, the flow experiences a larger resistance resulting from flow convergence due to a steady decrease of surface area towards the sphere center when a spherical cutting is assumed.

5.2 Anisotropy Effects

To restrict our study to the case of quantifying the anisotropy effects, we would mainly concern ourselves with cuttings of a cubic formulation to monitor the deviations in the responses, if any, only arising from the self induced anisotropy in the model.

It has already been demonstrated that curve fitting the responses obtained from a non-spherical model with a spherical model induces an error in the results. To quantify the impact of cutting anisotropy, we have defined offset as the deviation resulting from the anisotropic cases as compared to the standard isotropic response.

The properties and values presented in Table 5.3 have been assumed and kept constant for all the subsequent simulation runs pertaining to this section of the thesis. The value for viscosity is changed from case to case to keep the response time within the desired time range.

The cutting is modeled with 10 grid cells along each of the three axes, a number sufficient to help accurately capture the influx without exceeding the system resources available. Note that the 10 grid cells are actually dividing half the leg length of the cutting since the system modeled is describing one eighth of the cutting volume after splitting it about the no-flow boundaries.

Anisotropy was first simulated along one axis for cubic cuttings with leg lengths in accordance with keeping their net volumes equivalent to spheres of 2.5 mm and 5 mm in our simulation runs. Two of the axes were modeled having a base permeability first equal to 20 mD and then 50 mD. Anisotropy is simulated by changing the permeability of the third axis first to 0.5 and then to 1.5 times the base value. The three curves, the isotropic along with the two anisotropic responses, are plotted together and then individually in separate figures along with the curve fitting represented by the broken line to obtain more of a quantitative analysis. Note that this range was expected to appropriately highlight the influence of cutting anisotropy on the obtainable pressure

responses. The resultant pressure responses were analyzed both graphically and later quantitatively using the spherical model.

5.2.1 Uni-axial anisotropy case 1 (k = 20 mD)

A first set of simulation runs were made for a base permeability of 20 mD. Along with the isotropic case, the additional two cases were run keeping the permeability of one of the three axes equal to 10 mD and then 30 mD. The results for the cases are presented hereunder.

5.2.1.1 Equivalent diameter = 2.5 mm

With each of the three legs kept equal and a viscosity equivalent to 5000 cp, the results obtained from the simulator are presented in Figure 5.37.

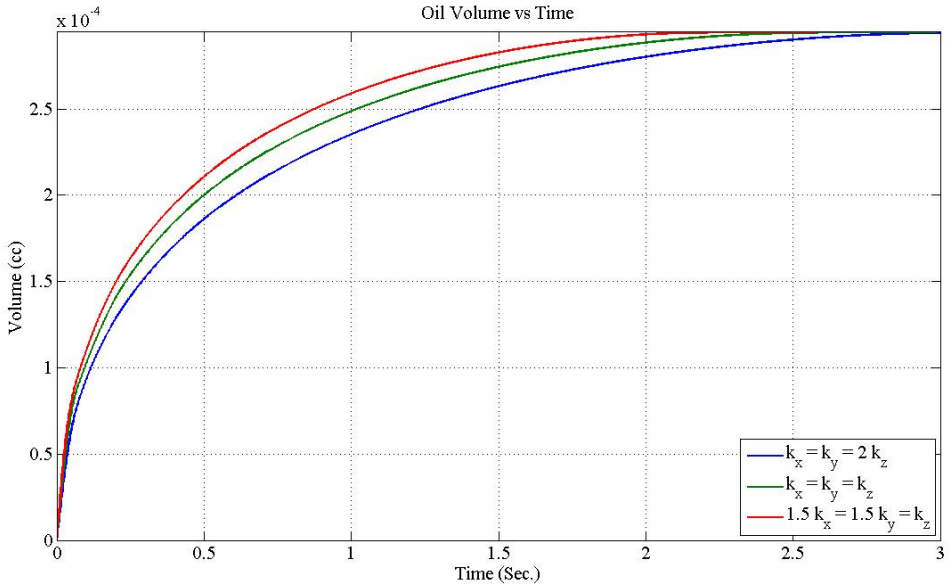

Figure 5.37: k_x=k_y=20 mD, E.D.=2.5 mm

The two anisotropic plots show variations about the isotropic curve. A quantitative analysis is conducted by curve fitting each of the obtained curves with the spherical model (Figure 5.38 to Figure 5.40).

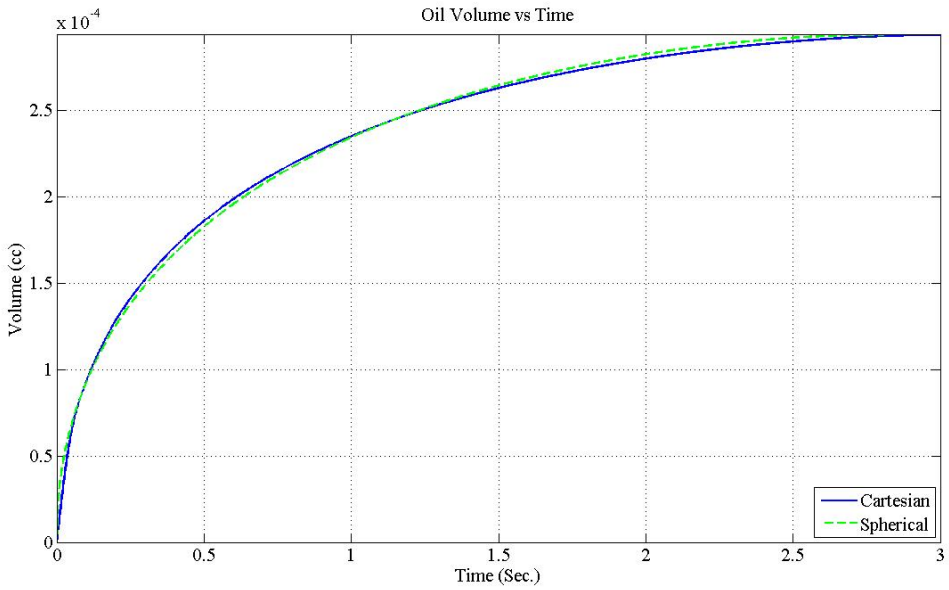

Figure 5.38: $k_x=k_y=20$ mD, E.D.=2.5 mm, $k_z=10$ mD (Interpreted k=20.82 mD)

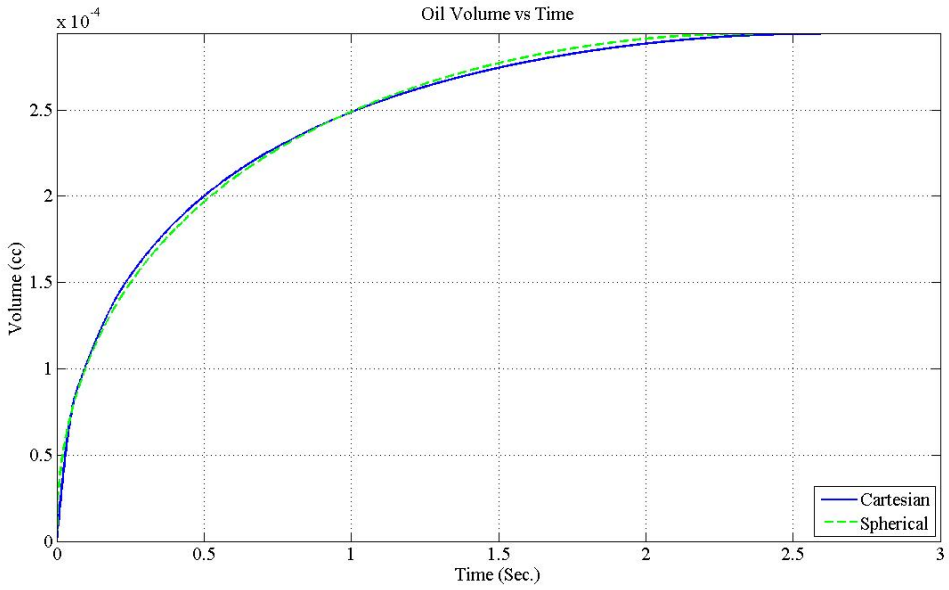

Figure 5.39: $k_x=k_y=20$ mD, E.D.=2.5 mm, $k_z=20$ mD (Interpreted k=25.14 mD)

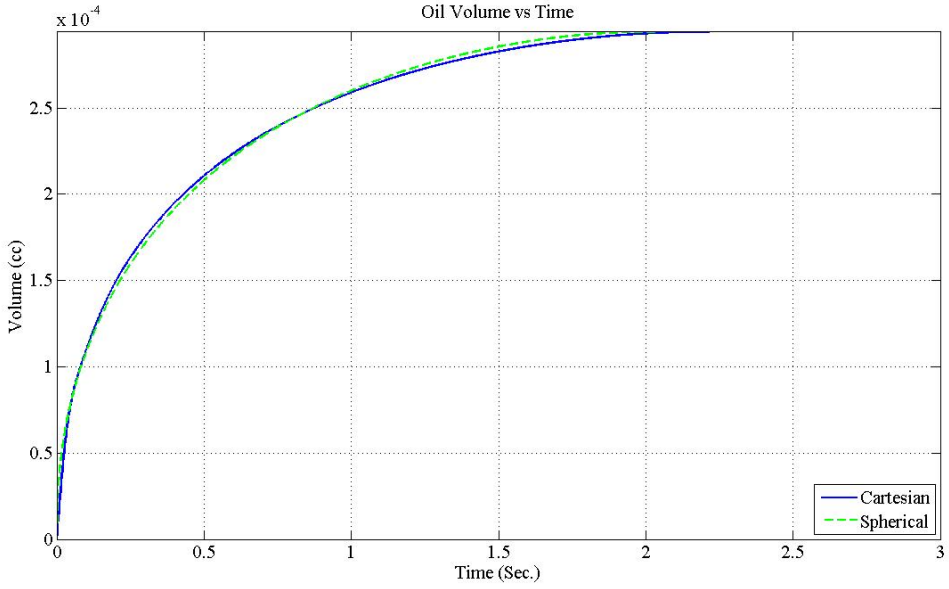

Figure 5.40: $k_x=k_y=20$ mD, E.D.=2.5 mm, $k_z=30$ mD (Interpreted k=29.2 mD)

Using the isotropic case as reference, we observe an offset of -17.17% for the 10 mD case and that of 16.15% for the 30 mD case.

5.2.1.2 Equivalent diameter = 5 mm

The cubic shaped cutting has a volume equivalent to that of a 5 mm diameter sphere. The increase in size allows us to use a smaller viscosity for the invading liquid. The value of viscosity used in the simulation run was kept at 1200 cp. Results obtained from the numerical simulator are displayed in Figure 5.41.

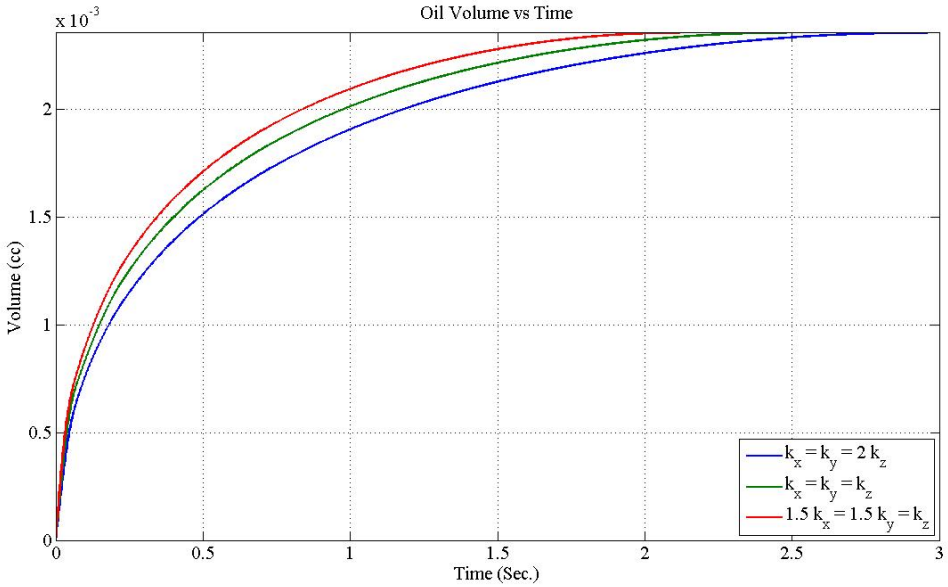

Figure 5.41: k_x=k_y=20 mD, E.D.=5 mm

Graphically, the results obtained appear to be quite similar to those for the 2.5 mm diameter cutting for similar initial and boundary conditions. Quantitative analysis is obtained when the individual responses are again curve fitted with the spherical model (Figure 5.42 to Figure 5.44).

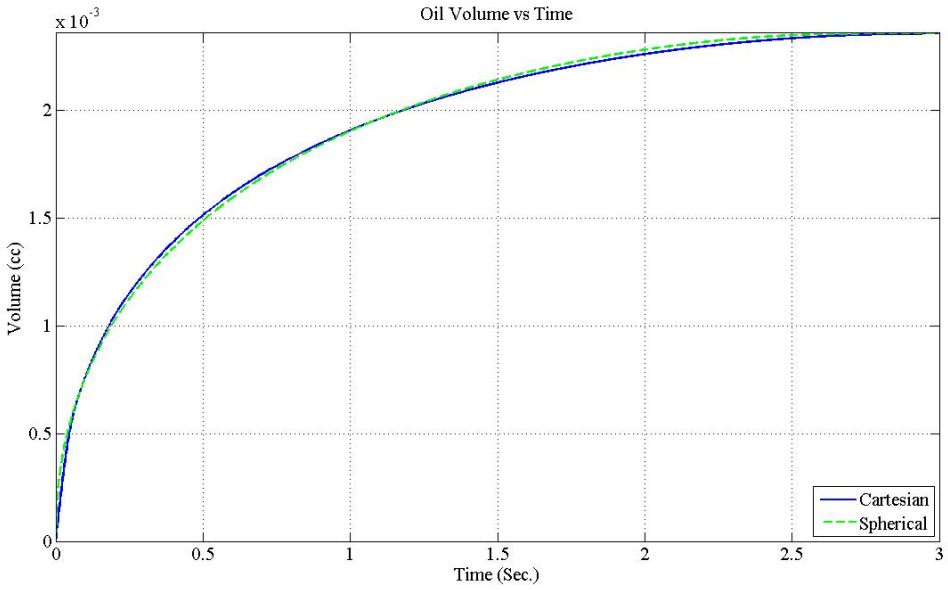

Figure 5.42: $k_x=k_y=20$ mD, E.D.=5 mm, $k_z=10$ mD (Interpreted k=20.82 mD)

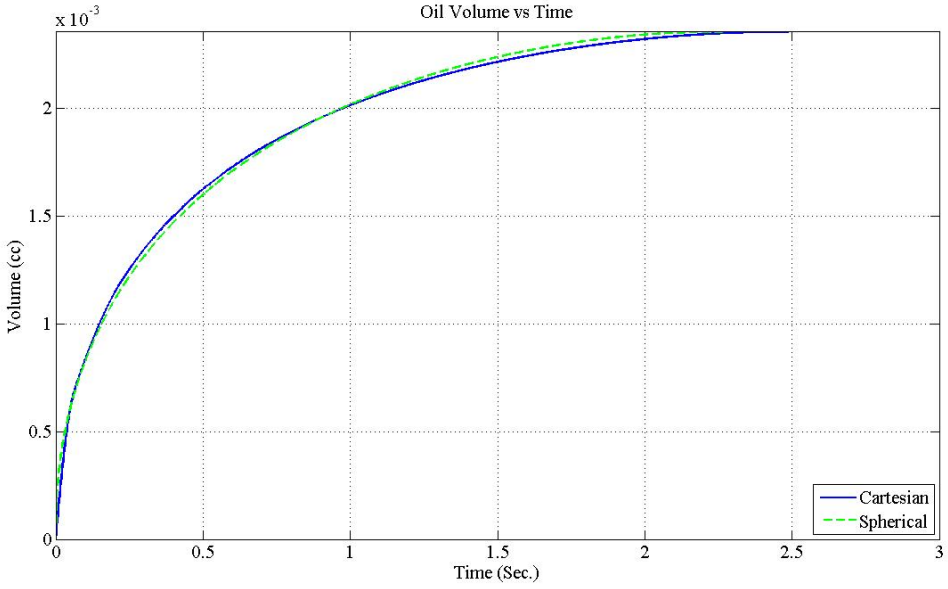

Figure 5.43: $k_x=k_y=20$ mD, E.D.=5 mm, $k_z=20$ mD (Interpreted k=25.13 mD)

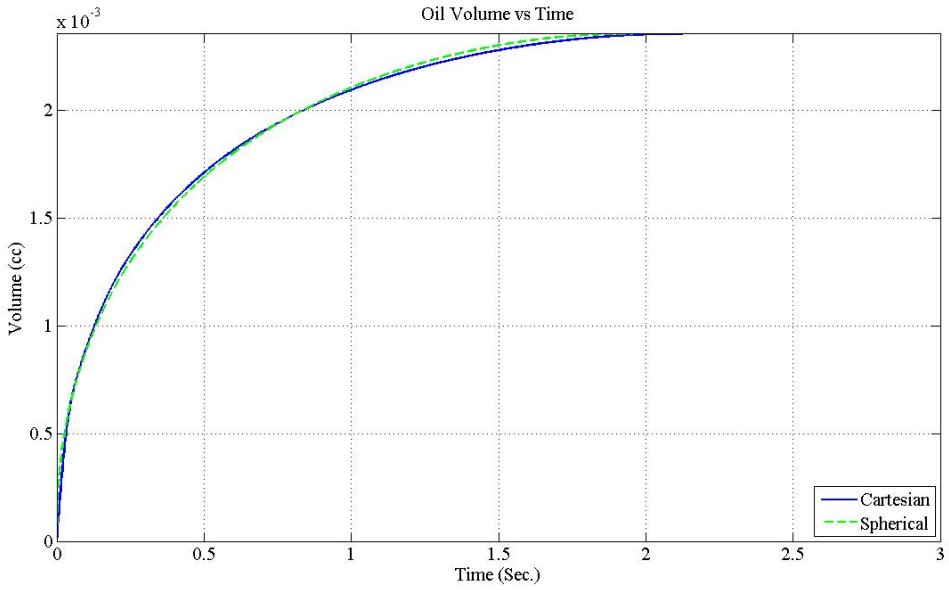

Figure 5.44: k_x=k_y=20 mD, E.D.=5 mm, k_z=30 mD (Interpreted k=29.18 mD)

Here again we observe an offset of -17.13% and 16.12% for the 10 mD and 30 mD anisotropies respectively about the isotropic results.

5.2.2 Uni-axial Anisotropy case 2 (k = 50 mD)

Next we carry out testing assuming the base or isotropic permeability to be 50 mD. All system properties and procedures are kept consistent with the 20 mD case which will help us highlight the trends and consistencies in the results, if any. Apart from the base, isotropic case, the anisotropy will again be introduced in the form of an arbitrary axis having 50% reduction and then an equal amount of exaggeration in permeability as opposed to the base value.

5.2.2.1 Equivalent diameter = 2.5 mm

Here again we start off our testing with the cubic cutting of volume equivalent to a 2.5 mm diameter sphere, with Figure 5.45 displaying the variation in the obtained responses graphically. The viscosity for the invading oil in this case needed to be increased to 12000 cp to remain within the time constraints.

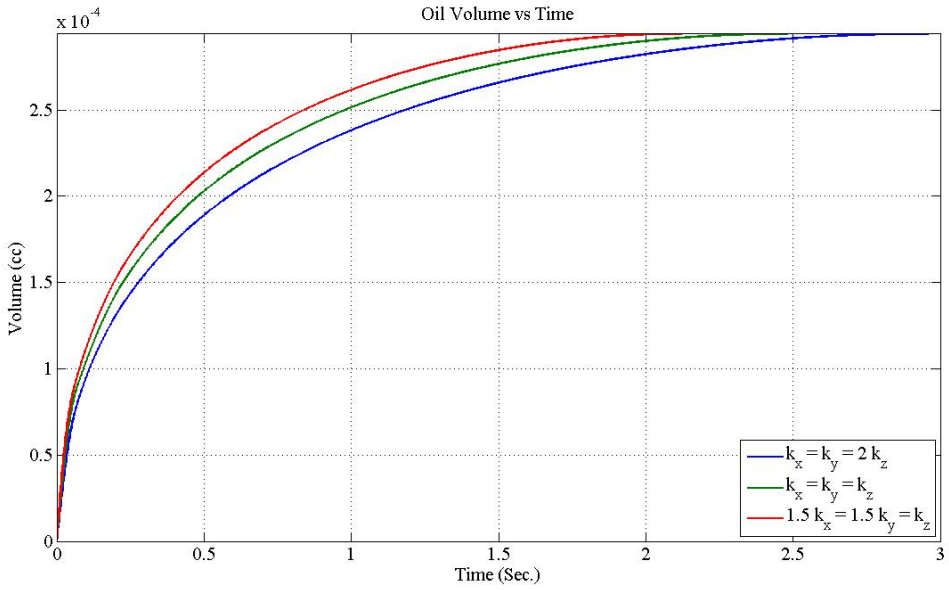

Figure 5.45: k_x=k_y=50 mD, E.D.=2.5 mm

Upon a cursory glance, the results again appear to be quite similar to those obtained for the 20 mD case for the same cutting size. The results are then followed by the curve fitting results presented in figures ranging from Figure 5.46 to Figure 5.48.

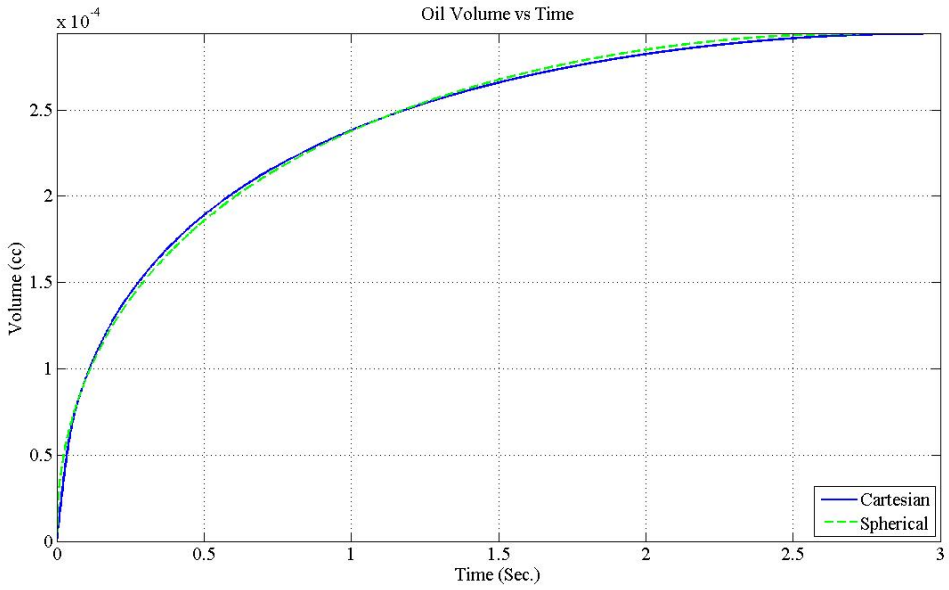

Figure 5.46: $k_x=k_y=50$ mD, E.D.=2.5 mm, $k_z=25$ mD (Interpreted k=52.04 mD)

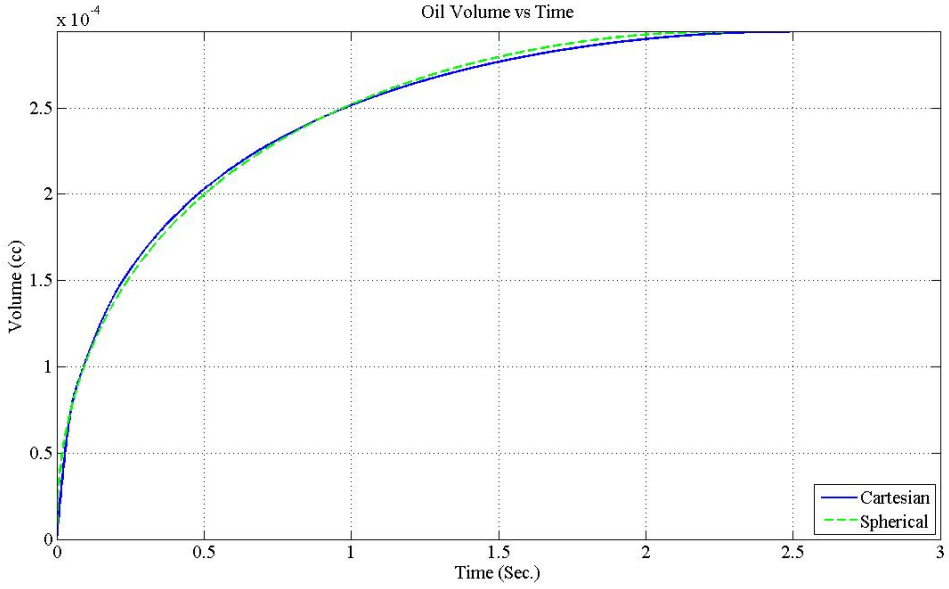

Figure 5.47: $k_x=k_y=50$ mD, E.D.=2.5 mm, $k_z=50$ mD (Interpreted k=62.84 mD)

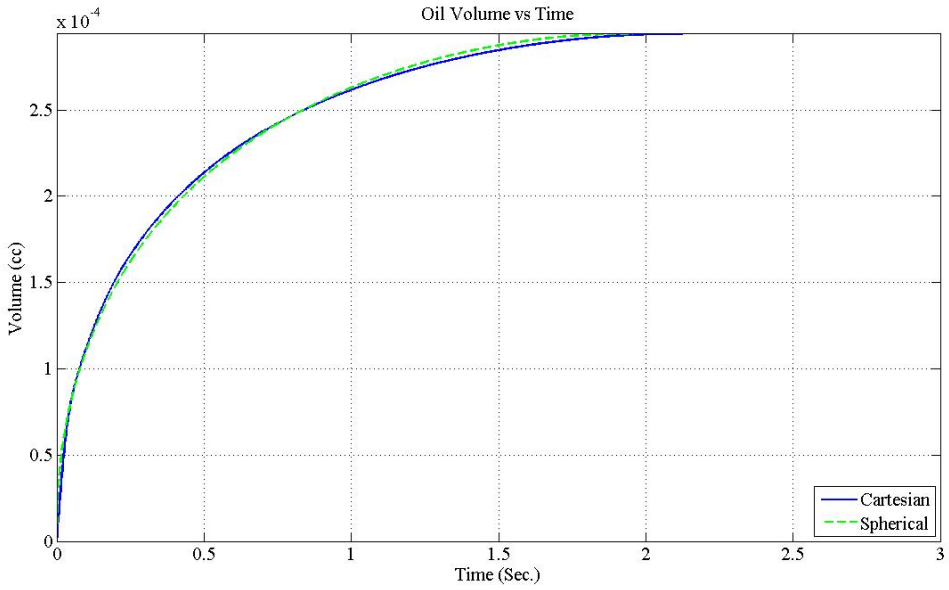

Figure 5.48: k_x=k_y=50 mD, E.D.=2.5 mm, k_z=75 mD (Interpreted k=72.95 mD)

Quantitative analysis reveals that the results are displaying an offset of -17.19% and 16.09% for the 25 mD and 75 mD cases from the base value respectively.

5.2.2.2 Equivalent diameter = 5 mm

The graphical results along with the curve fitting plots for the cubic cutting of a size equivalent to a diameter of 5 mm are presented in figures numbering from Figure 5.49 to Figure 5.52 respectively. Again the larger size of the cutting allowed us to reduce the viscosity of the viscous oil to 3000 cp.

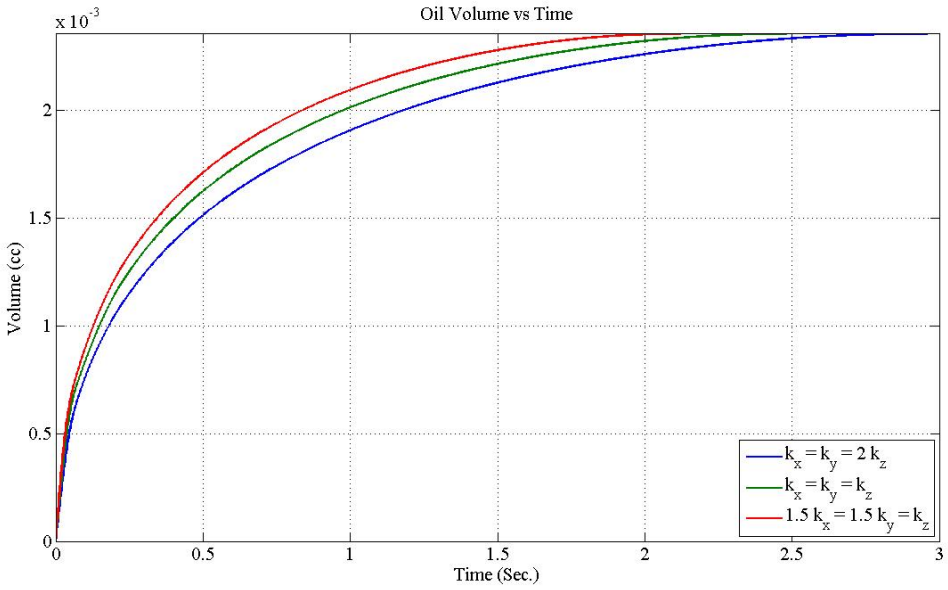

Figure 5.49: k_x=k_y=50 mD, E.D.=5 mm

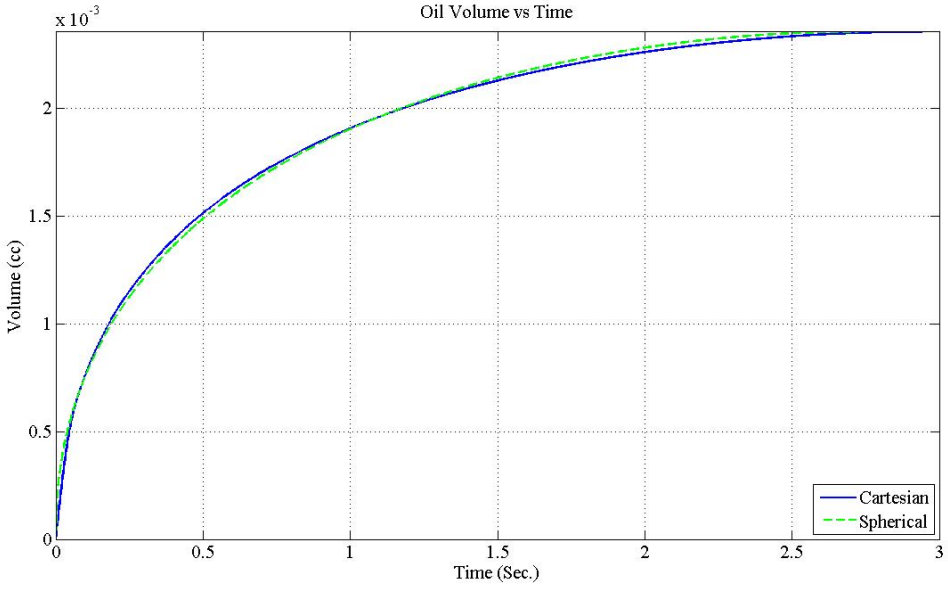

Figure 5.50: k_x=k_y=50 mD, E.D.=5 mm, k_z=25 mD (Interpreted k=52.04 mD)

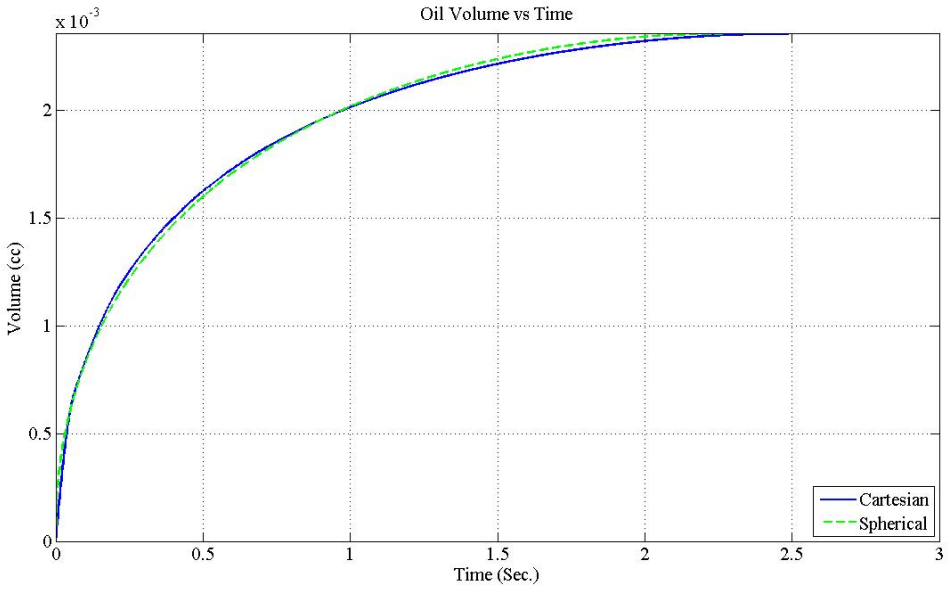

Figure 5.51: k_x=k_y=50 mD, E.D.=5 mm, k_z=50 mD (Interpreted k=62.84 mD)

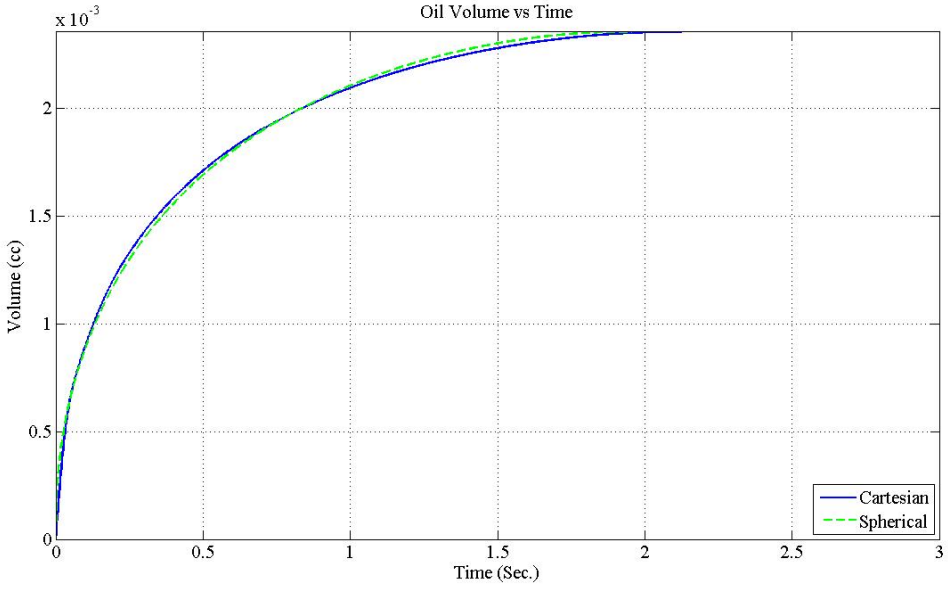

Figure 5.52: k_x=k_y=50 mD, E.D.=5 mm, k_z=75 mD (Interpreted k=72.95 mD)

The graphical as well as the quantitative results are in good agreement displaying an offset of -17.19% and 16.09% to either side of the isotropic curve consistently displaying a uniform shift in the interpreted values for similar conditions.

Upon a close inspection of the results obtained from all the cases, it is quite evident that similar percent increases or decreases in permeability results in a more or less similar increase or decrease in the interpretable results irrespective of the base permeability and cutting size. In each case, the percentage offset has been greater in magnitude for the permeability reduction as opposed to the contrary. A possible reason for this is the constant time step maintained for both cases. As the permeability increases, the higher influx rate requires that the time step size be reduced to more accurately capture the flow. Most of the previous simulation runs have shown that decreasing the time step size for a particular set of initial, boundary and system characteristics is interpreted as a slight increase in overall permeability of the system. A summary of the results is presented in Table 5.4.

Table 5.4: Anisotropy Effects (Single Direction)

$k_x = k_y$	E.D.	k_z / k_x	Estimated Permeability	Offset
mD	mm		mD	%
20	2.5	0.5	20.82	-17.2
20	5.0	0.5	20.82	-17.1
50	2.5	0.5	52.04	-17.2
50	5.0	0.5	52.04	-17.2
20	2.5	1.0	25.14	0.0
20	5.0	1.0	25.13	0.0
50	2.5	1.0	62.84	0.0
50	5.0	1.0	62.84	0.0
20	2.5	1.5	29.20	16.2
20	5.0	1.5	29.18	16.1
50	2.5	1.5	72.95	16.1
50	5.0	1.5	72.95	16.1

The results obtained from inducing anisotropy in one direction suggest that a given step change in permeability to either side of the mean value affects the response curve and in turn the interpretable permeability to a more or less similar extent. Thus, broadening the scope of that statement, we went about inducing multiple anisotropies in our model to capture or generalize the results and conclusions.

The multiple permeability cases were designed around a basic premise, for any given case, the permeability variations were kept such that the arithmetic average value arising from the three, since the cutting is always cubic, will be kept constant.

All the simulation runs were made around two arithmetic averages of 20 mD and 50 mD permeabilities respectively. As already stated, the cuttings were always modeled cubic so that the length factor would not play any influence upon the derived responses. Furthermore, all the simulation runs were made assuming a cutting bearing volume

equivalent to that of a 3.5 mm diameter sphere since it has already been established that the results are independent of the net cutting size.

5.2.3 Multi-axial Anisotropy case 1 (k_{avg} = 20 mD)

An oil viscosity of 2000 cp proved to be sufficient for all the variations averaging around the 20 mD mark. The results obtained for the various runs are presented in Figure 5.53.

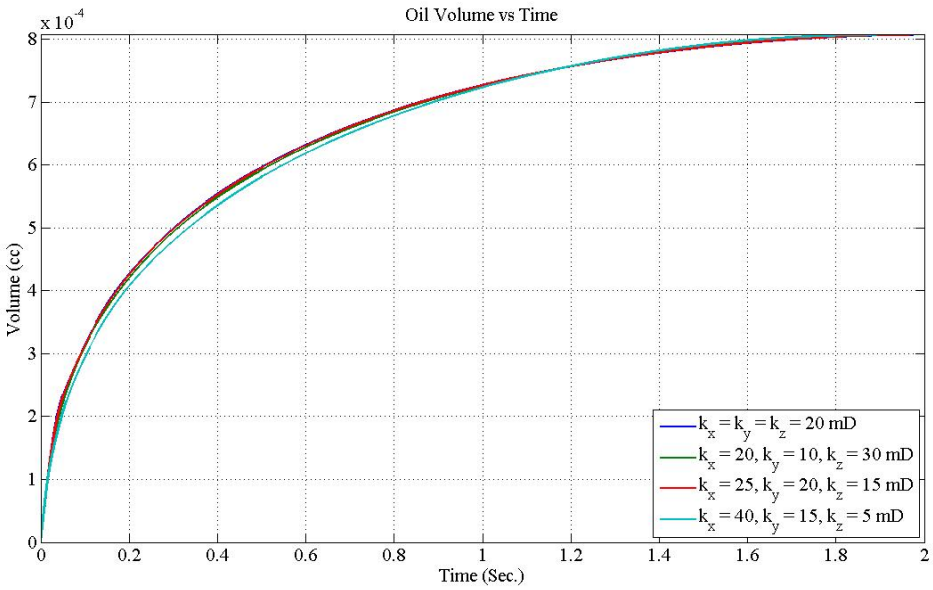

Figure 5.53: Average Permeability=20 mD, E.D.=3.5 mm

As can be seen in the plot, the curves lie very close to each other. To get a more objective idea, the results are quantitatively assessed using the spherical model. The results obtained from the curve fitting are presented in Figure 5.54, Figure 5.55, Figure 5.56 and Figure 5.57.

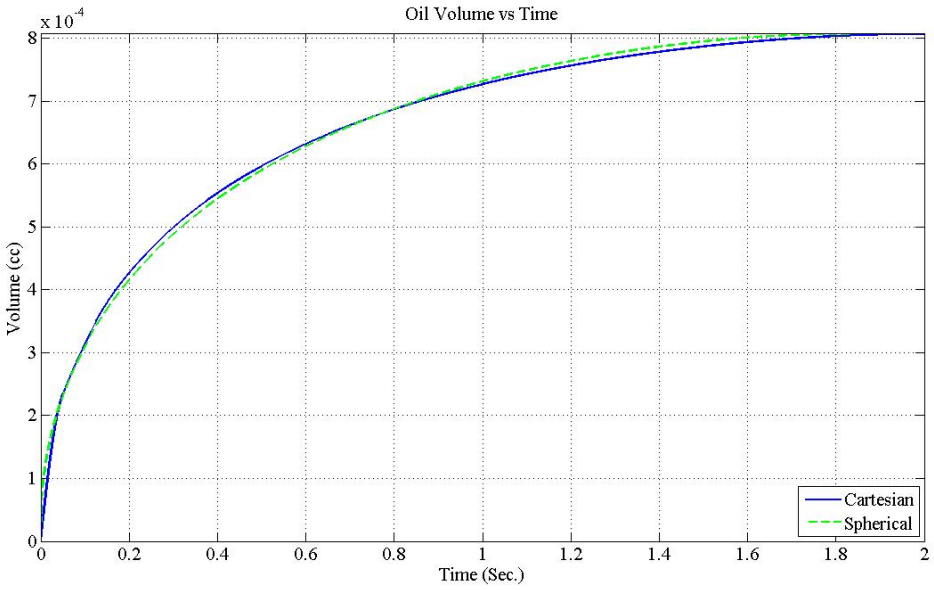

Figure 5.54: k_x=20 mD, k_y=20 mD, k_z=20 mD (Interpreted k=25.07 mD)

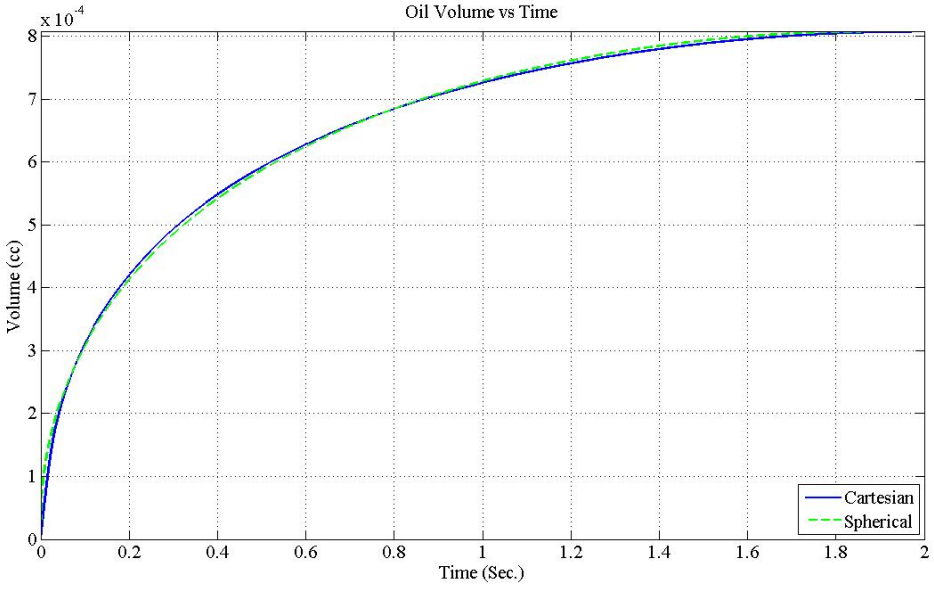

Figure 5.55: k_x=20 mD, k_y=10 mD, k_z=30 mD (Interpreted k=24.69 mD)

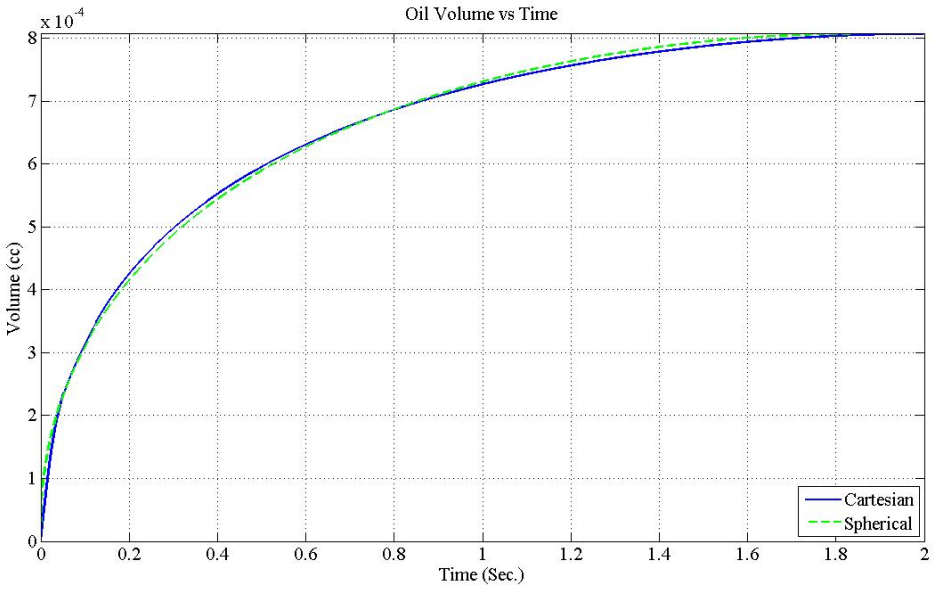

Figure 5.56: k_x=25 mD, k_y=20 mD, k_z=15 mD (Interpreted k=24.98 mD)

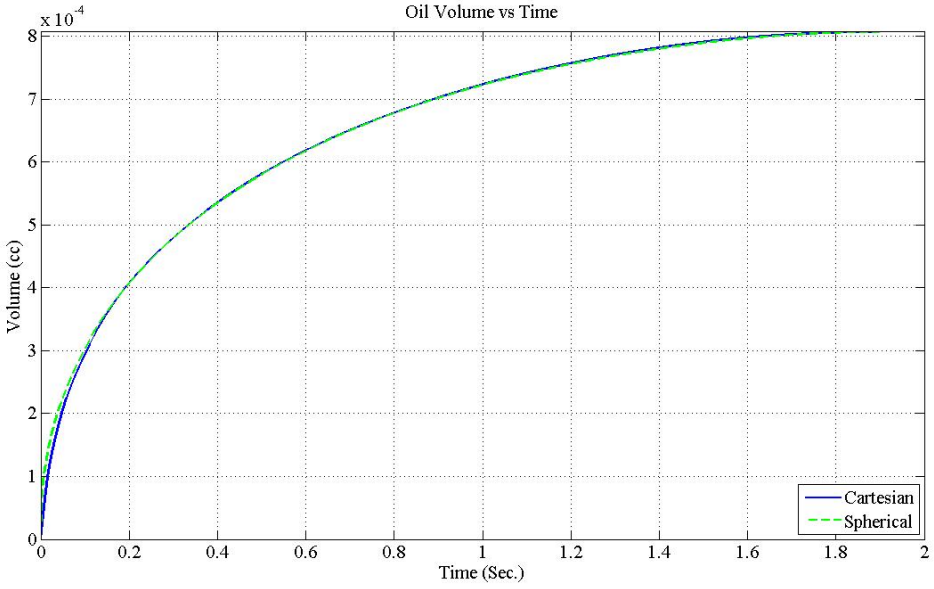

Figure 5.57: k_x=40 mD, k_y=15 mD, k_z=5 mD (Interpreted k=23.88 mD)

As can be seen from all the plots, all the curve-fits yield approximately the same values of permeability.

5.2.4 Multi-axial Anisotropy case 2 (k_{avg} = 50 mD)

The high permeability case required an increase in the prescribed viscosity of the invading oil modeled. An oil viscosity of 5000cp was used in all simulation runs for the 50mD average case. The results obtained for the various runs are presented in Figure 5.58.

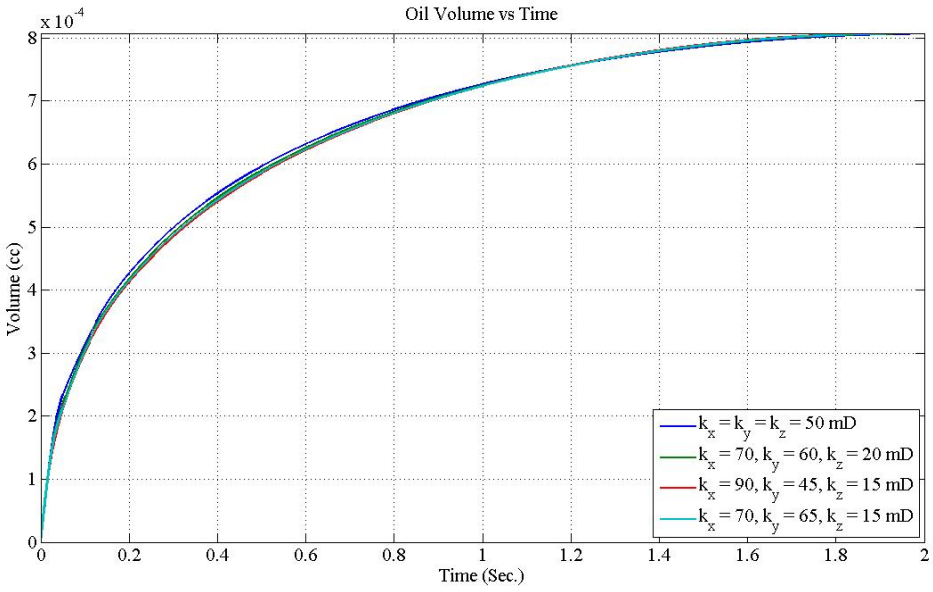

Figure 5.58: Average Permeability=50 mD, E.D.=3.5 mm

A quantitative assessment is made by curve fitting the obtained response curves with the spherical model to obtain the interpretable permeability (Figure 5.59 to Figure 5.62).

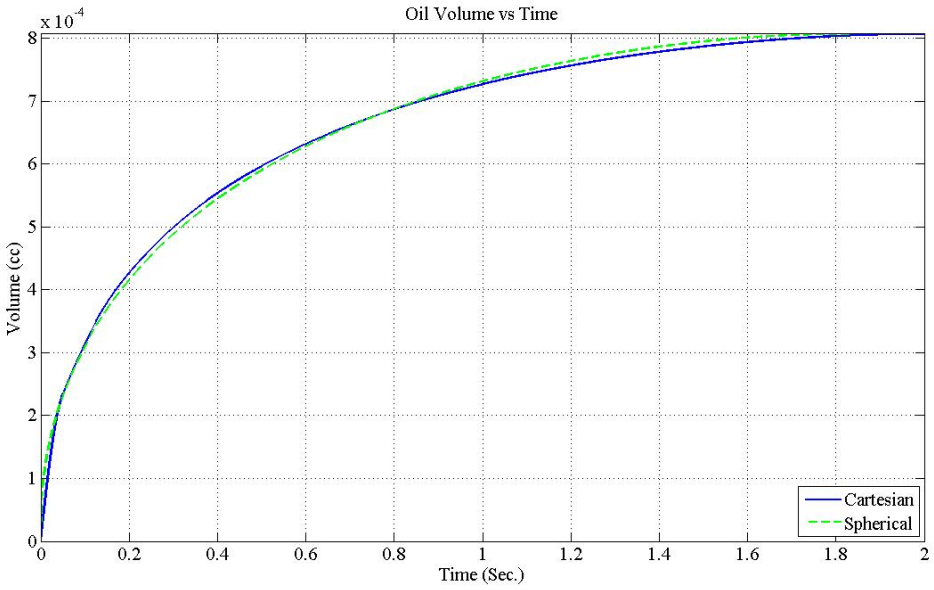

Figure 5.59: k_x=50 mD, k_y=50 mD, k_z=50 mD (Interpreted k=62.67 mD)

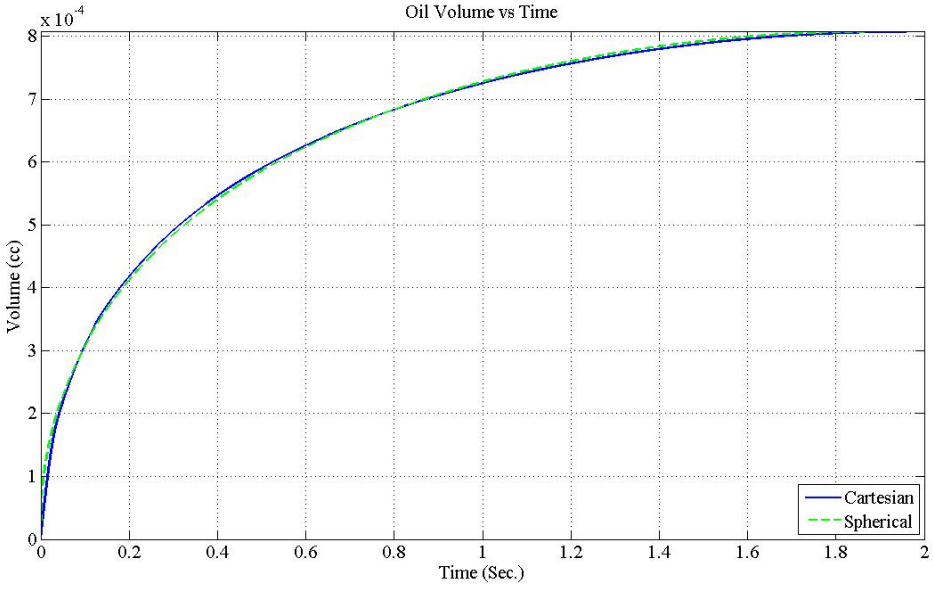

Figure 5.60: k_x=70 mD, k_y=60 mD, k_z=20 mD (Interpreted k=61.38 mD)

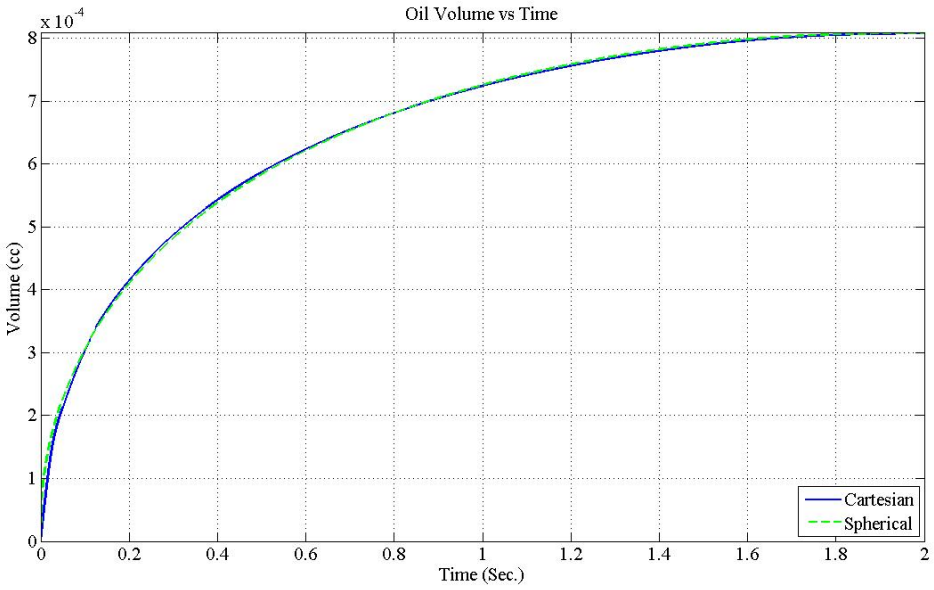

Figure 5.61: k_x=70 mD, k_y=65 mD, k_z=15 mD (Interpreted k=60.74 mD)

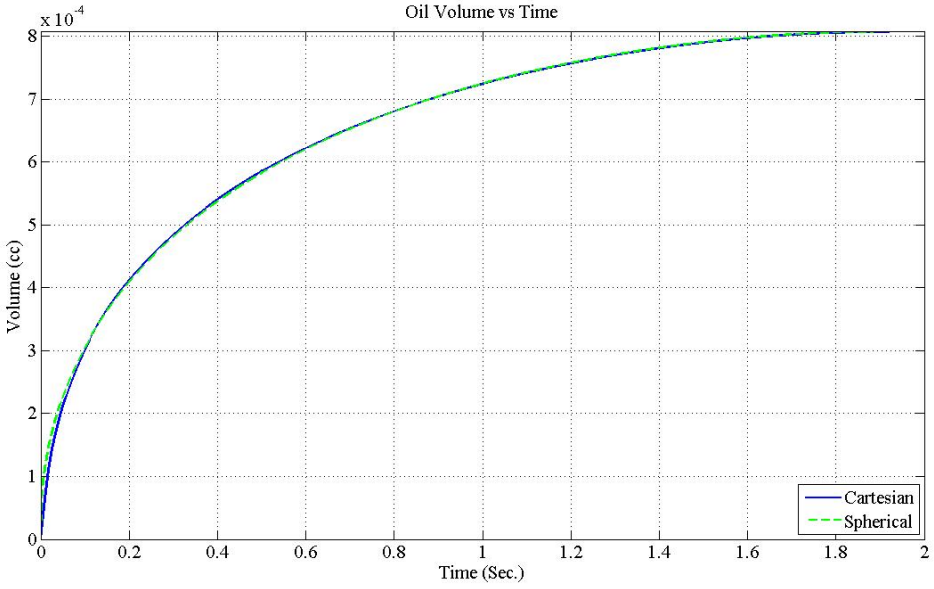

Figure 5.62: k_x=90 mD, k_y=45 mD, k_z=15 mD (Interpreted k=60.41 mD)

A summary of the results is presented in Table 5.5.

Table 5.5: Anisotropy Effects (Multiple Directions)

Average Permeability	k_x	k_y	k_z	Estimated Permeability	Offset
mD	mD	mD	mD	mD	%
20	20	20	20	25.07	0.0
20	20	10	30	24.69	-1.5
20	25	20	15	24.98	-0.3
20	40	15	5	23.88	-4.7
50	50	50	50	62.67	0.0
50	70	60	20	61.38	-2.1
50	70	65	15	60.74	-3.1
50	90	45	15	60.41	-3.6

The results for all anisotropic cases yield results which are always slightly less in magnitude than those for the isotropic cutting. This fact agrees with our previous findings where a slight decrease in permeability along one axis always marked a percentage shift larger in magnitude than a same percentage increase in permeability along that axis would render.

The results signify the fact that testing of anisotropic cuttings would render permeability values equivalent to those of isotropic cuttings having some area weighted average permeability of the anisotropic cases.

5.3 Experimental Results

This section is focused upon the experimental testing carried out using the Darcy Log equipment. Coarse simulation runs were carried out before shaping the cuttings to

ascertain that the formulated shapes would be able to demonstrate the expected contrast in the responses.

5.3.1 Directional Permeability Measurements

With our work aimed at establishing the influence of cutting shape and anisotropy on the permeability measurements made using the Darcy Log equipment, it became imperative to use cutting samples of a know shape and anisotropy so as the results might be quantified into more analytical terms.

Though having a control on the shape to a certain extent, since the cuttings could be cut off from any larger sample into prescribed shapes up to a certain size with relative convenience and use of simple tools, the assignment or more the measurement of the directional permeability of the cuttings presented a much more arduous task.

To mitigate this problem, it was decided to take a core plug exhibiting a sufficient permeability contrast along its axial and radial directions, measure the said permeabilities using the standard steady state method and then cut it into prescribed shapes for testing with the Darcy Log apparatus.

Problems were faced in finding the appropriate core plugs since the ones available were either carbonates from very tight formations or very high permeability sandstones (Berea) which could not be tested with even the fully concentrated glycerin available owing to an inadequate viscosity. Furthermore, the samples needed be free from any visible heterogeneities and cracks which could have an impact at throwing our measurements off board.

Though, given the system capabilities, an ideal choice would have been a sample with permeability in the range of 10 mD to 20 mD, the only one we had to work with in the end was one sample with an axial permeability of approximately 61 mD.

The complexity was to measure the permeability along the radial directions to get a complete three dimensional permeability profile of the available sample. The challenge was to cause radial flow across the core sample using a standard core holder.

The objective was achieved making slight modifications in the standard end pieces. Holes were drilled axially up till mid way through cylindrical metallic plugs with outer diameters equivalent to that of the end pieces provided with the available permeameter. A radial hole was then drilled horizontally from one of the cylindrical surfaces, coming to terminate at the existing axial passage.

The two radial holes are aligned at the opposite ends of the two sides of a chord running through the axis of the plug. The core sample is placed between them with a mesh screen running the length of the core plug from the drilled hole till a short distance from the opposite end piece. This way, we were able to ensure a radial flow of gas, nitrogen in our case, across the sample. The flow rates and the corresponding pressure differentials and overburden pressures were noted. The readings were then converted to give physical values of permeability using the model proposed by **Al-Yousef** [1].

The selected sample thus had a permeability of 61mD in the axial and a variation in the range of 34 mD to 36 mD along the radial directions. Since the variation was slight, we assumed a mean value of 35 mD for the radial directions as the variations might have been introduced due to experimental errors. The permeability range, though high for

testing small cuttings in the Darcy Log equipment, using comparable larger pieces cut out from the sample along each of the three major permeabilities had to suffice to keep the response times in perspective. The porosity displayed by the sample was measured to be 19.71%.

5.3.2 Darcy Log Procedure

IFP has developed a method to measure a wide range of permeability values from drill cuttings. Their proposed method has been modeled paying emphasis to simplicity to make the equipment and procedure straightforward enough to be employed at the drill site by a moderately trained crew. In their experimental procedure, to allow for measurement of higher permeability values, they established 'an effective flow of viscous oil, effectively to keep the mobility (k/μ) small enough to have an impact on the pressure regime, into the cuttings by compression of residual gas initially trapped into the cuttings. The pressure history is then history matched against the numerical model to obtain the value of permeability' [2].

The procedure requires roughly a volume of 3 - 3.5 g of cuttings to be placed in the pressure vessel. The cuttings are de-aired, preferably using helium since it has a very low volumetric diffusion into the oil, and saturated with viscous oil which completely fills the test chamber. Oil invasion into the cuttings results in a small volume of gas to get trapped inside the cuttings as disconnected ganglia. A pressure pulse applied to the chamber causes the viscous oil to enter into the cuttings, compressing the trapped gas.

As the step pressure diffuses, the pressure history is recorded to be history matched against the simulated pressure diffusion.

5.3.3 Results and Discussions

As many as five cuttings of different shapes and sizes were cut out from the sample. The number and sizes were more constrained by core plug properties and the chamber size of the available Darcy Log apparatus. The apparatus has been designed for the specific task of recording the pressure responses of cuttings of dimensions more representative of the actual ones obtainable form the field. While the maximum size was constrained by the chamber dimensions, the minimum limits were imposed by the physics of the whole procedure. Making the cuttings too small would require a very high viscosity oil to be able to at least ascertain a sufficient equilibrium time to register an interpretable response. The available viscous oil (glycerin in our case) had a maximum attainable viscosity under laboratory conditions of something close to 900 cp.

Furthermore, before fabricating the prescribed shapes, preliminary simulation runs were made to ascertain if the shapes would suffice to emphasize the influence of geometry and permeability directionality on the obtainable results.

Even with this viscosity of glycerin and the high permeability of the sample, it was very difficult to affect spontaneous imbibitions. The glycerin, thus, had to be force imbibed into the cuttings to result in discontinuous or irreducible gas saturation. Although the glycerin used in all simulation runs was of the same concentration (100%), slight

variations in temperature influenced the viscosity for the various experimental runs. The viscosity of the glycerin, thus, is stated separately for each sample tested.

Five fabricated cuttings, labeled alphabetically in the ascending order, representing two approximate bulk volumes were studied experimentally using the Darcy Log equipment. The complete description and interpretation of results for each case is presented henceforth.

The three values of permeability used along each of the three axes were, along with the effective porosity of the cutting determined are presented in Table 5.6.

Table 5.6: Core Plug Properties

k_x	61 mD
k_y	35 mD
k_z	35 mD
φ	19.71 %

For the properties defined for each sample, using the value of viscosity for the pertinent temperature for the concerned sample and the estimated residual gas saturation, simulation runs were made using the finite difference model. The value of permeability, thus estimated, was then compared with that obtained from the experimental process.

The first cutting size was selected based upon the smallest net volume necessary to keep the equilibrium or settling time in perspective. Note that the experimental procedure demands the pressure response to be curve fitted at least over one log cycle with the data below 0.2 seconds considered erroneous. Three shape variations roughly amounted to a volume which can be grouped together in this section.

5.3.3.1 Sample A (Volume 1)

The cutting geometry and other relevant fluid properties are presented in the Table 5.7.

Table 5.7: Geometry & Fluid Properties (Sample A)

x length	10.1 mm
y length	9.9 mm
z length	10.3 mm
μ_o	725 cp
S_g	0.173

The curve-fitted response is presented in Figure 5.63. The permeability was determined to be 55.45 mD.

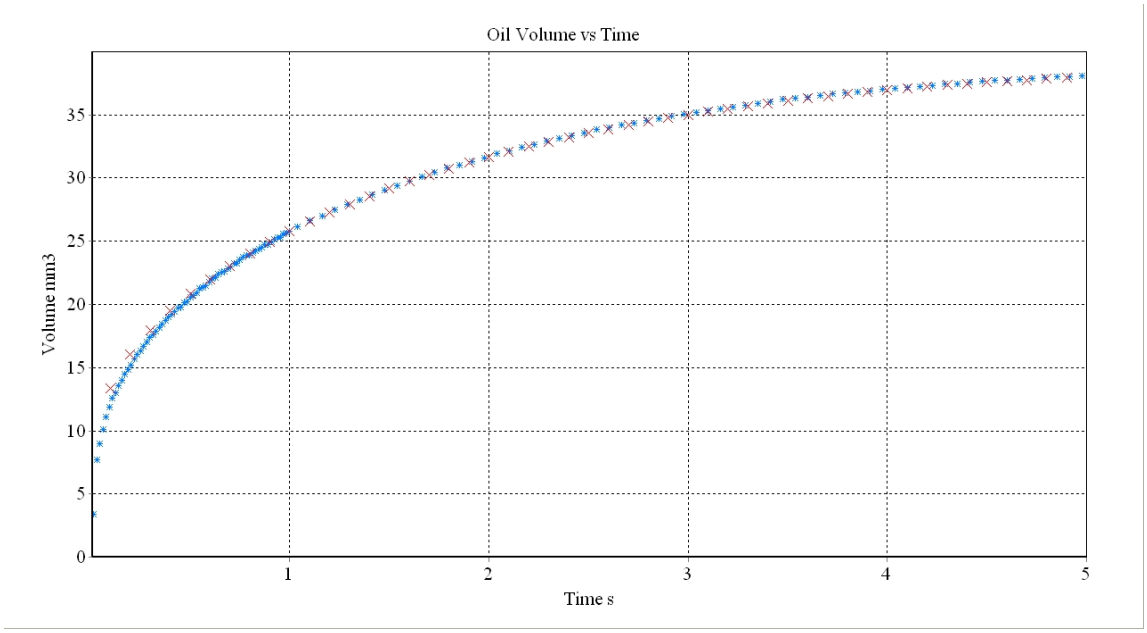

Figure 5.63: Experimental results for sample A (Measured k=55.45 mD)

Figure 5.64 presents the results obtained from the simulation run made for the same experimental conditions.

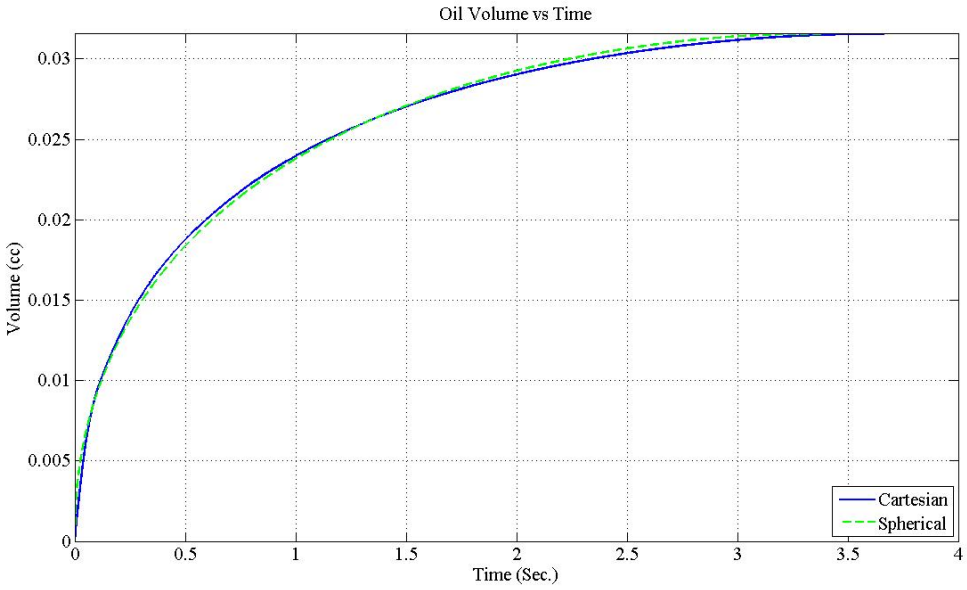

Figure 5.64: Simulation results for sample A (Estimated k=54.74 mD)

5.3.3.2 Sample B (Volume 1)

The cutting geometry and other relevant fluid properties are presented in Table 5.8.

Table 5.8: Geometry & Fluid Properties (Sample B)

x length	6.6 mm
y length	10.2 mm
z length	15.3 mm
μ_o	750 cp
S_g	0.173

The curve fitted response is presented in Figure 5.65. The permeability was determined to be 74.68 mD.

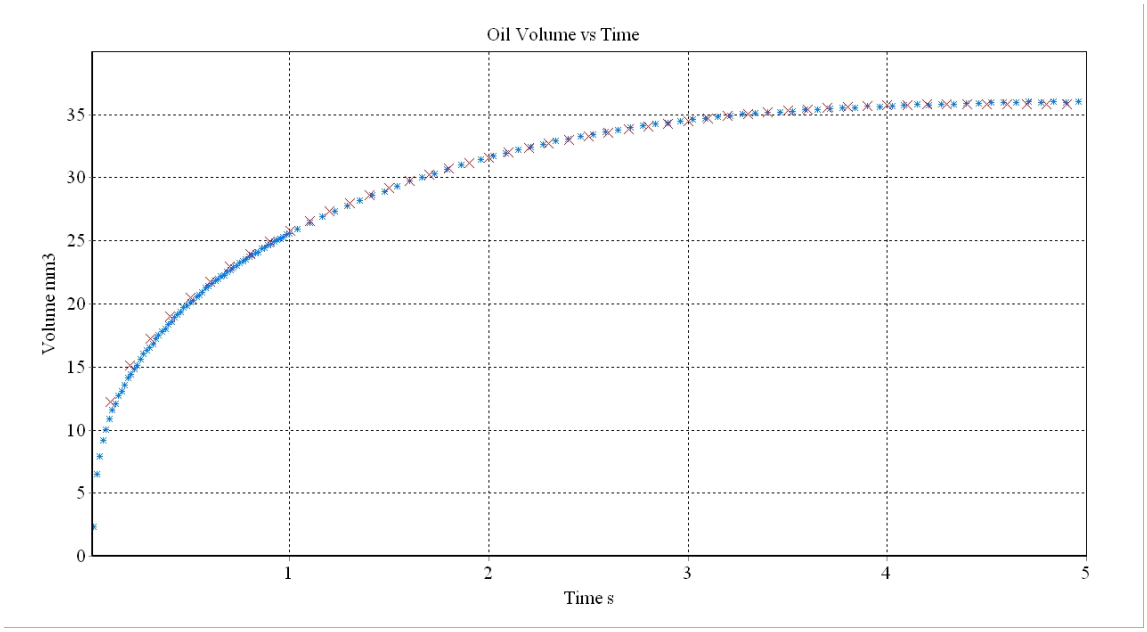

Figure 5.65: Experimental results for sample B (Measured k=74.68 mD)

The simulation runs for the same initial and boundary conditions for the measured rock and fluid properties are given in Figure 5.66.

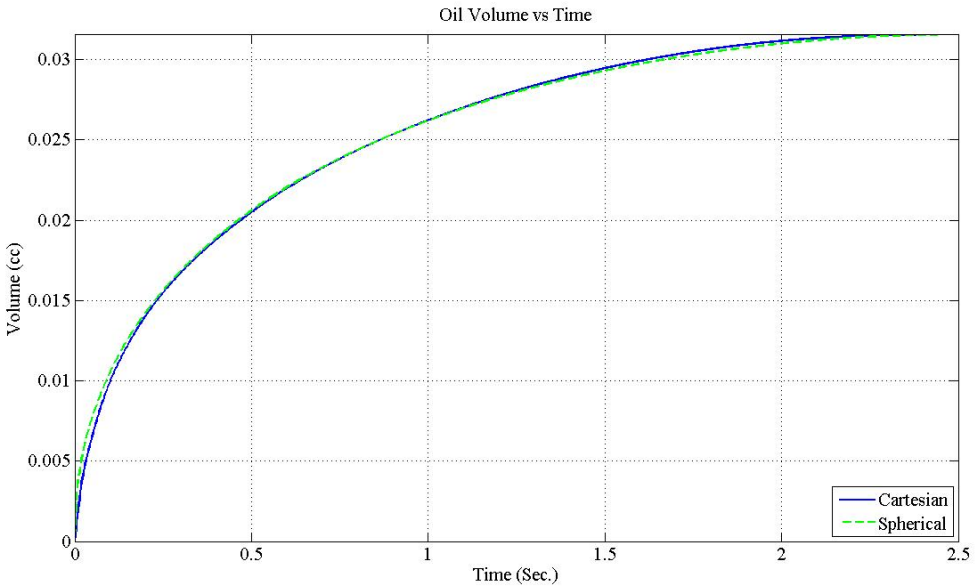

Figure 5.66: Simulation results for sample B (Estimated k=75.77 mD)

5.3.3.3 Sample C (Volume 1)

The cutting geometry and other relevant fluid properties are presented in the Table 5.9.

Table 5.9: Geometry & Fluid Properties (Sample C)

x length	13 mm
y length	7.7 mm
z length	10.5 mm
μ_o	826 cp
S_g	0.151

The curve fitted response is presented in Figure 5.67. The permeability was determined to be 53.29 mD.

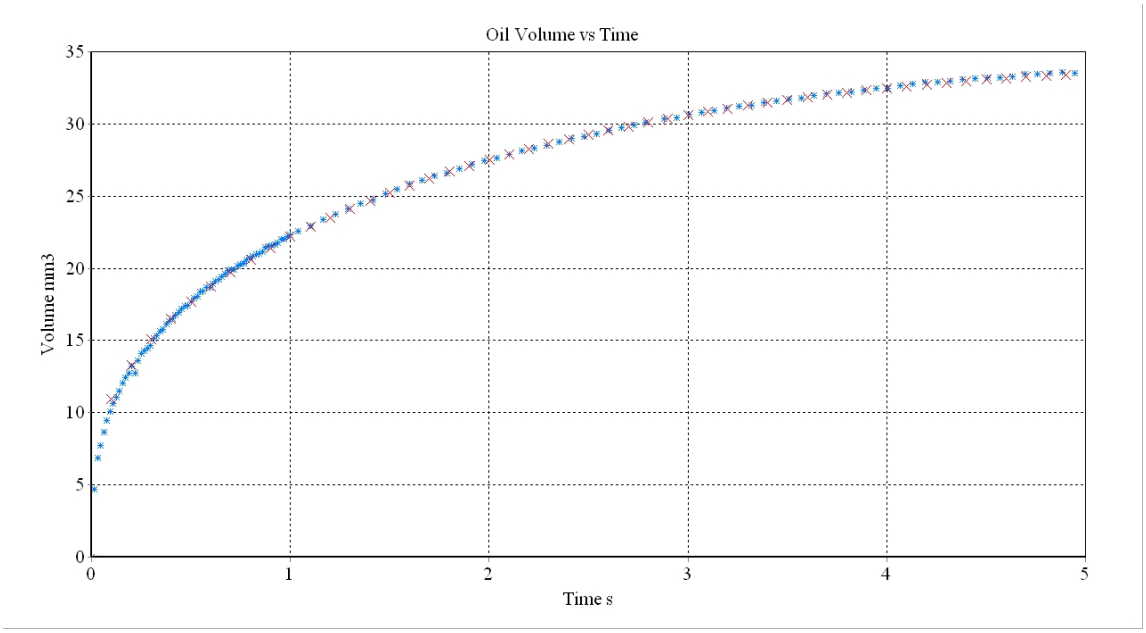

Figure 5.67: Experimental results for sample C (Measured k=53.29 mD)

A plot of the curve fit obtained for the simulated response is shown in Figure 5.68.

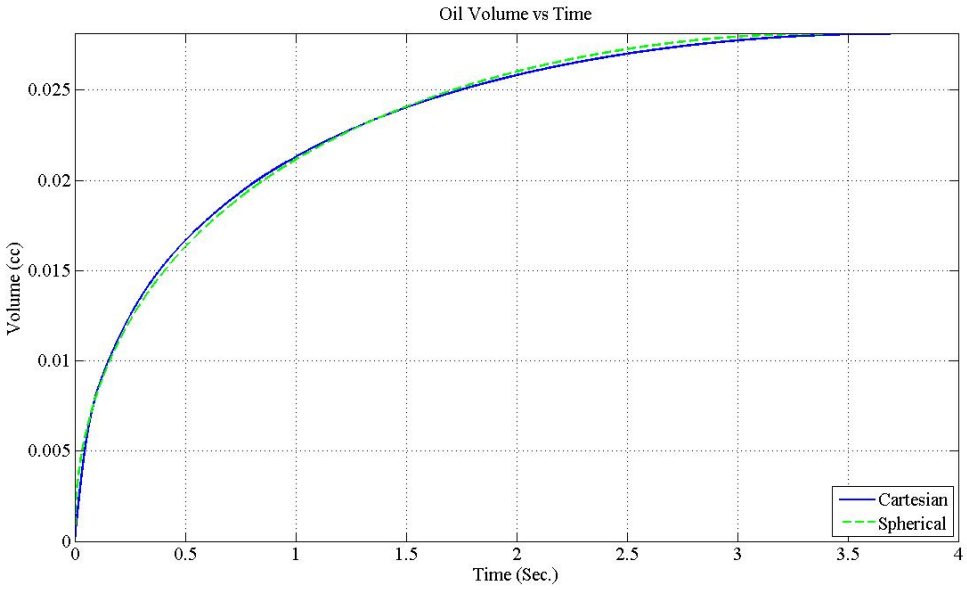

Figure 5.68: Simulation results for sample C (Estimated k=54.78 mD)

We ended off with the largest cutting volume, the shape variations of which could easily be accommodated inside the test chamber. The cubic formulation was not tested, since the purpose was just to ascertain the impact of permeability anisotropy. For each of the two non-cubic fabricated cuttings, the largest surface area was first kept perpendicular to the largest permeability (Sample D) and then later to the smallest permeability (Sample E). The responses were recorded and then interpreted assuming a spherical shape with the Darcy Log equipment and software.

5.3.3.4 Sample D (Volume 2)

The cutting geometry and other relevant fluid properties are presented in Table 5.10.

Table 5.10: Geometry & Fluid Properties (Sample D)

x length	10.6 mm
y length	10.7 mm
z length	24.5 mm
μ_o	752 cp
S_g	0.159

The curve fitted response is presented in Figure 5.69. The permeability was determined to be 72.44 mD.

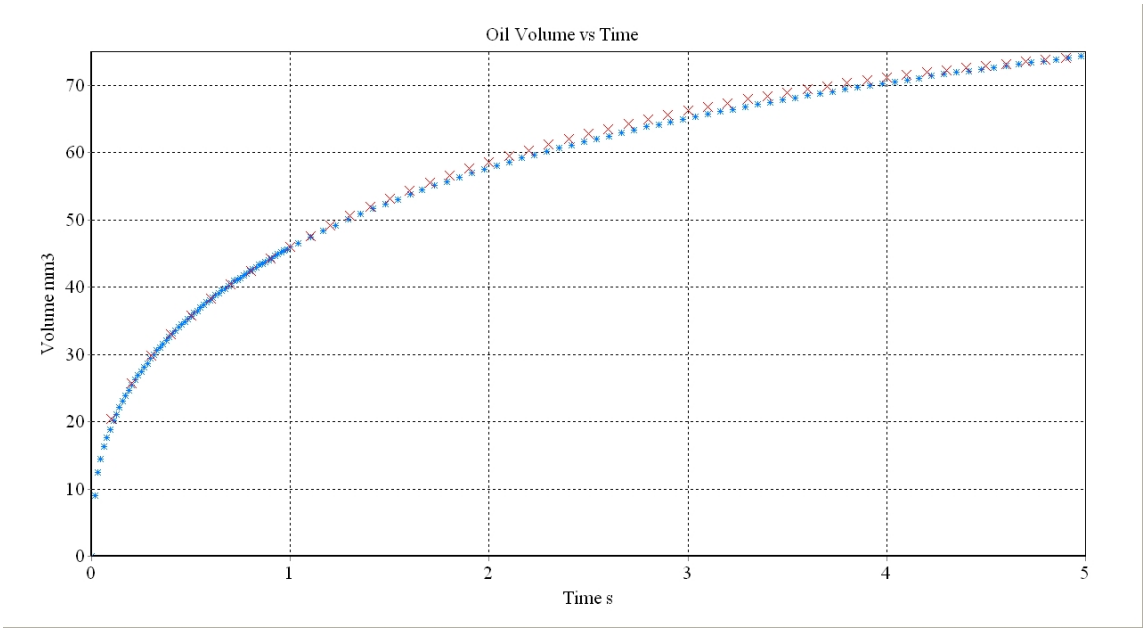

Figure 5.69: Experimental results for sample D (Measured k=72.44 mD)

Fig 5.70 presents the results obtained from the simulation run made for the same experimental conditions.

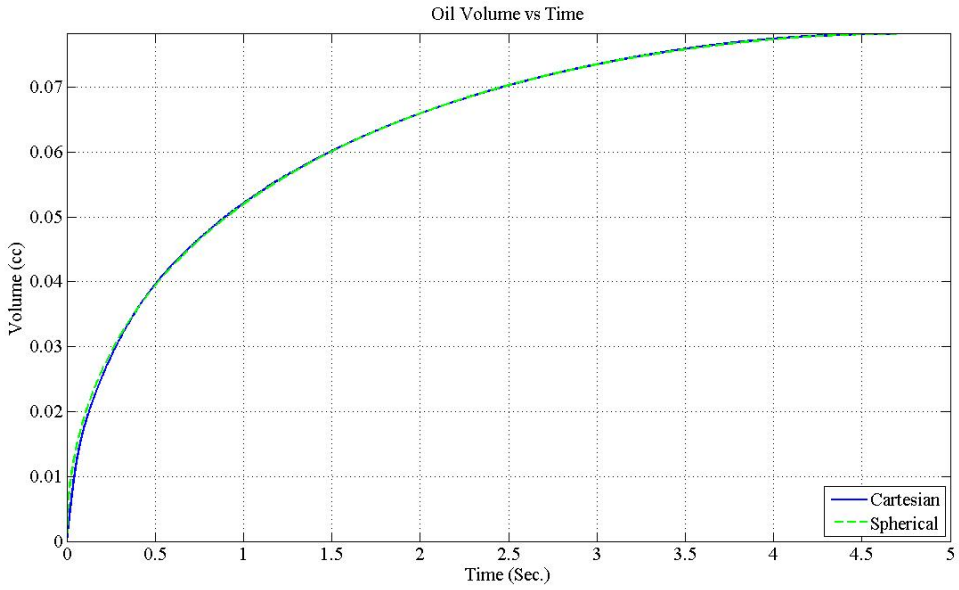

Figure 5.70: Simulation results for sample D (Estimated k=71.52 mD)

5.3.3.5 Sample E (Volume 2)

The cutting geometry and other relevant fluid properties are presented in Table 5.11.

Table 5.11: Geometry & Fluid Properties (Sample E)

x length	25.6 mm
y length	9.6 mm
z length	10.4 mm
μ_o	743 cp
S_g	0.159

The curve fitted response is presented in Figure 5.71. The permeability was determined to be 60.35 mD.

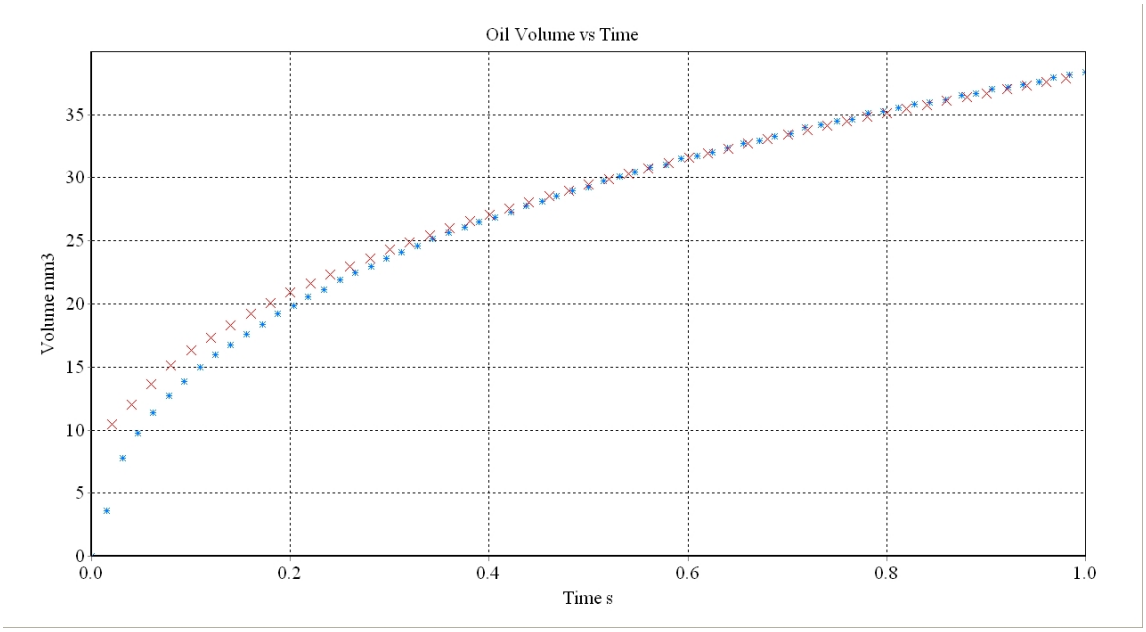

Figure 5.71: Experimental results for sample E (Measured k=60.35 mD)

The simulation runs for the same initial and boundary conditions for the measured rock and fluid properties are given in Figure 5.72.

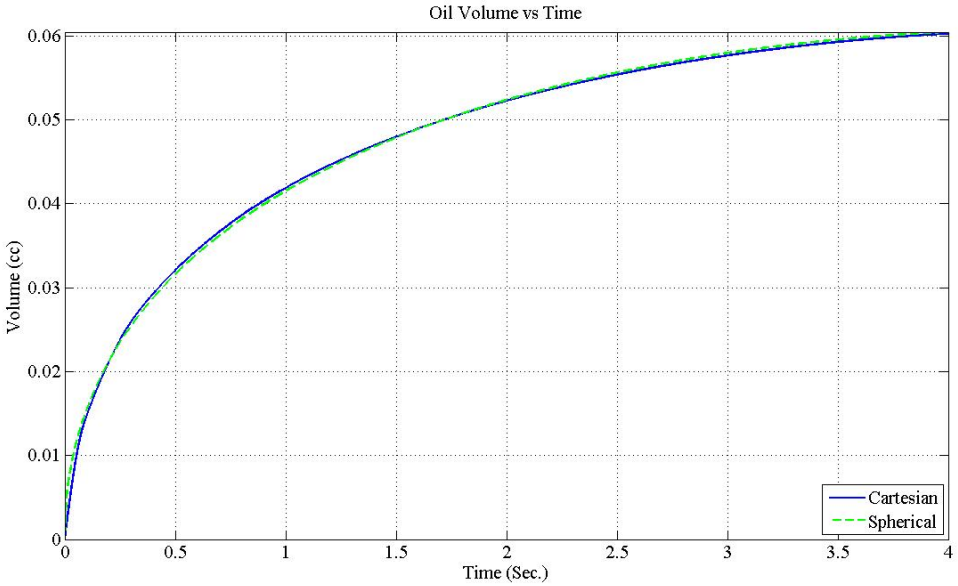

Figure 5.72: Simulation results for sample E (Estimated k=61.03 mD)

A summary of the results is presented in Table 5.12.

Table 5.12: Experimental vs. Simulated Results

Sample	Measured k mD	Simulated k mD	Error %
A	55.45	54.74	-1.28
B	74.68	75.77	1.46
C	53.29	54.78	2.8
D	72.44	71.52	-1.27
E	60.35	61.03	1.13

The table shows a very good agreement between the experimental and simulated results. Furthermore, the experimental results further go to help support our premise that the cutting geometry and anisotropy can have significant influence on the obtainable results from the pressure diffusion technique.

Note that the Darcy Log equipment has rendered best results for permeability ranges in the micro-Darcy to the few milli-Darcy range. A possible reason for accuracy in this range is owing to the fact that within this range, the permeability contrast, resulting from anisotropy or asymmetry is not so significant to cause a measureable error in the interpretable permeability.

CHAPTER 6

CONCLUSIONS AND RECOMMENDATIONS

6.1 Conclusions

A numerical model was developed to study the impact of cutting geometry and anisotropy on permeability measurements from drill cuttings. The results obtained from the numerical simulator were in excellent agreement with those obtained experimentally. Based on the results of this study, the following conclusions can be deduced:

1) The percentage deviation in the interpreted value of permeability in the absence of anisotropy is almost constant for same aspect ratios.
2) The larger interpreted value of permeability is a consequence of assuming the cutting spherical while curve fitting. The increased surface area is translated as a larger net value of permeability.
3) A percent decrease in the induced permeability along an arbitrary axis retards the stabilization time and the pressure response curve almost to the same degree as a percent increase would accelerate it under consistent initial and boundary conditions.
4) The permeability normal to the largest surface area would have the greatest influence upon the interpreted permeability for rectangular cuboids.

5) The testing of anisotropic cuttings would render permeability values equivalent to those from isotropic cuttings having some area weighted average permeability of the anisotropic cases.
6) Cutting shape has the largest influence on the resultant pressure responses.

6.2 Recommendations

Though the study has managed to highlight the impact of cutting geometry and anisotropy on permeability measurements from drill cuttings, the work was primarily restricted to regular shaped cuttings (rectangular cuboids). Furthermore, the experimental activity was also restricted to the various shapes and sizes obtainable from the one core sample due to the unavailability of core plugs displaying the desired degree of permeability anisotropy. Given the right degree of knowledge and resources, this work can be extended in the following areas:

1) Flexible grid model may in future be adopted to curve fit the pressure response to get a more accurate estimation of permeability.
2) Model the cutting using a finite element scheme to acquire more flexibility in defining irregular shapes to be numerically investigated.
3) Experimentally testing irregular shaped cuttings, both isotropic and anisotropic, to study the impact of shape and anisotropy on a broader spectrum.

Appendix A

Cartesian Model

Applying the central difference scheme to the second ordered pressure differential in Equation 4.17 we get,

$$\frac{\partial^2 P}{\partial x^2} = \frac{\left(\frac{\partial P}{\partial x}\right)_{i+\frac{1}{2}} - \left(\frac{\partial P}{\partial x}\right)_{i-\frac{1}{2}}}{x_{i+\frac{1}{2}} - x_{i-\frac{1}{2}}} \qquad \text{A.01}$$

Since,

$$x_{i+\frac{1}{2}} - x_{i-\frac{1}{2}} = \Delta x_i \qquad \text{A.02}$$

So,

$$\frac{\partial^2 P}{\partial x^2} = \frac{1}{\Delta x_i} \times \left[\frac{P_{i+1} - P_i}{x_{i+1} - x_i} - \frac{P_i - P_{i-1}}{x_i - x_{i-1}} \right] \qquad \text{A.03}$$

Similar steps can be taken for the other directions as well. Similarly, for time,

$$\frac{\partial P}{\partial t} = \frac{P_{node}^{n+1} - P_{node}^{n}}{\Delta t} \qquad \text{A.04}$$

Substituting back, Equation 4.17 becomes,

$$\frac{k_x}{\Delta x_i} \times \left[\frac{P_{i+1} - P_i}{x_{i+1} - x_i} - \frac{P_i - P_{i-1}}{x_i - x_{i-1}} \right] + \frac{k_y}{\Delta y_j} \times \left[\frac{P_{j+1} - P_j}{y_{j+1} - y_j} - \frac{P_j - P_{j-1}}{y_j - y_{j-1}} \right] +$$

$$\frac{k_z}{\Delta z_k} \times \left[\frac{P_{k+1} - P_k}{z_{k+1} - z_k} - \frac{P_k - P_{k-1}}{z_k - z_{k-1}} \right] = \phi \times \mu_o \times S_{g_{ini}} \times \frac{P_{ini}}{P^2} \times \frac{P^{n+1} - P^n}{\Delta t} \qquad \text{A.05}$$

Taking,

$$V_p = \phi \times \Delta x_i \times \Delta y_j \times \Delta z_k \tag{A.06}$$

Multiplying both sides of Equation A.05 by $\Delta x_i \times \Delta y_j \times \Delta z_k$, we get,

$$k_x \times \Delta y_j \times \Delta z_k \times \left[\frac{P_{i+1} - P_i}{x_{i+1} - x_i} - \frac{P_i - P_{i-1}}{x_i - x_{i-1}} \right] + k_y \times \Delta x_i \times \Delta z_k \times \left[\frac{P_{j+1} - P_j}{y_{j+1} - y_j} - \frac{P_j - P_{j-1}}{y_j - y_{j-1}} \right] +$$

$$k_z \times \Delta x_i \times \Delta y_j \times \left[\frac{P_{k+1} - P_k}{z_{k+1} - z_k} - \frac{P_k - P_{k-1}}{z_k - z_{k-1}} \right] = V_p \times \mu_o \times S_{g_{ini}} \times \frac{P_{ini}}{P^2} \times \frac{P^{n+1} - P^n}{\Delta t} \tag{A.07}$$

Since,

$$P_{ijk} = P_{node} \tag{A.08}$$

So,

$$k_x \times \Delta y_j \times \Delta z_k \times \left[\frac{P_{i+1} - P_{node}}{x_{i+1} - x_i} - \frac{P_{node} - P_{i-1}}{x_i - x_{i-1}} \right] + k_y \times \Delta x_i \times \Delta z_k \times \left[\frac{P_{j+1} - P_{node}}{y_{j+1} - y_j} - \frac{P_{node} - P_{j-1}}{y_j - y_{j-1}} \right] +$$

$$k_z \times \Delta x_i \times \Delta y_j \times \left[\frac{P_{k+1} - P_{node}}{z_{k+1} - z_k} - \frac{P_{node} - P_{k-1}}{z_k - z_{k-1}} \right] = V_p \times \mu_o \times S_{g_{ini}} \times \frac{P_{ini}}{P_{node}^2} \times \frac{P_{node}^{n+1} - P_{node}^n}{\Delta t} \tag{A.09}$$

Since,

$$x_i - x_{i-1} = \frac{\Delta x_i + \Delta x_{i-1}}{2} \tag{A.10}$$

$$x_{i+1} - x_i = \frac{\Delta x_{i+1} + \Delta x_i}{2} \tag{A.11}$$

$$y_j - y_{j-1} = \frac{\Delta y_j + \Delta y_{j-1}}{2} \tag{A.12}$$

$$y_{j+1} - y_j = \frac{\Delta y_{j+1} + \Delta y_j}{2} \tag{A.13}$$

$$z_k - z_{k-1} = \frac{\Delta z_k + \Delta z_{k-1}}{2} \qquad \text{A.14}$$

$$z_{k+1} - z_k = \frac{\Delta z_{k+1} + \Delta z_k}{2} \qquad \text{A.15}$$

Equation A.09 becomes,

$$2 \times k_x \times \Delta y_j \times \Delta z_k \times \left[\frac{P_{i+1} - P_{node}}{\Delta x_{i+1} + \Delta x_i} - \frac{P_{node} - P_{i-1}}{\Delta x_i + \Delta x_{i-1}} \right] + 2 \times k_y \times \Delta x_i \times \Delta z_k \times \left[\frac{P_{j+1} - P_{node}}{\Delta y_{j+1} + \Delta y_j} - \frac{P_{node} - P_{j-1}}{\Delta y_j + \Delta y_{j-1}} \right] +$$

$$2 \times k_z \times \Delta x_i \times \Delta y_j \times \left[\frac{P_{k+1} - P_{node}}{\Delta z_{k+1} + \Delta z_k} - \frac{P_{node} - P_{k-1}}{\Delta z_k + \Delta z_{k-1}} \right] = V_p \times \mu_o \times S_{g_{ini}} \times \frac{P_{ini}}{P_{node}^2} \times \frac{P_{node}^{n+1} - P_{node}^n}{\Delta t} \qquad \text{A.16}$$

Equation A.16 thus reached is suitable for all points other than those making up the boundaries. Considering a rectangular shaped chip immersed in a liquid applying equal pressure on each face, there will exist a no-flow boundary bisecting each length of the cutting. Thus, one eighth of the volume of the cutting can be used to simulate the pressure diffusion process with the face forming up the surfaces exposed directly to the liquid being represented by a constant or a specified pressure boundary. Thus,

When i = 1,

When j = 1,

When k = 1,

$$2 \times k_x \times \Delta y_j \times \Delta z_k \times \left[\frac{P_{i+1} - P_{node}}{\Delta x_{i+1} + \Delta x_i} - \frac{P_{node} - P_{cell}}{\Delta x_i} \right] + 2 \times k_y \times \Delta x_i \times \Delta z_k \times \left[\frac{P_{j+1} - P_{node}}{\Delta y_{j+1} + \Delta y_j} - \frac{P_{node} - P_{cell}}{\Delta y_j} \right] +$$

$$2 \times k_z \times \Delta x_i \times \Delta y_j \times \left[\frac{P_{k+1} - P_{node}}{\Delta z_{k+1} + \Delta z_k} - \frac{P_{node} - P_{cell}}{\Delta z_k} \right] = V_p \times \mu_o \times S_{g_{ini}} \times \frac{P_{ini}}{P_{node}^2} \times \frac{P_{node}^{n+1} - P_{node}^n}{\Delta t} \qquad \text{A.17}$$

When k = 2 to k = N – 1,

$$2\times k_x\times\Delta y_j\times\Delta z_k\times\left[\frac{P_{i+1}-P_{node}}{\Delta x_{i+1}+\Delta x_i}-\frac{P_{node}-P_{cell}}{\Delta x_i}\right]+2\times k_y\times\Delta x_i\times\Delta z_k\times\left[\frac{P_{j+1}-P_{node}}{\Delta y_{j+1}+\Delta y_j}-\frac{P_{node}-P_{cell}}{\Delta y_j}\right]+$$

$$2\times k_z\times\Delta x_i\times\Delta y_j\times\left[\frac{P_{k+1}-P_{node}}{\Delta z_{k+1}+\Delta z_k}-\frac{P_{node}-P_{k-1}}{\Delta z_k+\Delta z_{k-1}}\right]=V_p\times\mu_o\times S_{g_{ini}}\times\frac{P_{ini}}{P_{node}^2}\times\frac{P_{node}^{n+1}-P_{node}^{n}}{\Delta t} \quad \text{A.18}$$

When k = N,

$$2\times k_x\times\Delta y_j\times\Delta z_k\times\left[\frac{P_{i+1}-P_{node}}{\Delta x_{i+1}+\Delta x_i}-\frac{P_{node}-P_{cell}}{\Delta x_i}\right]+2\times k_y\times\Delta x_i\times\Delta z_k\times\left[\frac{P_{j+1}-P_{node}}{\Delta y_{j+1}+\Delta y_j}-\frac{P_{node}-P_{cell}}{\Delta y_j}\right]+$$

$$2\times k_z\times\Delta x_i\times\Delta y_j\times\left[0-\frac{P_{node}-P_{k-1}}{\Delta z_k+\Delta z_{k-1}}\right]=V_p\times\mu_o\times S_{g_{ini}}\times\frac{P_{ini}}{P_{node}^2}\times\frac{P_{node}^{n+1}-P_{node}^{n}}{\Delta t} \quad \text{A.19}$$

When j = 2 to j = N-1,

When k = 1,

$$2\times k_x\times\Delta y_j\times\Delta z_k\times\left[\frac{P_{i+1}-P_{node}}{\Delta x_{i+1}+\Delta x_i}-\frac{P_{node}-P_{cell}}{\Delta x_i}\right]+2\times k_y\times\Delta x_i\times\Delta z_k\times\left[\frac{P_{j+1}-P_{node}}{\Delta y_{j+1}+\Delta y_j}-\frac{P_{node}-P_{j-1}}{\Delta y_j+\Delta y_{j-1}}\right]+$$

$$2\times k_z\times\Delta x_i\times\Delta y_j\times\left[\frac{P_{k+1}-P_{node}}{\Delta z_{k+1}+\Delta z_k}-\frac{P_{node}-P_{cell}}{\Delta z_k}\right]=V_p\times\mu_o\times S_{g_{ini}}\times\frac{P_{ini}}{P_{node}^2}\times\frac{P_{node}^{n+1}-P_{node}^{n}}{\Delta t} \quad \text{A.20}$$

When k = 2 to k = N – 1,

$$2\times k_x\times\Delta y_j\times\Delta z_k\times\left[\frac{P_{i+1}-P_{node}}{\Delta x_{i+1}+\Delta x_i}-\frac{P_{node}-P_{cell}}{\Delta x_i}\right]+2\times k_y\times\Delta x_i\times\Delta z_k\times\left[\frac{P_{j+1}-P_{node}}{\Delta y_{j+1}+\Delta y_j}-\frac{P_{node}-P_{j-1}}{\Delta y_j+\Delta y_{j-1}}\right]+$$
$$2\times k_z\times\Delta x_i\times\Delta y_j\times\left[\frac{P_{k+1}-P_{node}}{\Delta z_{k+1}+\Delta z_k}-\frac{P_{node}-P_{k-1}}{\Delta z_k+\Delta z_{k-1}}\right]=V_p\times\mu_o\times S_{g_{ini}}\times\frac{P_{ini}}{P_{node}^2}\times\frac{P_{node}^{n+1}-P_{node}^{n}}{\Delta t} \quad \text{A.21}$$

When k = N,

$$2\times k_x\times\Delta y_j\times\Delta z_k\times\left[\frac{P_{i+1}-P_{node}}{\Delta x_{i+1}+\Delta x_i}-\frac{P_{node}-P_{cell}}{\Delta x_i}\right]+2\times k_y\times\Delta x_i\times\Delta z_k\times\left[\frac{P_{j+1}-P_{node}}{\Delta y_{j+1}+\Delta y_j}-\frac{P_{node}-P_{j-1}}{\Delta y_j+\Delta y_{j-1}}\right]+$$
$$2\times k_z\times\Delta x_i\times\Delta y_j\times\left[0-\frac{P_{node}-P_{k-1}}{\Delta z_k+\Delta z_{k-1}}\right]=V_p\times\mu_o\times S_{g_{ini}}\times\frac{P_{ini}}{P_{node}^2}\times\frac{P_{node}^{n+1}-P_{node}^n}{\Delta t} \quad \text{A.22}$$

When j =N,

When k = 1,

$$2\times k_x\times\Delta y_j\times\Delta z_k\times\left[\frac{P_{i+1}-P_{node}}{\Delta x_{i+1}+\Delta x_i}-\frac{P_{node}-P_{cell}}{\Delta x_i}\right]+2\times k_y\times\Delta x_i\times\Delta z_k\times\left[0-\frac{P_{node}-P_{j-1}}{\Delta y_j+\Delta y_{j-1}}\right]+$$
$$2\times k_z\times\Delta x_i\times\Delta y_j\times\left[\frac{P_{k+1}-P_{node}}{\Delta z_{k+1}+\Delta z_k}-\frac{P_{node}-P_{cell}}{\Delta z_k}\right]=V_p\times\mu_o\times S_{g_{ini}}\times\frac{P_{ini}}{P_{node}^2}\times\frac{P_{node}^{n+1}-P_{node}^n}{\Delta t} \quad \text{A.23}$$

When k = 2 to k = N – 1,

$$2\times k_x\times\Delta y_j\times\Delta z_k\times\left[\frac{P_{i+1}-P_{node}}{\Delta x_{i+1}+\Delta x_i}-\frac{P_{node}-P_{cell}}{\Delta x_i}\right]+2\times k_y\times\Delta x_i\times\Delta z_k\times\left[0-\frac{P_{node}-P_{j-1}}{\Delta y_j+\Delta y_{j-1}}\right]+$$
$$2\times k_z\times\Delta x_i\times\Delta y_j\times\left[\frac{P_{k+1}-P_{node}}{\Delta z_{k+1}+\Delta z_k}-\frac{P_{node}-P_{k-1}}{\Delta z_k+\Delta z_{k-1}}\right]=V_p\times\mu_o\times S_{g_{ini}}\times\frac{P_{ini}}{P_{node}^2}\times\frac{P_{node}^{n+1}-P_{node}^n}{\Delta t} \quad \text{A.24}$$

When k = N,

$$2\times k_x\times\Delta y_j\times\Delta z_k\times\left[\frac{P_{i+1}-P_{node}}{\Delta x_{i+1}+\Delta x_i}-\frac{P_{node}-P_{cell}}{\Delta x_i}\right]+2\times k_y\times\Delta x_i\times\Delta z_k\times\left[0-\frac{P_{node}-P_{j-1}}{\Delta y_j+\Delta y_{j-1}}\right]+$$
$$2\times k_z\times\Delta x_i\times\Delta y_j\times\left[0-\frac{P_{node}-P_{k-1}}{\Delta z_k+\Delta z_{k-1}}\right]=V_p\times\mu_o\times S_{g_{ini}}\times\frac{P_{ini}}{P_{node}^2}\times\frac{P_{node}^{n+1}-P_{node}^n}{\Delta t} \quad \text{A.25}$$

When i = 2 to i = N-1,

When j = 1,

When k = 1,

$$2\times k_x\times\Delta y_j\times\Delta z_k\times\left[\frac{P_{i+1}-P_{node}}{\Delta x_{i+1}+\Delta x_i}-\frac{P_{node}-P_{i-1}}{\Delta x_i+\Delta x_{i-1}}\right]+2\times k_y\times\Delta x_i\times\Delta z_k\times\left[\frac{P_{j+1}-P_{node}}{\Delta y_{j+1}+\Delta y_j}-\frac{P_{node}-P_{cell}}{\Delta y_j}\right]+$$

$$2\times k_z\times\Delta x_i\times\Delta y_j\times\left[\frac{P_{k+1}-P_{node}}{\Delta z_{k+1}+\Delta z_k}-\frac{P_{node}-P_{cell}}{\Delta z_k}\right]=V_p\times\mu_o\times S_{g_{ini}}\times\frac{P_{ini}}{P_{node}^2}\times\frac{P_{node}^{n+1}-P_{node}^n}{\Delta t} \quad \text{A.26}$$

When k = 2 to k = N – 1,

$$2\times k_x\times\Delta y_j\times\Delta z_k\times\left[\frac{P_{i+1}-P_{node}}{\Delta x_{i+1}+\Delta x_i}-\frac{P_{node}-P_{i-1}}{\Delta x_i+\Delta x_{i-1}}\right]+2\times k_y\times\Delta x_i\times\Delta z_k\times\left[\frac{P_{j+1}-P_{node}}{\Delta y_{j+1}+\Delta y_j}-\frac{P_{node}-P_{cell}}{\Delta y_j}\right]+$$

$$2\times k_z\times\Delta x_i\times\Delta y_j\times\left[\frac{P_{k+1}-P_{node}}{\Delta z_{k+1}+\Delta z_k}-\frac{P_{node}-P_{k-1}}{\Delta z_k+\Delta z_{k-1}}\right]=V_p\times\mu_o\times S_{g_{ini}}\times\frac{P_{ini}}{P_{node}^2}\times\frac{P_{node}^{n+1}-P_{node}^n}{\Delta t} \quad \text{A.27}$$

When k = N,

$$2\times k_x\times\Delta y_j\times\Delta z_k\times\left[\frac{P_{i+1}-P_{node}}{\Delta x_{i+1}+\Delta x_i}-\frac{P_{node}-P_{i-1}}{\Delta x_i+\Delta x_{i-1}}\right]+2\times k_y\times\Delta x_i\times\Delta z_k\times\left[\frac{P_{j+1}-P_{node}}{\Delta y_{j+1}+\Delta y_j}-\frac{P_{node}-P_{cell}}{\Delta y_j}\right]+$$

$$2\times k_z\times\Delta x_i\times\Delta y_j\times\left[0-\frac{P_{node}-P_{k-1}}{\Delta z_k+\Delta z_{k-1}}\right]=V_p\times\mu_o\times S_{g_{ini}}\times\frac{P_{ini}}{P_{node}^2}\times\frac{P_{node}^{n+1}-P_{node}^n}{\Delta t} \quad \text{A.28}$$

When j = 2 to j = N-1,

When k = 1,

$$2\times k_x\times\Delta y_j\times\Delta z_k\times\left[\frac{P_{i+1}-P_{node}}{\Delta x_{i+1}+\Delta x_i}-\frac{P_{node}-P_{i-1}}{\Delta x_i+\Delta x_{i-1}}\right]+2\times k_y\times\Delta x_i\times\Delta z_k\times\left[\frac{P_{j+1}-P_{node}}{\Delta y_{j+1}+\Delta y_j}-\frac{P_{node}-P_{j-1}}{\Delta y_j+\Delta y_{j-1}}\right]+$$

$$2\times k_z\times\Delta x_i\times\Delta y_j\times\left[\frac{P_{k+1}-P_{node}}{\Delta z_{k+1}+\Delta z_k}-\frac{P_{node}-P_{cell}}{\Delta z_k}\right]=V_p\times\mu_o\times S_{g_{ini}}\times\frac{P_{ini}}{P_{node}^2}\times\frac{P_{node}^{n+1}-P_{node}^n}{\Delta t} \quad \text{A.29}$$

When k = 2 to k = N – 1,

$$2\times k_x\times\Delta y_j\times\Delta z_k\times\left[\frac{P_{i+1}-P_{node}}{\Delta x_{i+1}+\Delta x_i}-\frac{P_{node}-P_{i-1}}{\Delta x_i+\Delta x_{i-1}}\right]+2\times k_y\times\Delta x_i\times\Delta z_k\times\left[\frac{P_{j+1}-P_{node}}{\Delta y_{j+1}+\Delta y_j}-\frac{P_{node}-P_{j-1}}{\Delta y_j+\Delta y_{j-1}}\right]+$$
$$2\times k_z\times\Delta x_i\times\Delta y_j\times\left[\frac{P_{k+1}-P_{node}}{\Delta z_{k+1}+\Delta z_k}-\frac{P_{node}-P_{k-1}}{\Delta z_k+\Delta z_{k-1}}\right]=V_p\times\mu_o\times S_{g_{ini}}\times\frac{P_{ini}}{P_{node}^2}\times\frac{P_{node}^{n+1}-P_{node}^n}{\Delta t} \quad \text{A.30}$$

When k = N,

$$2\times k_x\times\Delta y_j\times\Delta z_k\times\left[\frac{P_{i+1}-P_{node}}{\Delta x_{i+1}+\Delta x_i}-\frac{P_{node}-P_{i-1}}{\Delta x_i+\Delta x_{i-1}}\right]+2\times k_y\times\Delta x_i\times\Delta z_k\times\left[\frac{P_{j+1}-P_{node}}{\Delta y_{j+1}+\Delta y_j}-\frac{P_{node}-P_{j-1}}{\Delta y_j+\Delta y_{j-1}}\right]+$$
$$2\times k_z\times\Delta x_i\times\Delta y_j\times\left[0-\frac{P_{node}-P_{k-1}}{\Delta z_k+\Delta z_{k-1}}\right]=V_p\times\mu_o\times S_{g_{ini}}\times\frac{P_{ini}}{P_{node}^2}\times\frac{P_{node}^{n+1}-P_{node}^n}{\Delta t} \quad \text{A.31}$$

When j =N,

When k = 1,

$$2\times k_x\times\Delta y_j\times\Delta z_k\times\left[\frac{P_{i+1}-P_{node}}{\Delta x_{i+1}+\Delta x_i}-\frac{P_{node}-P_{i-1}}{\Delta x_i+\Delta x_{i-1}}\right]+2\times k_y\times\Delta x_i\times\Delta z_k\times\left[0-\frac{P_{node}-P_{j-1}}{\Delta y_j+\Delta y_{j-1}}\right]+$$
$$2\times k_z\times\Delta x_i\times\Delta y_j\times\left[\frac{P_{k+1}-P_{node}}{\Delta z_{k+1}+\Delta z_k}-\frac{P_{node}-P_{cell}}{\Delta z_k}\right]=V_p\times\mu_o\times S_{g_{ini}}\times\frac{P_{ini}}{P_{node}^2}\times\frac{P_{node}^{n+1}-P_{node}^n}{\Delta t} \quad \text{A.32}$$

When k = 2 to k = N – 1,

$$2\times k_x\times\Delta y_j\times\Delta z_k\times\left[\frac{P_{i+1}-P_{node}}{\Delta x_{i+1}+\Delta x_i}-\frac{P_{node}-P_{i-1}}{\Delta x_i+\Delta x_{i-1}}\right]+2\times k_y\times\Delta x_i\times\Delta z_k\times\left[0-\frac{P_{node}-P_{j-1}}{\Delta y_j+\Delta y_{j-1}}\right]+$$
$$2\times k_z\times\Delta x_i\times\Delta y_j\times\left[\frac{P_{k+1}-P_{node}}{\Delta z_{k+1}+\Delta z_k}-\frac{P_{node}-P_{k-1}}{\Delta z_k+\Delta z_{k-1}}\right]=V_p\times\mu_o\times S_{g_{ini}}\times\frac{P_{ini}}{P_{node}^2}\times\frac{P_{node}^{n+1}-P_{node}^n}{\Delta t} \quad \text{A.33}$$

When k = N,

$$2\times k_x\times\Delta y_j\times\Delta z_k\times\left[\frac{P_{i+1}-P_{node}}{\Delta x_{i+1}+\Delta x_i}-\frac{P_{node}-P_{i-1}}{\Delta x_i+\Delta x_{i-1}}\right]+2\times k_y\times\Delta x_i\times\Delta z_k\times\left[0-\frac{P_{node}-P_{j-1}}{\Delta y_j+\Delta y_{j-1}}\right]+$$

$$2\times k_z\times\Delta x_i\times\Delta y_j\times\left[0-\frac{P_{node}-P_{k-1}}{\Delta z_k+\Delta z_{k-1}}\right]=V_p\times\mu_o\times S_{g_{ini}}\times\frac{P_{ini}}{P_{node}^2}\times\frac{P_{node}^{n+1}-P_{node}^{n}}{\Delta t} \quad \text{A.34}$$

When i = N,

When j = 1,

When k = 1,

$$2\times k_x\times\Delta y_j\times\Delta z_k\times\left[0-\frac{P_{node}-P_{i-1}}{\Delta x_i+\Delta x_{i-1}}\right]+2\times k_y\times\Delta x_i\times\Delta z_k\times\left[\frac{P_{j+1}-P_{node}}{\Delta y_{j+1}+\Delta y_j}-\frac{P_{node}-P_{cell}}{\Delta y_j}\right]+$$

$$2\times k_z\times\Delta x_i\times\Delta y_j\times\left[\frac{P_{k+1}-P_{node}}{\Delta z_{k+1}+\Delta z_k}-\frac{P_{node}-P_{cell}}{\Delta z_k}\right]=V_p\times\mu_o\times S_{g_{ini}}\times\frac{P_{ini}}{P_{node}^2}\times\frac{P_{node}^{n+1}-P_{node}^{n}}{\Delta t} \quad \text{A.35}$$

When k = 2 to k = N – 1,

$$2\times k_x\times\Delta y_j\times\Delta z_k\times\left[0-\frac{P_{node}-P_{i-1}}{\Delta x_i+\Delta x_{i-1}}\right]+2\times k_y\times\Delta x_i\times\Delta z_k\times\left[\frac{P_{j+1}-P_{node}}{\Delta y_{j+1}+\Delta y_j}-\frac{P_{node}-P_{cell}}{\Delta y_j}\right]+$$

$$2\times k_z\times\Delta x_i\times\Delta y_j\times\left[\frac{P_{k+1}-P_{node}}{\Delta z_{k+1}+\Delta z_k}-\frac{P_{node}-P_{k-1}}{\Delta z_k+\Delta z_{k-1}}\right]=V_p\times\mu_o\times S_{g_{ini}}\times\frac{P_{ini}}{P_{node}^2}\times\frac{P_{node}^{n+1}-P_{node}^{n}}{\Delta t} \quad \text{A.36}$$

When k = N,

$$2\times k_x\times\Delta y_j\times\Delta z_k\times\left[0-\frac{P_{node}-P_{i-1}}{\Delta x_i+\Delta x_{i-1}}\right]+2\times k_y\times\Delta x_i\times\Delta z_k\times\left[\frac{P_{j+1}-P_{node}}{\Delta y_{j+1}+\Delta y_j}-\frac{P_{node}-P_{cell}}{\Delta y_j}\right]+$$

$$2\times k_z\times\Delta x_i\times\Delta y_j\times\left[0-\frac{P_{node}-P_{k-1}}{\Delta z_k+\Delta z_{k-1}}\right]=V_p\times\mu_o\times S_{g_{ini}}\times\frac{P_{ini}}{P_{node}^2}\times\frac{P_{node}^{n+1}-P_{node}^{n}}{\Delta t} \quad \text{A.37}$$

When j = 2 to j = N-1,

When k = 1,

$$2\times k_x\times\Delta y_j\times\Delta z_k\times\left[0-\frac{P_{node}-P_{i-1}}{\Delta x_i+\Delta x_{i-1}}\right]+2\times k_y\times\Delta x_i\times\Delta z_k\times\left[\frac{P_{j+1}-P_{node}}{\Delta y_{j+1}+\Delta y_j}-\frac{P_{node}-P_{j-1}}{\Delta y_j+\Delta y_{j-1}}\right]+$$

$$2\times k_z\times\Delta x_i\times\Delta y_j\times\left[\frac{P_{k+1}-P_{node}}{\Delta z_{k+1}+\Delta z_k}-\frac{P_{node}-P_{cell}}{\Delta z_k}\right]=V_p\times\mu_o\times S_{g_{ini}}\times\frac{P_{ini}}{P_{node}^2}\times\frac{P_{node}^{n+1}-P_{node}^n}{\Delta t} \quad \text{A.38}$$

When k = 2 to k = N – 1,

$$2\times k_x\times\Delta y_j\times\Delta z_k\times\left[0-\frac{P_{node}-P_{i-1}}{\Delta x_i+\Delta x_{i-1}}\right]+2\times k_y\times\Delta x_i\times\Delta z_k\times\left[\frac{P_{j+1}-P_{node}}{\Delta y_{j+1}+\Delta y_j}-\frac{P_{node}-P_{j-1}}{\Delta y_j+\Delta y_{j-1}}\right]+$$

$$2\times k_z\times\Delta x_i\times\Delta y_j\times\left[\frac{P_{k+1}-P_{node}}{\Delta z_{k+1}+\Delta z_k}-\frac{P_{node}-P_{k-1}}{\Delta z_k+\Delta z_{k-1}}\right]=V_p\times\mu_o\times S_{g_{ini}}\times\frac{P_{ini}}{P_{node}^2}\times\frac{P_{node}^{n+1}-P_{node}^n}{\Delta t} \quad \text{A.39}$$

When k = N,

$$2\times k_x\times\Delta y_j\times\Delta z_k\times\left[0-\frac{P_{node}-P_{i-1}}{\Delta x_i+\Delta x_{i-1}}\right]+2\times k_y\times\Delta x_i\times\Delta z_k\times\left[\frac{P_{j+1}-P_{node}}{\Delta y_{j+1}+\Delta y_j}-\frac{P_{node}-P_{j-1}}{\Delta y_j+\Delta y_{j-1}}\right]+$$

$$2\times k_z\times\Delta x_i\times\Delta y_j\times\left[0-\frac{P_{node}-P_{k-1}}{\Delta z_k+\Delta z_{k-1}}\right]=V_p\times\mu_o\times S_{g_{ini}}\times\frac{P_{ini}}{P_{node}^2}\times\frac{P_{node}^{n+1}-P_{node}^n}{\Delta t} \quad \text{A.40}$$

When j =N,

When k = 1,

$$2\times k_x\times\Delta y_j\times\Delta z_k\times\left[0-\frac{P_{node}-P_{i-1}}{\Delta x_i+\Delta x_{i-1}}\right]+2\times k_y\times\Delta x_i\times\Delta z_k\times\left[0-\frac{P_{node}-P_{j-1}}{\Delta y_j+\Delta y_{j-1}}\right]+$$

$$2\times k_z\times\Delta x_i\times\Delta y_j\times\left[\frac{P_{k+1}-P_{node}}{\Delta z_{k+1}+\Delta z_k}-\frac{P_{node}-P_{cell}}{\Delta z_k}\right]=V_p\times\mu_o\times S_{g_{ini}}\times\frac{P_{ini}}{P_{node}^2}\times\frac{P_{node}^{n+1}-P_{node}^n}{\Delta t} \quad \text{A.41}$$

When k = 2 to k = N – 1,

$$2\times k_x\times\Delta y_j\times\Delta z_k\times\left[0-\frac{P_{node}-P_{i-1}}{\Delta x_i+\Delta x_{i-1}}\right]+2\times k_y\times\Delta x_i\times\Delta z_k\times\left[0-\frac{P_{node}-P_{j-1}}{\Delta y_j+\Delta y_{j-1}}\right]+$$

$$2\times k_z\times\Delta x_i\times\Delta y_j\times\left[\frac{P_{k+1}-P_{node}}{\Delta z_{k+1}+\Delta z_k}-\frac{P_{node}-P_{k-1}}{\Delta z_k+\Delta z_{k-1}}\right]=V_p\times\mu_o\times S_{g_{ini}}\times\frac{P_{ini}}{P_{node}^2}\times\frac{P_{node}^{n+1}-P_{node}^n}{\Delta t} \quad \text{A.42}$$

When k = N,

$$2\times k_x\times\Delta y_j\times\Delta z_k\times\left[0-\frac{P_{node}-P_{i-1}}{\Delta x_i+\Delta x_{i-1}}\right]+2\times k_y\times\Delta x_i\times\Delta z_k\times\left[0-\frac{P_{node}-P_{j-1}}{\Delta y_j+\Delta y_{j-1}}\right]+$$

$$2\times k_z\times\Delta x_i\times\Delta y_j\times\left[0-\frac{P_{node}-P_{k-1}}{\Delta z_k+\Delta z_{k-1}}\right]=V_p\times\mu_o\times S_{g_{ini}}\times\frac{P_{ini}}{P_{node}^2}\times\frac{P_{node}^{n+1}-P_{node}^{n}}{\Delta t} \qquad \text{A.43}$$

An implicit solution of the equation reduces the concerns regarding stability. However, the reciprocal of pressure term being multiplied to the R.H.S (Equation A.17 to Equation A.43) makes the equations nonlinear. A way to reduce this problem is to take the pressure term at the old time level as an initial guess and then iterating until we get a reasonable match between the consecutive pressure values. Thus, solving the equations (Equation A.17 through Equation A.43) implicitly and resolving into its constituent components, we get,

When i = 1,

When j = 1,

When k = 1,

$$P_{node}^{n+1}\left[-2\times\left\{\begin{array}{l}k_x\times\Delta y_j\times\Delta z_k\times\left(\dfrac{1}{\Delta x_{i+1}+\Delta x_i}+\dfrac{1}{\Delta x_i}\right)+k_y\times\Delta x_i\times\Delta z_k\times\left(\dfrac{1}{\Delta y_{j+1}+\Delta y_j}+\dfrac{1}{\Delta y_j}\right)\\ +k_z\times\Delta x_i\times\Delta y_j\times\left(\dfrac{1}{\Delta z_{k+1}+\Delta z_k}+\dfrac{1}{\Delta z_k}\right)+\dfrac{1}{2}\times\dfrac{V_p\times\mu_o\times S_{g_{ini}}}{\Delta t}\times\dfrac{P_{ini}}{\left(P_{node}^{v}\right)^2}\end{array}\right\}\right]+$$

$$P_{k+1}^{n+1}\left[2\times k_z\times\frac{\Delta x_i\times\Delta y_j}{\Delta z_{k+1}+\Delta z_k}\right]+P_{j+1}^{n+1}\left[2\times k_y\times\frac{\Delta x_i\times\Delta z_k}{\Delta y_{j+1}+\Delta y_j}\right]+P_{i+1}^{n+1}\left[2\times k_x\times\frac{\Delta y_j\times\Delta z_k}{\Delta x_{i+1}+\Delta x_i}\right]$$

$$= P_{cell}^{n+1}\left[-2\times\left\{\begin{matrix} k_x\times\dfrac{\Delta y_j\times\Delta z_k}{\Delta x_i}+k_y\times\dfrac{\Delta x_i\times\Delta z_k}{\Delta y_j} \\ +k_z\times\dfrac{\Delta x_i\times\Delta y_j}{\Delta z_k}\end{matrix}\right\}\right]-\frac{V_p\times\mu_o\times S_{g_{ini}}}{\Delta t}\times\frac{P_{ini}\times P_{node}^{n}}{\left(P_{node}^{v}\right)^2} \quad \text{A.44}$$

When k = 2 to k = N – 1,

$$P_{k-1}^{n+1}\left[2\times k_z\times\frac{\Delta x_i\times\Delta y_j}{\Delta z_k+\Delta z_{k-1}}\right]+$$

$$P_{node}^{n+1}\left[-2\times\left\{\begin{matrix} k_x\times\Delta y_j\times\Delta z_k\times\left(\dfrac{1}{\Delta x_{i+1}+\Delta x_i}+\dfrac{1}{\Delta x_i}\right)+k_y\times\Delta x_i\times\Delta z_k\times\left(\dfrac{1}{\Delta y_{j+1}+\Delta y_j}+\dfrac{1}{\Delta y_j}\right) \\ +k_z\times\Delta x_i\times\Delta y_j\times\left(\dfrac{1}{\Delta z_{k+1}+\Delta z_k}+\dfrac{1}{\Delta z_k+\Delta z_{k-1}}\right)+\dfrac{1}{2}\times\dfrac{V_p\times\mu_o\times S_{g_{ini}}}{\Delta t}\times\dfrac{P_{ini}}{\left(P_{node}^{v}\right)^2}\end{matrix}\right\}\right]+$$

$$P_{k+1}^{n+1}\left[2\times k_z\times\frac{\Delta x_i\times\Delta y_j}{\Delta z_{k+1}+\Delta z_k}\right]+P_{j+1}^{n+1}\left[2\times k_y\times\frac{\Delta x_i\times\Delta z_k}{\Delta y_{j+1}+\Delta y_j}\right]+P_{i+1}^{n+1}\left[2\times k_x\times\frac{\Delta y_j\times\Delta z_k}{\Delta x_{i+1}+\Delta x_i}\right]$$

$$= P_{cell}^{n+1}\left[-2\times\left\{k_x\times\frac{\Delta y_j\times\Delta z_k}{\Delta x_i}+k_y\times\frac{\Delta x_i\times\Delta z_k}{\Delta y_j}\right\}\right]-\frac{V_p\times\mu_o\times S_{g_{ini}}}{\Delta t}\times\frac{P_{ini}\times P_{node}^{n}}{\left(P_{node}^{v}\right)^2} \quad \text{A.45}$$

When k = N,

$$P_{k-1}^{n+1}\left[2\times k_z\times\frac{\Delta x_i\times\Delta y_j}{\Delta z_k+\Delta z_{k-1}}\right]+$$

$$P_{node}^{n+1}\left[-2\times\left\{\begin{matrix} k_x\times\Delta y_j\times\Delta z_k\times\left(\dfrac{1}{\Delta x_{i+1}+\Delta x_i}+\dfrac{1}{\Delta x_i}\right)+k_y\times\Delta x_i\times\Delta z_k\times\left(\dfrac{1}{\Delta y_{j+1}+\Delta y_j}+\dfrac{1}{\Delta y_j}\right) \\ +k_z\times\Delta x_i\times\Delta y_j\times\left(\dfrac{1}{\Delta z_k+\Delta z_{k-1}}\right)+\dfrac{1}{2}\times\dfrac{V_p\times\mu_o\times S_{g_{ini}}}{\Delta t}\times\dfrac{P_{ini}}{\left(P_{node}^{v}\right)^2}\end{matrix}\right\}\right]+$$

$$P_{j+1}^{n+1}\left[2\times k_y\times\frac{\Delta x_i\times\Delta z_k}{\Delta y_{j+1}+\Delta y_j}\right]+P_{i+1}^{n+1}\left[2\times k_x\times\frac{\Delta y_j\times\Delta z_k}{\Delta x_{i+1}+\Delta x_i}\right]$$

$$= P_{cell}^{n+1}\left[-2\times\left\{k_x\times\frac{\Delta y_j\times\Delta z_k}{\Delta x_i}+k_y\times\frac{\Delta x_i\times\Delta z_k}{\Delta y_j}\right\}\right]-\frac{V_p\times\mu_o\times S_{g_{ini}}}{\Delta t}\times\frac{P_{ini}\times P_{node}^{n}}{\left(P_{node}^{v}\right)^2} \qquad \text{A.46}$$

When j = 2 to j = N-1,

When k = 1,

$$P_{j-1}^{n+1}\left[2\times k_y\times\frac{\Delta x_i\times\Delta z_k}{\Delta y_j+\Delta y_{j-1}}\right]+$$

$$P_{node}^{n+1}\left[-2\times\left\{\begin{array}{l}k_x\times\Delta y_j\times\Delta z_k\times\left(\dfrac{1}{\Delta x_{i+1}+\Delta x_i}+\dfrac{1}{\Delta x_i}\right)+k_y\times\Delta x_i\times\Delta z_k\times\left(\dfrac{1}{\Delta y_{j+1}+\Delta y_j}+\dfrac{1}{\Delta y_j+\Delta y_{j-1}}\right)\\ +k_z\times\Delta x_i\times\Delta y_j\times\left(\dfrac{1}{\Delta z_{k+1}+\Delta z_k}+\dfrac{1}{\Delta z_k}\right)+\dfrac{1}{2}\times\dfrac{V_p\times\mu_o\times S_{g_{ini}}}{\Delta t}\times\dfrac{P_{ini}}{\left(P_{node}^{v}\right)^2}\end{array}\right\}\right]+$$

$$P_{k+1}^{n+1}\left[2\times k_z\times\frac{\Delta x_i\times\Delta y_j}{\Delta z_{k+1}+\Delta z_k}\right]+P_{j+1}^{n+1}\left[2\times k_y\times\frac{\Delta x_i\times\Delta z_k}{\Delta y_{j+1}+\Delta y_j}\right]+P_{i+1}^{n+1}\left[2\times k_x\times\frac{\Delta y_j\times\Delta z_k}{\Delta x_{i+1}+\Delta x_i}\right]$$

$$= P_{cell}^{n+1}\left[-2\times\left\{k_x\times\frac{\Delta y_j\times\Delta z_k}{\Delta x_i}+k_z\times\frac{\Delta x_i\times\Delta y_j}{\Delta z_k}\right\}\right]-\frac{V_p\times\mu_o\times S_{g_{ini}}}{\Delta t}\times\frac{P_{ini}\times P_{node}^{n}}{\left(P_{node}^{v}\right)^2} \qquad \text{A.47}$$

When k = 2 to k = N – 1,

$$P_{k-1}^{n+1}\left[2\times k_z\times\frac{\Delta x_i\times\Delta y_j}{\Delta z_k+\Delta z_{k-1}}\right]+P_{j-1}^{n+1}\left[2\times k_y\times\frac{\Delta x_i\times\Delta z_k}{\Delta y_j+\Delta y_{j-1}}\right]+$$

$$P_{node}^{n+1}\left[-2\times\left\{\begin{array}{l}k_x\times\Delta y_j\times\Delta z_k\times\left(\dfrac{1}{\Delta x_{i+1}+\Delta x_i}+\dfrac{1}{\Delta x_i}\right)+k_y\times\Delta x_i\times\Delta z_k\times\left(\dfrac{1}{\Delta y_{j+1}+\Delta y_j}+\dfrac{1}{\Delta y_j+\Delta y_{j-1}}\right)\\ +k_z\times\Delta x_i\times\Delta y_j\times\left(\dfrac{1}{\Delta z_{k+1}+\Delta z_k}+\dfrac{1}{\Delta z_k+\Delta z_{k-1}}\right)+\dfrac{1}{2}\times\dfrac{V_p\times\mu_o\times S_{g_{ini}}}{\Delta t}\times\dfrac{P_{ini}}{\left(P_{node}^{v}\right)^2}\end{array}\right\}\right]+$$

$$P_{k+1}^{n+1}\left[2\times k_z\times\frac{\Delta x_i\times\Delta y_j}{\Delta z_{k+1}+\Delta z_k}\right]+P_{j+1}^{n+1}\left[2\times k_y\times\frac{\Delta x_i\times\Delta z_k}{\Delta y_{j+1}+\Delta y_j}\right]+P_{i+1}^{n+1}\left[2\times k_x\times\frac{\Delta y_j\times\Delta z_k}{\Delta x_{i+1}+\Delta x_i}\right]$$

$$=P_{cell}^{n+1}\left[-2\times k_x\times\frac{\Delta y_j\times\Delta z_k}{\Delta x_i}\right]-\frac{V_p\times\mu_o\times S_{g_{ini}}}{\Delta t}\times\frac{P_{ini}\times P_{node}^{n}}{\left(P_{node}^{v}\right)^2} \qquad \text{A.48}$$

When k = N,

$$P_{k-1}^{n+1}\left[2\times k_z\times\frac{\Delta x_i\times\Delta y_j}{\Delta z_k+\Delta z_{k-1}}\right]+P_{j-1}^{n+1}\left[2\times k_y\times\frac{\Delta x_i\times\Delta z_k}{\Delta y_j+\Delta y_{j-1}}\right]+$$

$$P_{node}^{n+1}\left[-2\times\left\{\begin{array}{l}k_x\times\Delta y_j\times\Delta z_k\times\left(\frac{1}{\Delta x_{i+1}+\Delta x_i}+\frac{1}{\Delta x_i}\right)+k_y\times\Delta x_i\times\Delta z_k\times\left(\frac{1}{\Delta y_{j+1}+\Delta y_j}+\frac{1}{\Delta y_j+\Delta y_{j-1}}\right)\\+k_z\times\Delta x_i\times\Delta y_j\times\left(\frac{1}{\Delta z_k+\Delta z_{k-1}}\right)+\frac{1}{2}\times\frac{V_p\times\mu_o\times S_{g_{ini}}}{\Delta t}\times\frac{P_{ini}}{\left(P_{node}^{v}\right)^2}\end{array}\right\}\right]+$$

$$P_{j+1}^{n+1}\left[2\times k_y\times\frac{\Delta x_i\times\Delta z_k}{\Delta y_{j+1}+\Delta y_j}\right]+P_{i+1}^{n+1}\left[2\times k_x\times\frac{\Delta y_j\times\Delta z_k}{\Delta x_{i+1}+\Delta x_i}\right]$$

$$=P_{cell}^{n+1}\left[-2\times k_x\times\frac{\Delta y_j\times\Delta z_k}{\Delta x_i}\right]-\frac{V_p\times\mu_o\times S_{g_{ini}}}{\Delta t}\times\frac{P_{ini}\times P_{node}^{n}}{\left(P_{node}^{v}\right)^2} \qquad \text{A.49}$$

When j =N,

When k = 1,

$$P_{j-1}^{n+1}\left[2\times k_y\times\frac{\Delta x_i\times\Delta z_k}{\Delta y_j+\Delta y_{j-1}}\right]+$$

$$P_{node}^{n+1}\left[-2\times\left\{\begin{array}{l}k_x\times\Delta y_j\times\Delta z_k\times\left(\dfrac{1}{\Delta x_{i+1}+\Delta x_i}+\dfrac{1}{\Delta x_i}\right)+k_y\times\Delta x_i\times\Delta z_k\times\left(\dfrac{1}{\Delta y_j+\Delta y_{j-1}}\right)\\ +k_z\times\Delta x_i\times\Delta y_j\times\left(\dfrac{1}{\Delta z_{k+1}+\Delta z_k}+\dfrac{1}{\Delta z_k}\right)+\dfrac{1}{2}\times\dfrac{V_p\times\mu_o\times S_{g_{ini}}}{\Delta t}\times\dfrac{P_{ini}}{\left(P_{node}^{v}\right)^2}\end{array}\right\}\right]+$$

$$P_{k+1}^{n+1}\left[2\times k_z\times\frac{\Delta x_i\times\Delta y_j}{\Delta z_{k+1}+\Delta z_k}\right]+P_{i+1}^{n+1}\left[2\times k_x\times\frac{\Delta y_j\times\Delta z_k}{\Delta x_{i+1}+\Delta x_i}\right]$$

$$=P_{cell}^{n+1}\left[-2\times\left\{k_x\times\frac{\Delta y_j\times\Delta z_k}{\Delta x_i}+k_z\times\frac{\Delta x_i\times\Delta y_j}{\Delta z_k}\right\}\right]-\frac{V_p\times\mu_o\times S_{g_{ini}}}{\Delta t}\times\frac{P_{ini}\times P_{node}^{n}}{\left(P_{node}^{v}\right)^2}\qquad\text{A.50}$$

When k = 2 to k = N – 1,

$$P_{k-1}^{n+1}\left[2\times k_z\times\frac{\Delta x_i\times\Delta y_j}{\Delta z_k+\Delta z_{k-1}}\right]+P_{j-1}^{n+1}\left[2\times k_y\times\frac{\Delta x_i\times\Delta z_k}{\Delta y_j+\Delta y_{j-1}}\right]+$$

$$P_{node}^{n+1}\left[-2\times\left\{\begin{array}{l}k_x\times\Delta y_j\times\Delta z_k\times\left(\dfrac{1}{\Delta x_{i+1}+\Delta x_i}+\dfrac{1}{\Delta x_i}\right)+k_y\times\Delta x_i\times\Delta z_k\times\left(\dfrac{1}{\Delta y_j+\Delta y_{j-1}}\right)\\ +k_z\times\Delta x_i\times\Delta y_j\times\left(\dfrac{1}{\Delta z_{k+1}+\Delta z_k}+\dfrac{1}{\Delta z_k+\Delta z_{k-1}}\right)+\dfrac{1}{2}\times\dfrac{V_p\times\mu_o\times S_{g_{ini}}}{\Delta t}\times\dfrac{P_{ini}}{\left(P_{node}^{v}\right)^2}\end{array}\right\}\right]+$$

$$P_{k+1}^{n+1}\left[2\times k_z\times\frac{\Delta x_i\times\Delta y_j}{\Delta z_{k+1}+\Delta z_k}\right]+P_{i+1}^{n+1}\left[2\times k_x\times\frac{\Delta y_j\times\Delta z_k}{\Delta x_{i+1}+\Delta x_i}\right]$$

$$=P_{cell}^{n+1}\left[-2\times k_x\times\frac{\Delta y_j\times\Delta z_k}{\Delta x_i}\right]-\frac{V_p\times\mu_o\times S_{g_{ini}}}{\Delta t}\times\frac{P_{ini}\times P_{node}^{n}}{\left(P_{node}^{v}\right)^2}\qquad\text{A.51}$$

When k = N,

$$P_{k-1}^{n+1}\left[2\times k_z\times\frac{\Delta x_i\times\Delta y_j}{\Delta z_k+\Delta z_{k-1}}\right]+P_{j-1}^{n+1}\left[2\times k_y\times\frac{\Delta x_i\times\Delta z_k}{\Delta y_j+\Delta y_{j-1}}\right]+$$

$$P_{node}^{n+1}\left[-2\times\left\{\begin{array}{l}k_x\times\Delta y_j\times\Delta z_k\times\left(\dfrac{1}{\Delta x_{i+1}+\Delta x_i}+\dfrac{1}{\Delta x_i}\right)+k_y\times\Delta x_i\times\Delta z_k\times\left(\dfrac{1}{\Delta y_j+\Delta y_{j-1}}\right)\\ +k_z\times\Delta x_i\times\Delta y_j\times\left(\dfrac{1}{\Delta z_k+\Delta z_{k-1}}\right)+\dfrac{1}{2}\times\dfrac{V_p\times\mu_o\times S_{g_{ini}}}{\Delta t}\times\dfrac{P_{ini}}{\left(P_{node}^{v}\right)^2}\end{array}\right\}\right]+$$

$$P_{i+1}^{n+1}\left[2\times k_x\times\frac{\Delta y_j\times\Delta z_k}{\Delta x_{i+1}+\Delta x_i}\right]$$

$$=P_{cell}^{n+1}\left[-2\times k_x\times\frac{\Delta y_j\times\Delta z_k}{\Delta x_i}\right]-\frac{V_p\times\mu_o\times S_{g_{ini}}}{\Delta t}\times\frac{P_{ini}\times P_{node}^{n}}{\left(P_{node}^{v}\right)^2}\qquad\text{A.52}$$

When i = 2 to i = N-1,

When j = 1,

When k = 1,

$$P_{i-1}^{n+1}\left[2\times k_x\times\frac{\Delta y_j\times\Delta z_k}{\Delta x_i+\Delta x_{i-1}}\right]+$$

$$P_{node}^{n+1}\left[-2\times\left\{\begin{array}{l}k_x\times\Delta y_j\times\Delta z_k\times\left(\dfrac{1}{\Delta x_{i+1}+\Delta x_i}+\dfrac{1}{\Delta x_i+\Delta x_{i-1}}\right)+k_y\times\Delta x_i\times\Delta z_k\times\left(\dfrac{1}{\Delta y_{j+1}+\Delta y_j}+\dfrac{1}{\Delta y_j}\right)\\ +k_z\times\Delta x_i\times\Delta y_j\times\left(\dfrac{1}{\Delta z_{k+1}+\Delta z_k}+\dfrac{1}{\Delta z_k}\right)+\dfrac{1}{2}\times\dfrac{V_p\times\mu_o\times S_{g_{ini}}}{\Delta t}\times\dfrac{P_{ini}}{\left(P_{node}^{v}\right)^2}\end{array}\right\}\right]+$$

$$P_{k+1}^{n+1}\left[2\times k_z\times\frac{\Delta x_i\times\Delta y_j}{\Delta z_{k+1}+\Delta z_k}\right]+P_{j+1}^{n+1}\left[2\times k_y\times\frac{\Delta x_i\times\Delta z_k}{\Delta y_{j+1}+\Delta y_j}\right]+P_{i+1}^{n+1}\left[2\times k_x\times\frac{\Delta y_j\times\Delta z_k}{\Delta x_{i+1}+\Delta x_i}\right]$$

$$=P_{cell}^{n+1}\left[-2\times\left\{k_y\times\frac{\Delta x_i\times\Delta z_k}{\Delta y_j}+k_z\times\frac{\Delta x_i\times\Delta y_j}{\Delta z_k}\right\}\right]-\frac{V_p\times\mu_o\times S_{g_{ini}}}{\Delta t}\times\frac{P_{ini}\times P_{node}^{n}}{\left(P_{node}^{v}\right)^2}\qquad\text{A.53}$$

When k = 2 to k = N – 1,

$$P_{k-1}^{n+1}\left[2\times k_z\times\frac{\Delta x_i\times\Delta y_j}{\Delta z_k+\Delta z_{k-1}}\right]+P_{i-1}^{n+1}\left[2\times k_x\times\frac{\Delta y_j\times\Delta z_k}{\Delta x_i+\Delta x_{i-1}}\right]+$$

$$P_{node}^{n+1}\left[-2\times\left\{\begin{array}{l}k_x\times\Delta y_j\times\Delta z_k\times\left(\frac{1}{\Delta x_{i+1}+\Delta x_i}+\frac{1}{\Delta x_i+\Delta x_{i-1}}\right)+k_y\times\Delta x_i\times\Delta z_k\times\left(\frac{1}{\Delta y_{j+1}+\Delta y_j}+\frac{1}{\Delta y_j}\right)\\+k_z\times\Delta x_i\times\Delta y_j\times\left(\frac{1}{\Delta z_{k+1}+\Delta z_k}+\frac{1}{\Delta z_k+\Delta z_{k-1}}\right)+\frac{1}{2}\times\frac{V_p\times\mu_o\times S_{g_{ini}}}{\Delta t}\times\frac{P_{ini}}{\left(P_{node}^{v}\right)^2}\end{array}\right\}\right]+$$

$$P_{k+1}^{n+1}\left[2\times k_z\times\frac{\Delta x_i\times\Delta y_j}{\Delta z_{k+1}+\Delta z_k}\right]+P_{j+1}^{n+1}\left[2\times k_y\times\frac{\Delta x_i\times\Delta z_k}{\Delta y_{j+1}+\Delta y_j}\right]+P_{i+1}^{n+1}\left[2\times k_x\times\frac{\Delta y_j\times\Delta z_k}{\Delta x_{i+1}+\Delta x_i}\right]$$

$$=P_{cell}^{n+1}\left[-2\times k_y\times\frac{\Delta x_i\times\Delta z_k}{\Delta y_j}\right]-\frac{V_p\times\mu_o\times S_{g_{ini}}}{\Delta t}\times\frac{P_{ini}\times P_{node}^{n}}{\left(P_{node}^{v}\right)^2}\qquad\text{A.54}$$

When k = N,

$$P_{k-1}^{n+1}\left[2\times k_z\times\frac{\Delta x_i\times\Delta y_j}{\Delta z_k+\Delta z_{k-1}}\right]+P_{i-1}^{n+1}\left[2\times k_x\times\frac{\Delta y_j\times\Delta z_k}{\Delta x_i+\Delta x_{i-1}}\right]+$$

$$P_{node}^{n+1}\left[-2\times\left\{\begin{array}{l}k_x\times\Delta y_j\times\Delta z_k\times\left(\frac{1}{\Delta x_{i+1}+\Delta x_i}+\frac{1}{\Delta x_i+\Delta x_{i-1}}\right)+k_y\times\Delta x_i\times\Delta z_k\times\left(\frac{1}{\Delta y_{j+1}+\Delta y_j}+\frac{1}{\Delta y_j}\right)\\+k_z\times\Delta x_i\times\Delta y_j\times\left(\frac{1}{\Delta z_k+\Delta z_{k-1}}\right)+\frac{1}{2}\times\frac{V_p\times\mu_o\times S_{g_{ini}}}{\Delta t}\times\frac{P_{ini}}{\left(P_{node}^{v}\right)^2}\end{array}\right\}\right]+$$

$$P_{j+1}^{n+1}\left[2\times k_y\times\frac{\Delta x_i\times\Delta z_k}{\Delta y_{j+1}+\Delta y_j}\right]+P_{i+1}^{n+1}\left[2\times k_x\times\frac{\Delta y_j\times\Delta z_k}{\Delta x_{i+1}+\Delta x_i}\right]$$

$$=P_{cell}^{n+1}\left[-2\times k_y\times\frac{\Delta x_i\times\Delta z_k}{\Delta y_j}\right]-\frac{V_p\times\mu_o\times S_{g_{ini}}}{\Delta t}\times\frac{P_{ini}\times P_{node}^{n}}{\left(P_{node}^{v}\right)^2}\qquad\text{A.55}$$

When j = 2 to j = N-1,

When k = 1,

$$P_{j-1}^{n+1}\left[2\times k_y\times\frac{\Delta x_i\times\Delta z_k}{\Delta y_j+\Delta y_{j-1}}\right]+P_{i-1}^{n+1}\left[2\times k_x\times\frac{\Delta y_j\times\Delta z_k}{\Delta x_i+\Delta x_{i-1}}\right]+$$

$$P_{node}^{n+1}\left[-2\times\left\{\begin{array}{l}k_x\times\Delta y_j\times\Delta z_k\times\left(\frac{1}{\Delta x_{i+1}+\Delta x_i}+\frac{1}{\Delta x_i+\Delta x_{i-1}}\right)+k_y\times\Delta x_i\times\Delta z_k\times\left(\frac{1}{\Delta y_{j+1}+\Delta y_j}+\frac{1}{\Delta y_j+\Delta y_{j-1}}\right)\\+k_z\times\Delta x_i\times\Delta y_j\times\left(\frac{1}{\Delta z_{k+1}+\Delta z_k}+\frac{1}{\Delta z_k}\right)+\frac{1}{2}\times\frac{V_p\times\mu_o\times S_{g_{ini}}}{\Delta t}\times\frac{P_{ini}}{\left(P_{node}^v\right)^2}\end{array}\right\}\right]+$$

$$P_{k+1}^{n+1}\left[2\times k_z\times\frac{\Delta x_i\times\Delta y_j}{\Delta z_{k+1}+\Delta z_k}\right]+P_{j+1}^{n+1}\left[2\times k_y\times\frac{\Delta x_i\times\Delta z_k}{\Delta y_{j+1}+\Delta y_j}\right]+P_{i+1}^{n+1}\left[2\times k_x\times\frac{\Delta y_j\times\Delta z_k}{\Delta x_{i+1}+\Delta x_i}\right]$$

$$=P_{cell}^{n+1}\left[-2\times k_z\times\frac{\Delta x_i\times\Delta y_j}{\Delta z_k}\right]-\frac{V_p\times\mu_o\times S_{g_{ini}}}{\Delta t}\times\frac{P_{ini}\times P_{node}^n}{\left(P_{node}^v\right)^2}$$

A.56

When k = 2 to k = N – 1,

$$P_{k-1}^{n+1}\left[2\times k_z\times\frac{\Delta x_i\times\Delta y_j}{\Delta z_k+\Delta z_{k-1}}\right]+P_{j-1}^{n+1}\left[2\times k_y\times\frac{\Delta x_i\times\Delta z_k}{\Delta y_j+\Delta y_{j-1}}\right]+P_{i-1}^{n+1}\left[2\times k_x\times\frac{\Delta y_j\times\Delta z_k}{\Delta x_i+\Delta x_{i-1}}\right]+$$

$$P_{node}^{n+1}\left[-2\times\left\{\begin{array}{l}k_x\times\Delta y_j\times\Delta z_k\times\left(\frac{1}{\Delta x_{i+1}+\Delta x_i}+\frac{1}{\Delta x_i+\Delta x_{i-1}}\right)+k_y\times\Delta x_i\times\Delta z_k\times\left(\frac{1}{\Delta y_{j+1}+\Delta y_j}+\frac{1}{\Delta y_j+\Delta y_{j-1}}\right)\\+k_z\times\Delta x_i\times\Delta y_j\times\left(\frac{1}{\Delta z_{k+1}+\Delta z_k}+\frac{1}{\Delta z_k+\Delta z_{k-1}}\right)+\frac{1}{2}\times\frac{V_p\times\mu_o\times S_{g_{ini}}}{\Delta t}\times\frac{P_{ini}}{\left(P_{node}^v\right)^2}\end{array}\right\}\right]+$$

$$P_{k+1}^{n+1}\left[2\times k_z\times\frac{\Delta x_i\times\Delta y_j}{\Delta z_{k+1}+\Delta z_k}\right]+P_{j+1}^{n+1}\left[2\times k_y\times\frac{\Delta x_i\times\Delta z_k}{\Delta y_{j+1}+\Delta y_j}\right]+P_{i+1}^{n+1}\left[2\times k_x\times\frac{\Delta y_j\times\Delta z_k}{\Delta x_{i+1}+\Delta x_i}\right]$$

$$=-\frac{V_p\times\mu_o\times S_{g_{ini}}}{\Delta t}\times\frac{P_{ini}\times P_{node}^n}{\left(P_{node}^v\right)^2}$$

A.57

When k = N,

$$P_{k-1}^{n+1}\left[2\times k_z\times\frac{\Delta x_i\times\Delta y_j}{\Delta z_k+\Delta z_{k-1}}\right]+P_{j-1}^{n+1}\left[2\times k_y\times\frac{\Delta x_i\times\Delta z_k}{\Delta y_j+\Delta y_{j-1}}\right]+P_{i-1}^{n+1}\left[2\times k_x\times\frac{\Delta y_j\times\Delta z_k}{\Delta x_i+\Delta x_{i-1}}\right]+$$

$$P_{node}^{n+1}\left[-2\times\left\{\begin{array}{l}k_x\times\Delta y_j\times\Delta z_k\times\left(\frac{1}{\Delta x_{i+1}+\Delta x_i}+\frac{1}{\Delta x_i+\Delta x_{i-1}}\right)+k_y\times\Delta x_i\times\Delta z_k\times\left(\frac{1}{\Delta y_{j+1}+\Delta y_j}+\frac{1}{\Delta y_j+\Delta y_{j-1}}\right)\\+k_z\times\Delta x_i\times\Delta y_j\times\left(\frac{1}{\Delta z_k+\Delta z_{k-1}}\right)+\frac{1}{2}\times\frac{V_p\times\mu_o\times S_{g_{ini}}}{\Delta t}\times\frac{P_{ini}}{\left(P_{node}^v\right)^2}\end{array}\right\}\right]+$$

$$P_{j+1}^{n+1}\left[2\times k_y\times\frac{\Delta x_i\times\Delta z_k}{\Delta y_{j+1}+\Delta y_j}\right]+P_{i+1}^{n+1}\left[2\times k_x\times\frac{\Delta y_j\times\Delta z_k}{\Delta x_{i+1}+\Delta x_i}\right]$$

$$=-\frac{V_p\times\mu_o\times S_{g_{ini}}}{\Delta t}\times\frac{P_{ini}\times P_{node}^n}{\left(P_{node}^v\right)^2}\qquad\text{A.58}$$

When j =N,

When k = 1,

$$P_{j-1}^{n+1}\left[2\times k_y\times\frac{\Delta x_i\times\Delta z_k}{\Delta y_j+\Delta y_{j-1}}\right]+P_{i-1}^{n+1}\left[2\times k_x\times\frac{\Delta y_j\times\Delta z_k}{\Delta x_i+\Delta x_{i-1}}\right]+$$

$$P_{node}^{n+1}\left[-2\times\left\{\begin{array}{l}k_x\times\Delta y_j\times\Delta z_k\times\left(\frac{1}{\Delta x_{i+1}+\Delta x_i}+\frac{1}{\Delta x_i+\Delta x_{i-1}}\right)+k_y\times\Delta x_i\times\Delta z_k\times\left(\frac{1}{\Delta y_j+\Delta y_{j-1}}\right)\\+k_z\times\Delta x_i\times\Delta y_j\times\left(\frac{1}{\Delta z_{k+1}+\Delta z_k}+\frac{1}{\Delta z_k}\right)+\frac{1}{2}\times\frac{V_p\times\mu_o\times S_{g_{ini}}}{\Delta t}\times\frac{P_{ini}}{\left(P_{node}^v\right)^2}\end{array}\right\}\right]+$$

$$P_{k+1}^{n+1}\left[2\times k_z\times\frac{\Delta x_i\times\Delta y_j}{\Delta z_{k+1}+\Delta z_k}\right]+P_{i+1}^{n+1}\left[2\times k_x\times\frac{\Delta y_j\times\Delta z_k}{\Delta x_{i+1}+\Delta x_i}\right]$$

$$=P_{cell}^{n+1}\left[-2\times k_z\times\frac{\Delta x_i\times\Delta y_j}{\Delta z_k}\right]-\frac{V_p\times\mu_o\times S_{g_{ini}}}{\Delta t}\times\frac{P_{ini}\times P_{node}^n}{\left(P_{node}^v\right)^2}\qquad\text{A.59}$$

When k = 2 to k = N – 1,

$$P_{k-1}^{n+1}\left[2\times k_z\times\frac{\Delta x_i\times\Delta y_j}{\Delta z_k+\Delta z_{k-1}}\right]+P_{j-1}^{n+1}\left[2\times k_y\times\frac{\Delta x_i\times\Delta z_k}{\Delta y_j+\Delta y_{j-1}}\right]+P_{i-1}^{n+1}\left[2\times k_x\times\frac{\Delta y_j\times\Delta z_k}{\Delta x_i+\Delta x_{i-1}}\right]+$$

$$P_{node}^{n+1}\left[-2\times\left\{\begin{array}{l}k_x\times\Delta y_j\times\Delta z_k\times\left(\frac{1}{\Delta x_{i+1}+\Delta x_i}+\frac{1}{\Delta x_i+\Delta x_{i-1}}\right)+k_y\times\Delta x_i\times\Delta z_k\times\left(\frac{1}{\Delta y_j+\Delta y_{j-1}}\right)\\+k_z\times\Delta x_i\times\Delta y_j\times\left(\frac{1}{\Delta z_{k+1}+\Delta z_k}+\frac{1}{\Delta z_k+\Delta z_{k-1}}\right)+\frac{1}{2}\times\frac{V_p\times\mu_o\times S_{g_{ini}}}{\Delta t}\times\frac{P_{ini}}{\left(P_{node}^v\right)^2}\end{array}\right\}\right]+$$

$$P_{k+1}^{n+1}\left[2\times k_z\times\frac{\Delta x_i\times\Delta y_j}{\Delta z_{k+1}+\Delta z_k}\right]+P_{i+1}^{n+1}\left[2\times k_x\times\frac{\Delta y_j\times\Delta z_k}{\Delta x_{i+1}+\Delta x_i}\right]$$

$$=-\frac{V_p\times\mu_o\times S_{g_{ini}}}{\Delta t}\times\frac{P_{ini}\times P_{node}^n}{\left(P_{node}^v\right)^2}\qquad\text{A.60}$$

When k = N,

$$P_{k-1}^{n+1}\left[2\times k_z\times\frac{\Delta x_i\times\Delta y_j}{\Delta z_k+\Delta z_{k-1}}\right]+P_{j-1}^{n+1}\left[2\times k_y\times\frac{\Delta x_i\times\Delta z_k}{\Delta y_j+\Delta y_{j-1}}\right]+P_{i-1}^{n+1}\left[2\times k_x\times\frac{\Delta y_j\times\Delta z_k}{\Delta x_i+\Delta x_{i-1}}\right]+$$

$$P_{node}^{n+1}\left[-2\times\left\{\begin{array}{l}k_x\times\Delta y_j\times\Delta z_k\times\left(\frac{1}{\Delta x_{i+1}+\Delta x_i}+\frac{1}{\Delta x_i+\Delta x_{i-1}}\right)+k_y\times\Delta x_i\times\Delta z_k\times\left(\frac{1}{\Delta y_j+\Delta y_{j-1}}\right)\\+k_z\times\Delta x_i\times\Delta y_j\times\left(\frac{1}{\Delta z_k+\Delta z_{k-1}}\right)+\frac{1}{2}\times\frac{V_p\times\mu_o\times S_{g_{ini}}}{\Delta t}\times\frac{P_{ini}}{\left(P_{node}^v\right)^2}\end{array}\right\}\right]+$$

$$P_{i+1}^{n+1}\left[2\times k_x\times\frac{\Delta y_j\times\Delta z_k}{\Delta x_{i+1}+\Delta x_i}\right]$$

$$=-\frac{V_p\times\mu_o\times S_{g_{ini}}}{\Delta t}\times\frac{P_{ini}\times P_{node}^n}{\left(P_{node}^v\right)^2}\qquad\text{A.61}$$

When i = N,

When j = 1,

When k = 1,

$$P_{i-1}^{n+1}\left[2\times k_x\times\frac{\Delta y_j\times\Delta z_k}{\Delta x_i+\Delta x_{i-1}}\right]+$$

$$P_{node}^{n+1}\left[-2\times\left\{\begin{array}{l}k_x\times\Delta y_j\times\Delta z_k\times\left(\dfrac{1}{\Delta x_i+\Delta x_{i-1}}\right)+k_y\times\Delta x_i\times\Delta z_k\times\left(\dfrac{1}{\Delta y_{j+1}+\Delta y_j}+\dfrac{1}{\Delta y_j}\right)\\ +k_z\times\Delta x_i\times\Delta y_j\times\left(\dfrac{1}{\Delta z_{k+1}+\Delta z_k}+\dfrac{1}{\Delta z_k}\right)+\dfrac{1}{2}\times\dfrac{V_p\times\mu_o\times S_{g_{ini}}}{\Delta t}\times\dfrac{P_{ini}}{\left(P_{node}^{v}\right)^2}\end{array}\right\}\right]+$$

$$P_{k+1}^{n+1}\left[2\times k_z\times\frac{\Delta x_i\times\Delta y_j}{\Delta z_{k+1}+\Delta z_k}\right]+P_{j+1}^{n+1}\left[2\times k_y\times\frac{\Delta x_i\times\Delta z_k}{\Delta y_{j+1}+\Delta y_j}\right]$$

$$=P_{cell}^{n+1}\left[-2\times\left\{k_y\times\frac{\Delta x_i\times\Delta z_k}{\Delta y_j}+k_z\times\frac{\Delta x_i\times\Delta y_j}{\Delta z_k}\right\}\right]-\frac{V_p\times\mu_o\times S_{g_{ini}}}{\Delta t}\times\frac{P_{ini}\times P_{node}^{n}}{\left(P_{node}^{v}\right)^2}\qquad\text{A.62}$$

When k = 2 to k = N – 1,

$$P_{k-1}^{n+1}\left[2\times k_z\times\frac{\Delta x_i\times\Delta y_j}{\Delta z_k+\Delta z_{k-1}}\right]+P_{i-1}^{n+1}\left[2\times k_x\times\frac{\Delta y_j\times\Delta z_k}{\Delta x_i+\Delta x_{i-1}}\right]+$$

$$P_{node}^{n+1}\left[-2\times\left\{\begin{array}{l}k_x\times\Delta y_j\times\Delta z_k\times\left(\dfrac{1}{\Delta x_i+\Delta x_{i-1}}\right)+k_y\times\Delta x_i\times\Delta z_k\times\left(\dfrac{1}{\Delta y_{j+1}+\Delta y_j}+\dfrac{1}{\Delta y_j}\right)\\ +k_z\times\Delta x_i\times\Delta y_j\times\left(\dfrac{1}{\Delta z_{k+1}+\Delta z_k}+\dfrac{1}{\Delta z_k+\Delta z_{k-1}}\right)+\dfrac{1}{2}\times\dfrac{V_p\times\mu_o\times S_{g_{ini}}}{\Delta t}\times\dfrac{P_{ini}}{\left(P_{node}^{v}\right)^2}\end{array}\right\}\right]+$$

$$P_{k+1}^{n+1}\left[2\times k_z\times\frac{\Delta x_i\times\Delta y_j}{\Delta z_{k+1}+\Delta z_k}\right]+P_{j+1}^{n+1}\left[2\times k_y\times\frac{\Delta x_i\times\Delta z_k}{\Delta y_{j+1}+\Delta y_j}\right]$$

$$=P_{cell}^{n+1}\left[-2\times k_y\times\frac{\Delta x_i\times\Delta z_k}{\Delta y_j}\right]-\frac{V_p\times\mu_o\times S_{g_{ini}}}{\Delta t}\times\frac{P_{ini}\times P_{node}^{n}}{\left(P_{node}^{v}\right)^2}\qquad\text{A.63}$$

When k = N,

$$P_{k-1}^{n+1}\left[2\times k_z\times\frac{\Delta x_i\times\Delta y_j}{\Delta z_k+\Delta z_{k-1}}\right]+P_{i-1}^{n+1}\left[2\times k_x\times\frac{\Delta y_j\times\Delta z_k}{\Delta x_i+\Delta x_{i-1}}\right]+$$

$$P_{node}^{n+1}\left[-2\times\left\{\begin{array}{l}k_x\times\Delta y_j\times\Delta z_k\times\left(\frac{1}{\Delta x_i+\Delta x_{i-1}}\right)+k_y\times\Delta x_i\times\Delta z_k\times\left(\frac{1}{\Delta y_{j+1}+\Delta y_j}+\frac{1}{\Delta y_j}\right)\\+k_z\times\Delta x_i\times\Delta y_j\times\left(\frac{1}{\Delta z_k+\Delta z_{k-1}}\right)+\frac{1}{2}\times\frac{V_p\times\mu_o\times S_{g_{ini}}}{\Delta t}\times\frac{P_{ini}}{\left(P_{node}^{v}\right)^2}\end{array}\right\}\right]+$$

$$P_{j+1}^{n+1}\left[2\times k_y\times\frac{\Delta x_i\times\Delta z_k}{\Delta y_{j+1}+\Delta y_j}\right]$$

$$=P_{cell}^{n+1}\left[-2\times k_y\times\frac{\Delta x_i\times\Delta z_k}{\Delta y_j}\right]-\frac{V_p\times\mu_o\times S_{g_{ini}}}{\Delta t}\times\frac{P_{ini}\times P_{node}^{n}}{\left(P_{node}^{v}\right)^2}\qquad\text{A.64}$$

When j = 2 to j = N-1,

When k = 1,

$$P_{j-1}^{n+1}\left[2\times k_y\times\frac{\Delta x_i\times\Delta z_k}{\Delta y_j+\Delta y_{j-1}}\right]+P_{i-1}^{n+1}\left[2\times k_x\times\frac{\Delta y_j\times\Delta z_k}{\Delta x_i+\Delta x_{i-1}}\right]+$$

$$P_{node}^{n+1}\left[-2\times\left\{\begin{array}{l}k_x\times\Delta y_j\times\Delta z_k\times\left(\frac{1}{\Delta x_i+\Delta x_{i-1}}\right)+k_y\times\Delta x_i\times\Delta z_k\times\left(\frac{1}{\Delta y_{j+1}+\Delta y_j}+\frac{1}{\Delta y_j+\Delta y_{j-1}}\right)\\+k_z\times\Delta x_i\times\Delta y_j\times\left(\frac{1}{\Delta z_{k+1}+\Delta z_k}+\frac{1}{\Delta z_k}\right)+\frac{1}{2}\times\frac{V_p\times\mu_o\times S_{g_{ini}}}{\Delta t}\times\frac{P_{ini}}{\left(P_{node}^{v}\right)^2}\end{array}\right\}\right]+$$

$$P_{k+1}^{n+1}\left[2\times k_z\times\frac{\Delta x_i\times\Delta y_j}{\Delta z_{k+1}+\Delta z_k}\right]+P_{j+1}^{n+1}\left[2\times k_y\times\frac{\Delta x_i\times\Delta z_k}{\Delta y_{j+1}+\Delta y_j}\right]$$

$$=P_{cell}^{n+1}\left[-2\times k_z\times\frac{\Delta x_i\times\Delta y_j}{\Delta z_k}\right]-\frac{V_p\times\mu_o\times S_{g_{ini}}}{\Delta t}\times\frac{P_{ini}\times P_{node}^{n}}{\left(P_{node}^{v}\right)^2}\qquad\text{A.65}$$

When k = 2 to k = N – 1,

$$P_{k-1}^{n+1}\left[2\times k_z\times\frac{\Delta x_i\times\Delta y_j}{\Delta z_k+\Delta z_{k-1}}\right]+P_{j-1}^{n+1}\left[2\times k_y\times\frac{\Delta x_i\times\Delta z_k}{\Delta y_j+\Delta y_{j-1}}\right]+P_{i-1}^{n+1}\left[2\times k_x\times\frac{\Delta y_j\times\Delta z_k}{\Delta x_i+\Delta x_{i-1}}\right]+$$

$$P_{node}^{n+1}\left[-2\times\left\{\begin{array}{l}k_x\times\Delta y_j\times\Delta z_k\times\left(\frac{1}{\Delta x_i+\Delta x_{i-1}}\right)+k_y\times\Delta x_i\times\Delta z_k\times\left(\frac{1}{\Delta y_{j+1}+\Delta y_j}+\frac{1}{\Delta y_j+\Delta y_{j-1}}\right)\\+k_z\times\Delta x_i\times\Delta y_j\times\left(\frac{1}{\Delta z_{k+1}+\Delta z_k}+\frac{1}{\Delta z_k+\Delta z_{k-1}}\right)+\frac{1}{2}\times\frac{V_p\times\mu_o\times S_{g_{ini}}}{\Delta t}\times\frac{P_{ini}}{\left(P_{node}^v\right)^2}\end{array}\right\}\right]+$$

$$P_{k+1}^{n+1}\left[2\times k_z\times\frac{\Delta x_i\times\Delta y_j}{\Delta z_{k+1}+\Delta z_k}\right]+P_{j+1}^{n+1}\left[2\times k_y\times\frac{\Delta x_i\times\Delta z_k}{\Delta y_{j+1}+\Delta y_j}\right]$$

$$=-\frac{V_p\times\mu_o\times S_{g_{ini}}}{\Delta t}\times\frac{P_{ini}\times P_{node}^n}{\left(P_{node}^v\right)^2}\qquad\text{A.66}$$

When k = N,

$$P_{k-1}^{n+1}\left[2\times k_z\times\frac{\Delta x_i\times\Delta y_j}{\Delta z_k+\Delta z_{k-1}}\right]+P_{j-1}^{n+1}\left[2\times k_y\times\frac{\Delta x_i\times\Delta z_k}{\Delta y_j+\Delta y_{j-1}}\right]+P_{i-1}^{n+1}\left[2\times k_x\times\frac{\Delta y_j\times\Delta z_k}{\Delta x_i+\Delta x_{i-1}}\right]+$$

$$P_{node}^{n+1}\left[-2\times\left\{\begin{array}{l}k_x\times\Delta y_j\times\Delta z_k\times\left(\frac{1}{\Delta x_i+\Delta x_{i-1}}\right)+k_y\times\Delta x_i\times\Delta z_k\times\left(\frac{1}{\Delta y_{j+1}+\Delta y_j}+\frac{1}{\Delta y_j+\Delta y_{j-1}}\right)\\+k_z\times\Delta x_i\times\Delta y_j\times\left(\frac{1}{\Delta z_k+\Delta z_{k-1}}\right)+\frac{1}{2}\times\frac{V_p\times\mu_o\times S_{g_{ini}}}{\Delta t}\times\frac{P_{ini}}{\left(P_{node}^v\right)^2}\end{array}\right\}\right]+$$

$$P_{j+1}^{n+1}\left[2\times k_y\times\frac{\Delta x_i\times\Delta z_k}{\Delta y_{j+1}+\Delta y_j}\right]$$

$$=-\frac{V_p\times\mu_o\times S_{g_{ini}}}{\Delta t}\times\frac{P_{ini}\times P_{node}^n}{\left(P_{node}^v\right)^2}\qquad\text{A.67}$$

When j =N,

When k = 1,

$$P_{j-1}^{n+1}\left[2\times k_y\times\frac{\Delta x_i\times\Delta z_k}{\Delta y_j+\Delta y_{j-1}}\right]+P_{i-1}^{n+1}\left[2\times k_x\times\frac{\Delta y_j\times\Delta z_k}{\Delta x_i+\Delta x_{i-1}}\right]+$$

$$P_{node}^{n+1}\left[-2\times\left\{\begin{array}{l}k_x\times\Delta y_j\times\Delta z_k\times\left(\frac{1}{\Delta x_i+\Delta x_{i-1}}\right)+k_y\times\Delta x_i\times\Delta z_k\times\left(\frac{1}{\Delta y_j+\Delta y_{j-1}}\right)\\+k_z\times\Delta x_i\times\Delta y_j\times\left(\frac{1}{\Delta z_{k+1}+\Delta z_k}+\frac{1}{\Delta z_k}\right)+\frac{1}{2}\times\frac{V_p\times\mu_o\times S_{g_{ini}}}{\Delta t}\times\frac{P_{ini}}{\left(P_{node}^{v}\right)^2}\end{array}\right\}\right]+$$

$$P_{k+1}^{n+1}\left[2\times k_z\times\frac{\Delta x_i\times\Delta y_j}{\Delta z_{k+1}+\Delta z_k}\right]$$

$$=P_{cell}^{n+1}\left[-2\times k_z\times\frac{\Delta x_i\times\Delta y_j}{\Delta z_k}\right]-\frac{V_p\times\mu_o\times S_{g_{ini}}}{\Delta t}\times\frac{P_{ini}\times P_{node}^{n}}{\left(P_{node}^{v}\right)^2}\qquad\text{A.68}$$

When k = 2 to k = N – 1,

$$P_{k-1}^{n+1}\left[2\times k_z\times\frac{\Delta x_i\times\Delta y_j}{\Delta z_k+\Delta z_{k-1}}\right]+P_{j-1}^{n+1}\left[2\times k_y\times\frac{\Delta x_i\times\Delta z_k}{\Delta y_j+\Delta y_{j-1}}\right]+P_{i-1}^{n+1}\left[2\times k_x\times\frac{\Delta y_j\times\Delta z_k}{\Delta x_i+\Delta x_{i-1}}\right]+$$

$$P_{node}^{n+1}\left[-2\times\left\{\begin{array}{l}k_x\times\Delta y_j\times\Delta z_k\times\left(\frac{1}{\Delta x_i+\Delta x_{i-1}}\right)+k_y\times\Delta x_i\times\Delta z_k\times\left(\frac{1}{\Delta y_j+\Delta y_{j-1}}\right)\\+k_z\times\Delta x_i\times\Delta y_j\times\left(\frac{1}{\Delta z_{k+1}+\Delta z_k}+\frac{1}{\Delta z_k+\Delta z_{k-1}}\right)+\frac{1}{2}\times\frac{V_p\times\mu_o\times S_{g_{ini}}}{\Delta t}\times\frac{P_{ini}}{\left(P_{node}^{v}\right)^2}\end{array}\right\}\right]+$$

$$P_{k+1}^{n+1}\left[2\times k_z\times\frac{\Delta x_i\times\Delta y_j}{\Delta z_{k+1}+\Delta z_k}\right]$$

$$=-\frac{V_p\times\mu_o\times S_{g_{ini}}}{\Delta t}\times\frac{P_{ini}\times P_{node}^{n}}{\left(P_{node}^{v}\right)^2}\qquad\text{A.69}$$

When k = N,

$$P_{k-1}^{n+1}\left[2\times k_z\times\frac{\Delta x_i\times\Delta y_j}{\Delta z_k+\Delta z_{k-1}}\right]+P_{j-1}^{n+1}\left[2\times k_y\times\frac{\Delta x_i\times\Delta z_k}{\Delta y_j+\Delta y_{j-1}}\right]+P_{i-1}^{n+1}\left[2\times k_x\times\frac{\Delta y_j\times\Delta z_k}{\Delta x_i+\Delta x_{i-1}}\right]+$$

$$P_{node}^{n+1}\left[-2\times\left\{\begin{array}{l}k_x\times\Delta y_j\times\Delta z_k\times\left(\dfrac{1}{\Delta x_i+\Delta x_{i-1}}\right)+k_y\times\Delta x_i\times\Delta z_k\times\left(\dfrac{1}{\Delta y_j+\Delta y_{j-1}}\right)\\ +k_z\times\Delta x_i\times\Delta y_j\times\left(\dfrac{1}{\Delta z_k+\Delta z_{k-1}}\right)+\dfrac{1}{2}\times\dfrac{V_p\times\mu_o\times S_{g_{ini}}}{\Delta t}\times\dfrac{P_{ini}}{\left(P_{node}^{v}\right)^2}\end{array}\right\}\right]+$$

$$=-\frac{V_p\times\mu_o\times S_{g_{ini}}}{\Delta t}\times\frac{P_{ini}\times P_{node}^{n}}{\left(P_{node}^{v}\right)^2} \qquad \text{A.70}$$

Appendix B

Spherical Model

Applying the central difference in space to Equation 4.18,

$$\frac{\partial}{\partial r}\left(r^2 \times \frac{\partial P}{\partial r}\right) = \frac{\left(r^2 \times \frac{\partial P}{\partial r}\right)_{j+\frac{1}{2}} - \left(r^2 \times \frac{\partial P}{\partial r}\right)_{j-\frac{1}{2}}}{r_{j+\frac{1}{2}} - r_{j-\frac{1}{2}}} \qquad \text{B.01}$$

$$= \frac{r^2_{j+\frac{1}{2}} \times \left(\frac{\partial P}{\partial r}\right)_{j+\frac{1}{2}} - r^2_{j-\frac{1}{2}} \times \left(\frac{\partial P}{\partial r}\right)_{j-\frac{1}{2}}}{r_{j+\frac{1}{2}} - r_{j-\frac{1}{2}}} \qquad \text{B.02}$$

Applying backward difference in time,

$$\frac{\partial P}{\partial t} = \frac{P^{n+1}_{node} - P^{n}_{node}}{\Delta t} \qquad \text{B.03}$$

So Equation B.02 may be written as,

$$\frac{r^2_{j+\frac{1}{2}} \times \left(\frac{\partial P}{\partial r}\right)_{j+\frac{1}{2}} - r^2_{j-\frac{1}{2}} \times \left(\frac{\partial P}{\partial r}\right)_{j-\frac{1}{2}}}{r_{j+\frac{1}{2}} - r_{j-\frac{1}{2}}} = \alpha \times \frac{r_j^2}{P_j^2} \times \frac{P_j^{n+1} - P_j^n}{\Delta t} \qquad \text{B.04}$$

Re-arranging,

$$r^2_{j+\frac{1}{2}} \times \left(\frac{\partial P}{\partial r}\right)_{j+\frac{1}{2}} - r^2_{j-\frac{1}{2}} \times \left(\frac{\partial P}{\partial r}\right)_{j-\frac{1}{2}} = r_j^2 \times \left(r_{j+\frac{1}{2}} - r_{j-\frac{1}{2}}\right) \times \frac{\alpha}{P_j^2} \times \frac{P_j^{n+1} - P_j^n}{\Delta t} \qquad \text{B.05}$$

Since,

$$r_j^2 \times \left(r_{j+\frac{1}{2}} - r_{j-\frac{1}{2}} \right) = \frac{1}{3} \times \left(r^3_{j+\frac{1}{2}} - r^3_{j-\frac{1}{2}} \right) \quad \text{B.06}$$

Replacing back into Equation B.05,

$$r^2_{j+\frac{1}{2}} \times \left(\frac{\partial P}{\partial r} \right)_{j+\frac{1}{2}} - r^2_{j-\frac{1}{2}} \times \left(\frac{\partial P}{\partial r} \right)_{j-\frac{1}{2}} = \frac{1}{3} \times \left(r^3_{j+\frac{1}{2}} - r^3_{j-\frac{1}{2}} \right) \times \frac{\alpha}{P_j^2} \times \frac{P_j^{n+1} - P_j^n}{\Delta t} \quad \text{B.07}$$

Since,

$$\text{Volume of a sphere} = \frac{4}{3} \times \pi \times r^3 \quad \text{B.08}$$

Volume of a differential element can be given by,

$$V_j = \frac{4}{3} \times \pi \times \left(r^3_{j+\frac{1}{2}} - r^3_{j-\frac{1}{2}} \right) \quad \text{B.09}$$

Substituting into Equation B.07,

$$r^2_{j+\frac{1}{2}} \times \left(\frac{\partial P}{\partial r} \right)_{j+\frac{1}{2}} - r^2_{j-\frac{1}{2}} \times \left(\frac{\partial P}{\partial r} \right)_{j-\frac{1}{2}} = \frac{V_j}{4 \times \pi} \times \frac{\alpha}{P_j^2} \times \frac{P_j^{n+1} - P_j^n}{\Delta t} \quad \text{B.10}$$

Now, at the first node, which exists at the center of the cutting, there would exist a no flow boundary condition so Equation B.10 can be written as,

First Node,

$$r^2_{j+\frac{1}{2}} \times \left(\frac{\partial P}{\partial r} \right)_{j+\frac{1}{2}} = \frac{1}{4 \times \pi} \times V_j \times \frac{\alpha}{P_j^2} \times \frac{P_j^{n+1} - P_j^n}{\Delta t} \quad \text{B.11}$$

Solving further by applying our center difference scheme in space,

$$r^2_{j+\frac{1}{2}} \times \left(\frac{P_{j+1} - P_j}{r_{j+1} - r_j} \right) = \frac{V_j}{4 \times \pi} \times \frac{\alpha}{P_j^2} \times \frac{P_j^{n+1} - P_j^n}{\Delta t} \quad \text{B.12}$$

Middle Nodes,

$$r_{j+\frac{1}{2}}^2 \times \left(\frac{\partial P}{\partial r}\right)_{j+\frac{1}{2}} - r_{j-\frac{1}{2}}^2 \times \left(\frac{\partial P}{\partial r}\right)_{j-\frac{1}{2}} = \frac{V_j}{4\times\pi} \times \frac{\alpha}{P_j^2} \times \frac{P_j^{n+1} - P_j^n}{\Delta t} \qquad \text{B.13}$$

Expanding the equation using center difference in space further, we get,

$$r_{j+\frac{1}{2}}^2 \times \left(\frac{P_{j+1} - P_j}{r_{j+1} - r_j}\right) - r_{j-\frac{1}{2}}^2 \times \left(\frac{P_j - P_{j-1}}{r_j - r_{j-1}}\right) = \frac{V_j}{4\times\pi} \times \frac{\alpha}{P_j^2} \times \frac{P_j^{n+1} - P_j^n}{\Delta t} \qquad \text{B.14}$$

Boundary Node,

$$r_{j+\frac{1}{2}}^2 \times \left(\frac{\partial P}{\partial r}\right)_{j+\frac{1}{2}} - r_{j-\frac{1}{2}}^2 \times \left(\frac{\partial P}{\partial r}\right)_{j-\frac{1}{2}} = \frac{V_j}{4\times\pi} \times \frac{\alpha}{P_j^2} \times \frac{P_j^{n+1} - P_j^n}{\Delta t} \qquad \text{B.15}$$

Can be expanded to give,

$$r_e^2 \times \left(\frac{P_{cell} - P_j}{r_e - r_j}\right) - r_{j-\frac{1}{2}}^2 \times \left(\frac{P_j - P_{j-1}}{r_j - r_{j-1}}\right) = \frac{V_j}{4\times\pi} \times \frac{\alpha}{P_j^2} \times \frac{P_j^{n+1} - P_j^n}{\Delta t} \qquad \text{B.16}$$

An implicit solution of the equation reduces the concerns regarding stability. However, the reciprocal of pressure term being multiplied to the R.H.S (Equation B.11 through Equation B.16) makes the equations non-linear. A way to pacify this concern is to take the pressure term at the old time level as an initial guess and then iterating until we get a reasonable match between the consecutive pressure values. Thus, solving the equations implicitly and resolving into its constituent components, we get,

First Node,

$$r_{j+\frac{1}{2}}^2 \times \left(\frac{P_{j+1}^{n+1} - P_j^{n+1}}{r_{j+1} - r_j}\right) = \frac{V_j}{4\times\pi} \times \frac{\alpha}{\left(P_j^v\right)^2} \times \frac{P_j^{n+1} - P_j^n}{\Delta t} \qquad \text{B.17}$$

Re-arranging,

$$P_j^{n+1}\left[-r_{j+\frac{1}{2}}^2\times\frac{\Delta t}{r_{j+1}-r_j}-\frac{V_j}{4\times\pi}\times\frac{\alpha}{\left(P_j^v\right)^2}\right]+P_{j+1}^{n+1}\left[r_{j+\frac{1}{2}}^2\times\frac{\Delta t}{r_{j+1}-r_j}\right]=-\frac{V_j}{4\times\pi}\times\frac{\alpha}{\left(P_j^v\right)^2}\times P_j^n \quad \text{B.18}$$

Middle Nodes,

$$r_{j+\frac{1}{2}}^2\times\left(\frac{P_{j+1}^{n+1}-P_j^{n+1}}{r_{j+1}-r_j}\right)-r_{j-\frac{1}{2}}^2\times\left(\frac{P_j^{n+1}-P_{j-1}^{n+1}}{r_j-r_{j-1}}\right)=\frac{V_j}{4\times\pi}\times\frac{\alpha}{\left(P_j^v\right)^2}\times\frac{P_j^{n+1}-P_j^n}{\Delta t} \quad \text{B.19}$$

Re-arranging,

$$P_{j-1}^{n+1}\left[r_{j-\frac{1}{2}}^2\times\frac{\Delta t}{r_j-r_{j-1}}\right]+P_j^{n+1}\left[-r_{j-\frac{1}{2}}^2\times\frac{\Delta t}{r_j-r_{j-1}}-r_{j+\frac{1}{2}}^2\times\frac{\Delta t}{r_{j+1}-r_j}-\frac{V_j}{4\times\pi}\times\frac{\alpha}{\left(P_j^v\right)^2}\right]$$
$$+P_{j+1}^{n+1}\left[r_{j+\frac{1}{2}}^2\times\frac{\Delta t}{r_{j+1}-r_j}\right]=-\frac{V_j}{4\times\pi}\times\frac{\alpha}{\left(P_j^v\right)^2}\times P_j^n \quad \text{B.20}$$

Boundary Node,

$$r_e^2\times\left(\frac{P_{cell}^{n+1}-P_j^{n+1}}{r_e-r_j}\right)-r_{j-\frac{1}{2}}^2\times\left(\frac{P_j^{n+1}-P_{j-1}^{n+1}}{r_j-r_{j-1}}\right)=\frac{V_j}{4\times\pi}\times\frac{\alpha}{\left(P_j^v\right)^2}\times\frac{P_j^{n+1}-P_j^n}{\Delta t} \quad \text{B.21}$$

Re-arranging,

$$P_{j-1}^{n+1}\left[r_{j-\frac{1}{2}}^2\times\frac{\Delta t}{r_j-r_{j-1}}\right]+P_j^{n+1}\left[-r_{j-\frac{1}{2}}^2\times\frac{\Delta t}{r_j-r_{j-1}}-r_e^2\times\frac{\Delta t}{r_e-r_j}-\frac{V_j}{4\times\pi}\times\frac{\alpha}{\left(P_j^v\right)^2}\right]$$
$$=-\frac{V_j}{4\times\pi}\times\frac{\alpha}{\left(P_j^v\right)^2}\times P_j^n-P_{cell}^{n+1}\left[r_e^2\times\frac{\Delta t}{r_e-r_j}\right] \quad \text{B.22}$$

Nomenclature

$\hat{i}$	Unit vector along x-axis
$\hat{j}$	Unit vector along y-axis
$\hat{k}$	Unit vector along z-axis
k	Isotropic permeability, Darcy
k_x	Permeability along x-axis, Darcy
k_y	Permeability along y-axis, Darcy
k_z	Permeability along z-axis, Darcy
P	Pressure, Atm.
P^n	Pressure at present time level, atm.
P^{n+1}	Pressure at next time level, atm.
P^v	Iterative pressure for next time level, atm.
P_i	Pressure at cell center of current node along x-axis, atm.
P_{i-1}	Pressure at cell center of previous node along x-axis, atm.
P_{i+1}	Pressure at cell center of next node along x-axis, atm.
P_j	Pressure at cell center of current node along y-axis, atm.
P_{j-1}	Pressure at cell center of previous node along y-axis, atm.
P_{j+1}	Pressure at cell center of next node along y-axis, atm.

P_k	Pressure at cell center of current node along z-axis, atm.
P_{k-1}	Pressure at cell center of previous node along z-axis, atm.
P_{k+1}	Pressure at cell center of next node along z-axis, atm.
P_{cell}	Applied chamber pressure, atm.
P_{ini}	Initial pressure, atm.
P_{node}	Pressure at cell center of current node, atm.
∂P	Pressure change, atm.
r_e	Radius of the cutting, cm
r_j	Radial distance to center of current differential volume element, cm
$r_{j-\frac{1}{2}}$	Radial distance to near boundary of differential volume element, cm
$r_{j+\frac{1}{2}}$	Radial distance to far boundary of differential volume element, cm
r_{j-1}	Radial distance to center of previous differential volume element, cm
r_{j+1}	Radial distance to center of next differential volume element, cm
∂r	Differential radius, cm
S_{fluid}	Fluid Saturation
S_g	Gas saturation
$S_{g_{ini}}$	Initial gas saturation
S_o	Oil saturation

∂S_o	Change in oil saturation
t	Time, sec
Δt	Time Step size, sec
∂t	Time differential, sec
V	Volume, cm^3
V_j	Volume of current volume element, cm^3
V_{ini}	Initial Volume, cm^3
V_{fluid}	Fluid Volume, cm^3
V_p	Pore Volume, cm^3
$\vec{v}_o$	Oil flow velocity vector, cm/sec
$\vec{v}_x$	Fluid flow velocity along x-axis, cm/sec
x_i	x-axis distance to center of current differential length element, cm
$x_{i-\frac{1}{2}}$	x-axis distance to near boundary of differential length element, cm
$x_{i+\frac{1}{2}}$	x-axis distance to far boundary of differential length element, cm
x_{i-1}	x-axis distance to center of previous differential length element, cm
x_{i+1}	x-axis distance to center of next differential length element, cm
Δx_i	Current differential length element along x-axis, cm
Δx_{i-1}	Differential length element along x-axis of previous element, cm

Δx_{i+1}	Differential length element along x-axis of next element, cm
∂x	Differential length element along x-axis, cm
$x \quad length$	Length of cutting along x-axis, mm
y_j	y-axis distance to center of current differential length element, cm
y_{j-1}	y-axis distance to center of previous differential length element, cm
y_{j+1}	y-axis distance to center of next differential length element, cm
Δy_j	Current differential length element along y-axis, cm
Δy_{j-1}	Differential length element along y-axis of previous element, cm
Δy_{j+1}	Differential length element along y-axis of next element, cm
∂y	Differential length element along y-axis, cm
$y \quad length$	Length of cutting along y-axis, mm
z_k	z-axis distance to center of current differential length element, cm
z_{k-1}	z-axis distance to center of previous differential length element, cm
z_{k+1}	z-axis distance to center of next differential length element, cm
Δz_k	Current differential length element along z-axis, cm
Δz_{k-1}	Differential length element along z-axis of previous element, cm
Δz_{k+1}	Differential length element along z-axis of next element, cm
∂z	Differential length element along z-axis, cm
$z \quad length$	Length of cutting along z-axis, mm

∇	Divergence
ϕ	Cutting porosity
μ	Fluid viscosity, cp
μ_o	Oil Viscosity, cp

References

[1] Al-Yousef, H. Y.: "Permeability Anisotropy Measurements on Whole Cores – Analytical Solution and Application," paper SPE 93559 presented at the 14th SPE Middle East Oil & Gas Show and Conference, Bahrain, 12 – 15 March 2005.

[2] Egermann, P., Lenormand, R., Longeron, D. and Zarcone, C.: "A Fast and Direct Method of Permeability Measurements on Drill Cuttings," paper SPE 77563 presented at the SPE Annual Technical Conference and Exhibition, San Antonio, TX, September 29 – 2 October 2002.

[3] Egermann, P., Doerler, N., Fleury, M., Behot, J., Deflandre, F. and Lenormand, R.: "Petrophysical Measurements from Drill Cuttings, an Added Value for Reservoir Characterization Process," paper SPE 88684 presented at the 11th Abu Dhabi International Petroleum Exhibition and Conference, Abu Dhabi, U.A.E., 10 – 13 October 2004.

[4] Darcy, H., Les Fontaines Publiques de la Ville de Dijon, Dalmont, Paris (1856).

[5] Kamath, J.: "Evaluation of Accuracy of Estimating Air Permeability from Mercury-Injection Data," Journal SPE Formation Evaluation, 4, pp 304-310, 1992.

[6] Larson, R. G. and Morrow, N. R.: "Effect of Sample Size on Capillary Pressures in Porous Media," Powder Technology, 30, pp 123-138, 1981.

[7] Lenormand, R. and Fonta, O.: "Advances in Measuring Porosity and Permeability from Drill Cuttings," paper SPE 111286 presented at the 2007 SPE/EAGE Reservoir Characterization and Simulation Conference, Abu Dhabi, U.A.E., 38 – 31 October 2007.

[8] Luffel, D.L., Hopkins, C.W. and Schettler Jr., P.D.: "Matrix Permeability Measurement of Gas Productive Shales," paper SPE 26633 presented at the SPE Annual Technical Conference and Exhibition, Dallas, TX, 3 – 6 October 1993.

[9] Marsala, A.F., Zausa, F., Martera, M.D. and Santarelli, F.J.: "Sonic While Drilling: Have You Thought about Cuttings," paper SPE 30545 presented at the SPE Annual Technical Conference and Exhibition, Dallas, TX, 22 – 25 October 1995.

[10] Marsala, A.F., Figoni, A. and Brignoli, M.: "Transient Method Implemented under Un-Steady State Conditions for Low and Very Low Permebility Measurements on Cuttings," paper SPE 47202 presented at the SPE/ISRM Eurock, Trondheim, Norway, 8 – 10 July 1996.

[11] Marsala, A.F., et al.: "Petrophysical Characterization of Reservoir Rocks by Measurements on Cuttings," paper presented at the Offshore Mediterranean Conference, Ravenna, Italy, 1997.

[12] Nigh, E. and Taylor, M.: "Well Site Determination of Porosity and Permeability Using Drill Cuttings," C.W.-L Society, 10th Formation Evaluation Symposium 1985.

[13] Santarelli, F.J., Marsala, A.F., Brignoli, M., Rossi, E. and Bona, N.: "Formation Evaluation From Logging on Cuttings," paper SPE 36851 presented at the SPE Permian Basin Oil and Gas Recovery Conference, Midland, TX, 27 – 29 March 1996.

[14] Swanson, B.F.: "A Simple Correlation between Permeabilities and Mercury Capillary Pressures," JPT, pp 2498-2504, Dec. 1981.

[15] Timur, A.: “An Investigation of Permeability, Porosity and Residual Water Saturation Relationships,” SPWLA 1968.

Vita

Name:	**Sheharyar Mansur**
Nationality:	Pakistani
Email:	sheharyarmansur@gmail.com
Address:	H # 3, National Housing Scheme Phase 2, Adiala Road, Rawalpindi (46000), Pakistan
Education:	**MS (Petroleum Engineering), June 2009** King Fahd University of Petroleum and Minerals, Dhahran (31261), Saudi Arabia **B.E. (Mechanical Engineering), May 2002** National University of Sciences and Technology, Rawalpindi (46000), Pakistan
Areas of Interest:	Reservoir Simulation and Management, Enhanced Oil Recovery